Coastal Circulation and Sediment Dynamics in Pelekane and Kawaihae Bays, Hawaii

Measurements of waves, currents, temperature, salinity, turbidity, and geochronology: November 2010–March 2011

By Curt D. Storlazzi, Michael E. Field, M. Katherine Presto, Peter W. Swarzenski, Joshua B. Logan, Thomas E. Reiss, Timothy C. Elfers, Susan A. Cochran, Michael E. Torresan, and Hank Chezar

Top: Image of Pelekane and Kawaihae Bays on a typical trade-wind day.
Bottom: Image of Pelekane and Kawaihae Bays during the November 2010 flood.

U.S. Department of the Interior
KEN SALAZAR, Secretary

U.S. Geological Survey
Marcia K. McNutt, Director

U.S. Geological Survey, Reston, Virginia: 2013

Contents

Figures

Tables

Appendixes

Abbreviations and acronyms

USGS	United States Geological Survey
NOAA	National Oceanic and Atmospheric Administration
ARRA	American Recovery and Reinvestment Act
CRAMP	Coral Reef Assessment and Monitoring Program
WCP	water column profiler
ADCP	acoustic Doppler current profiler
MP	MiniProbe
CT	conductivity and temperature
SLOBS	self-logging optical backscatter sensor
NTU	Nephelometric Turbidity Units
TIS	terrestrial imaging system
CIS	coral imaging system
SG	stream gage
STT	simple tube trap
RST	rotary sediment trap
GPS	Global Positioning System
NOS	National Ocean Servicec
MLLW	mean lower low water
MSL	mean sea level
RMS	root mean square
IDW	inverse distance weighting
SC	short core
PC	long core
WAAS	wide area augmentation system
DGPS	differential Global Positioning System
IAEA	International Atomic Energy Agency
SHOALS	Scanning Hydrographic Operational Airborne Lidar Survey
Lidar	light detection and ranging
PAR	photosynthetically-available radiation

Coastal Circulation and Sediment Dynamics in Pelekane and Kawaihae Bays, Hawaii

Measurements of waves, currents, temperature, salinity, turbidity, and geochronology: November 2010–March 2011

By Curt D. Storlazzi, Michael E. Field, M. Katherine Presto, Peter W. Swarzenski, Joshua B. Logan, Thomas E. Reiss, Timothy C. Elfers, Susan A. Cochran, Michael E. Torresan, and Hank Chezar.

U.S. Geological Survey, Pacific Coastal and Marine Science Center, 400 Natural Bridges Drive, Santa Cruz, CA 95060.

Introduction

Project Objectives

Coral reef communities on the Island of Hawaii have been heavily affected by the construction of Kawaihae Harbor in the 1950s and by subsequent changes in land use in the adjacent watershed. Sedimentation and other forms of land-based pollution have led to declines in water quality and coral reef health over the past two decades (Tissot, 1998). Erosion mitigation efforts are underway on land, and there is a need to evaluate the impact of these actions on the adjacent coastal ecosystem.

The Kohala Center and Kohala Watershed Partnership was awarded $2.69 million from the National Oceanographic and Atmospheric Administration's (NOAA) Restoration Center as part of the American Recovery and Reinvestment Act of 2009 to stabilize soil and improve land-use practices in the Pelekane Bay watershed. The grant allowed the Kohala Watershed Partnership to implement various upland watershed management activities to reduce land-based sources of pollution into Pelekane Bay. However, a number of questions must be answered in order to: (1) evaluate the effectiveness of the terrestrial watershed remediation efforts; (2) understand the potential of the local marine ecosystem to recover; and (3) understand the potential threat that existing mud deposits in the bay pose to adjacent, relatively pristine coral reef ecosystems. The goal of this experiment was to help address these questions and establish a framework to evaluate the success of the Kohala Watershed Partnership restoration efforts. This research program will also provide resource managers with information relevant to other watershed restoration efforts currently being planned in neighboring watersheds.

This project involved an interdisciplinary team of coral reef biologists from the University of Hawaii Coral Reef Assessment and Monitoring Program, who focused on the impact of sedimentation on the biota of Pelekane Bay, and a team of geologists and

oceanographers from the U.S. Geological Survey (USGS), who focused on the circulation and sediment dynamics in Pelekane and Kawaihae Bays. The initial findings from the USGS research program are described in this report. These measurements support the ongoing studies being conducted as part of the USGS Coastal and Marine Geology Program's Pacific Coral Reef Project to better understand the effect of geologic and oceanographic processes on coral reef systems.

Study Area

Spatial and temporal measurements of meteorologic, oceanographic, and sedimentological data were made during the 2010-2011 winter in Pelekane and Kawaihae Bays, on the Kohala coast of the northwest side of the Island of Hawaii (fig. 1), to describe and assess circulation and sediment dynamics in the area. Pelekane Bay is a small, inshore portion of the larger Kawaihae Bay that is located just south of the harbor. Instruments were deployed and measurements made from north of Kawaihae Harbor south to Puako in order to understand circulation and sediment transport in Pelekane and Kawaihae Bays, their connection to the adjacent watersheds, and give the focused study in Pelekane Bay a more regional context. The bathymetric and geochemical studies were conducted only in Pelekane Bay to describe and evaluate the terrigenous sediment deposited after the construction of Kawaihae Harbor.

The climate in the study area is exceptionally arid (Thornberry-Ehrlich, 2011); measured average rainfall rates at the coast are a little more than 10 cm/yr. This is in sharp contrast to precipitation rates recorded at the summit of Kohala Mountain (elevation = 1600 m) in the upper Pelekane watershed, where precipitation can approach 400 cm/yr. The Pelekane watershed (50 square kilometers) is typically dry except during periods of heavy rainfall, which occur most frequently in winter. During these events, a series of erosional gullies fill with sediment-laden runoff and transport their muddy loads to the sea as ephemeral, flashy flows (Hoover and Gold, 2006). Two distributary gulch systems (Makeahua and Pohaukole) collect this surface runoff and converge just before emptying into Pelekane Bay.

Rocks in the watershed are mostly volcanic, and the soils include sandy to silty loams that are easily erodible and further weathered during down-stream transport. Pelekane Bay is littered with many rocks and small boulders of varying sizes that were transported downstream during flash-flood events. From modeling, it has been estimated that roughly 4200 metric tons of sediment are delivered annually to Pelekane Bay by runoff (Group 70 International, Inc. and Oceanit Center, 2007).

Operations

This section provides information about the personnel, equipment, and field operations used during the study. See table 1 for a list of personnel involved in the experiment and tables 2–5 for complete listings of instrument and deployment information.

The circulation and sediment-dynamics portion of the study consisted of three suites of instruments, deployed to provide an integrated understanding of circulation and sediment dynamics: terrestrial instruments, bottom-mounted time-series oceanographic instrument packages, and oceanographic survey instruments that profiled the water column. The terrestrial instruments consisted of a weather station, stream gauge, and a digital imaging system (fig. 1).
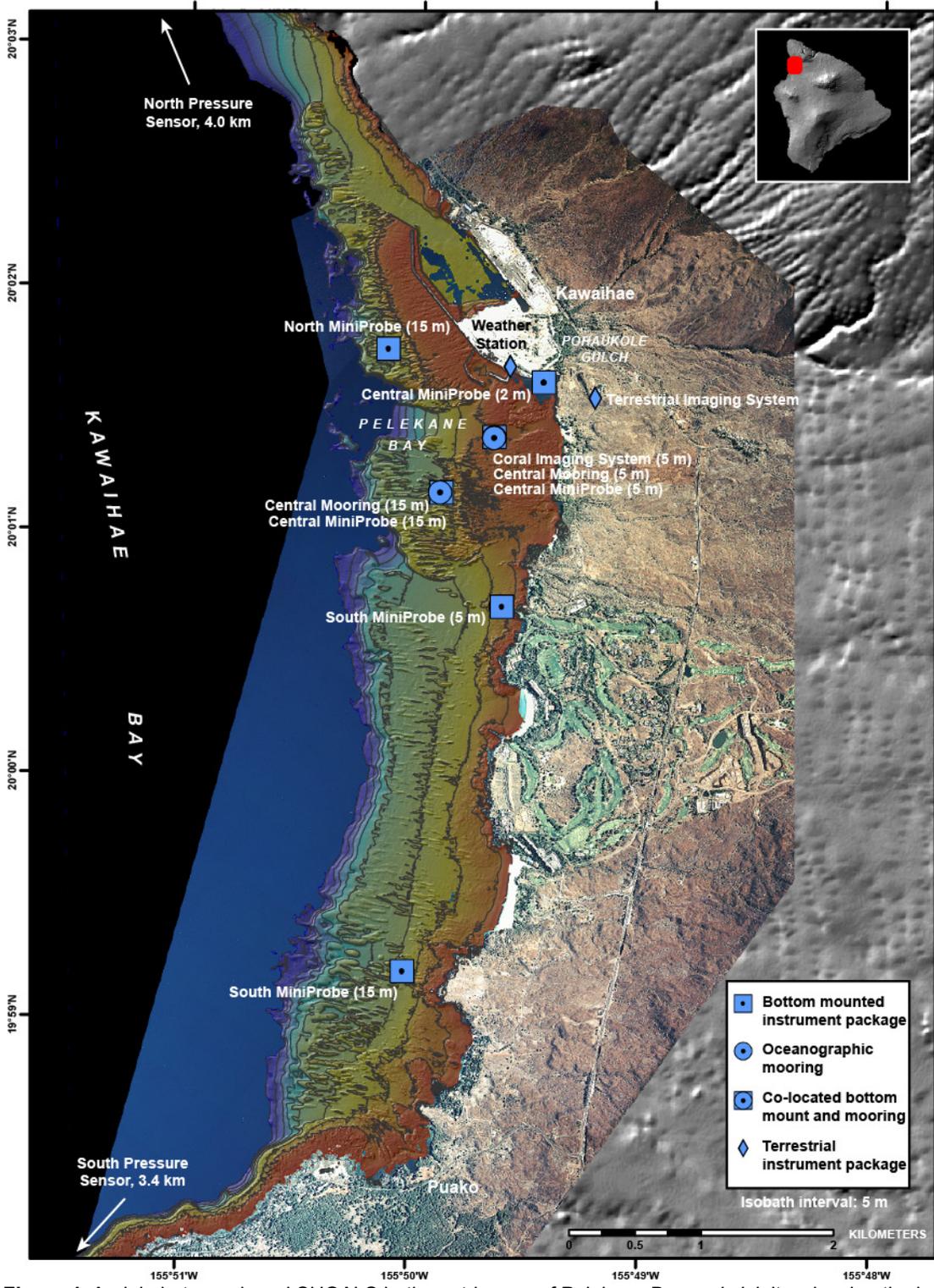
Figure 1. Aerial photograph and SHOALS bathymetric map of Pelekane Bay and vicinity, showing the locations of instrument packages and major landmarks; the location of the study area on the Island of Hawaii (the "Big Island") is shown in the inset, upper right.

Bottom-mounted oceanographic instrument packages were deployed along the 5-m and 15-m isobaths, as well as a cross-shore array in the central region of Kawaihae Bay. This cross-shore array included three bottom-mounted oceanographic instrument packages on the 2-m, 5-m, and 15-m isobaths, and two moorings on the 5-m and 15-m isobaths (fig. 1). In addition to these fixed, bottom-mounted, time-series measurements, spatial surveys of water-column properties were made in Pelekane and Kawaihae Bays at the beginning and end of the experiment.

In order to understand the nature and thickness of the terrigenous sediment deposit in Pelekane Bay, a topographic/bathymetric survey was conducted for comparison with pre-Kawaihae Harbor surveys. In addition, two complementary geochemical and geophysical techniques were used to assess the sediment dynamics within Pelekane Bay: short-lived radionuclides (that is, ^{210}Pb, ^{137}Cs, and ^{7}Be) were used to develop a modern sediment geochronology; and multichannel electrical resistivity surveys were employed to estimate lithologic change and sediment thickness within the bay.

Research Platform and Field Operations

The instrument deployments and recoveries were conducted using the F/V *Alyce C*. Vessel operations, including mobilization and demobilization, were based out of Kawaihae Harbor, Hawaii. The water-column profiler (WCP) casts were conducted from a U.S. National Park Service vessel using a hand line. The starboard quarterdeck was outfitted with a davit for the profiler to be lowered into the water for water-column surveys. The topographic/bathymetric survey was conducted from shore either on foot or using a small inflatable boat.

Equipment and Data Review

Acoustic Doppler Current Profilers (ADCP)

Six upward-looking acoustic Doppler current profilers (ADCPs) were mounted on MiniProbes (MPs) along the 2-m, 5-m, and 15-m isobaths in Pelekane and Kawaihae Bays (fig. 2*A*). Please see appendix 1 for information about instrument settings to collect current and wave data from the ADCPs deployed at 2-m, 5-m, and 15-m isobaths. The ADCPs deployed on the 15-m isobath and collected data for 50 s at 2 Hz every 15 min, measuring mean current speeds (m/s), and mean current directions (given as "going to," in degrees clockwise from true north, °True) from 1.5 m above the sea floor up to the surface in 1-m bins, to allow calculation of tidal heights (given in m). Directional wave data were recorded for 1024 s at 2 Hz every hour; these data included significant wave height (m), dominant wave period (s), mean wave direction (°True), and directional spread (°). The ADCPs deployed along the 2-m and 5-m isobaths collected data for 480 s at 2 Hz every 15 min, in 0.5-m bins from 1.0 m above the sea floor up to the surface. Directional wave data were recorded by a setup similar to those used with the ADCPs deployed along the 5-m and 15-m isobaths. Acoustic backscatter data (dB) collected from the ADCPs for the current measurements also provide information on the volume of particulates scattering the acoustic signals in the water column and are used as a qualitative measurement of turbidity. The sensor locations are listed in table 3; complete sensor and processing information is listed in appendix 1.
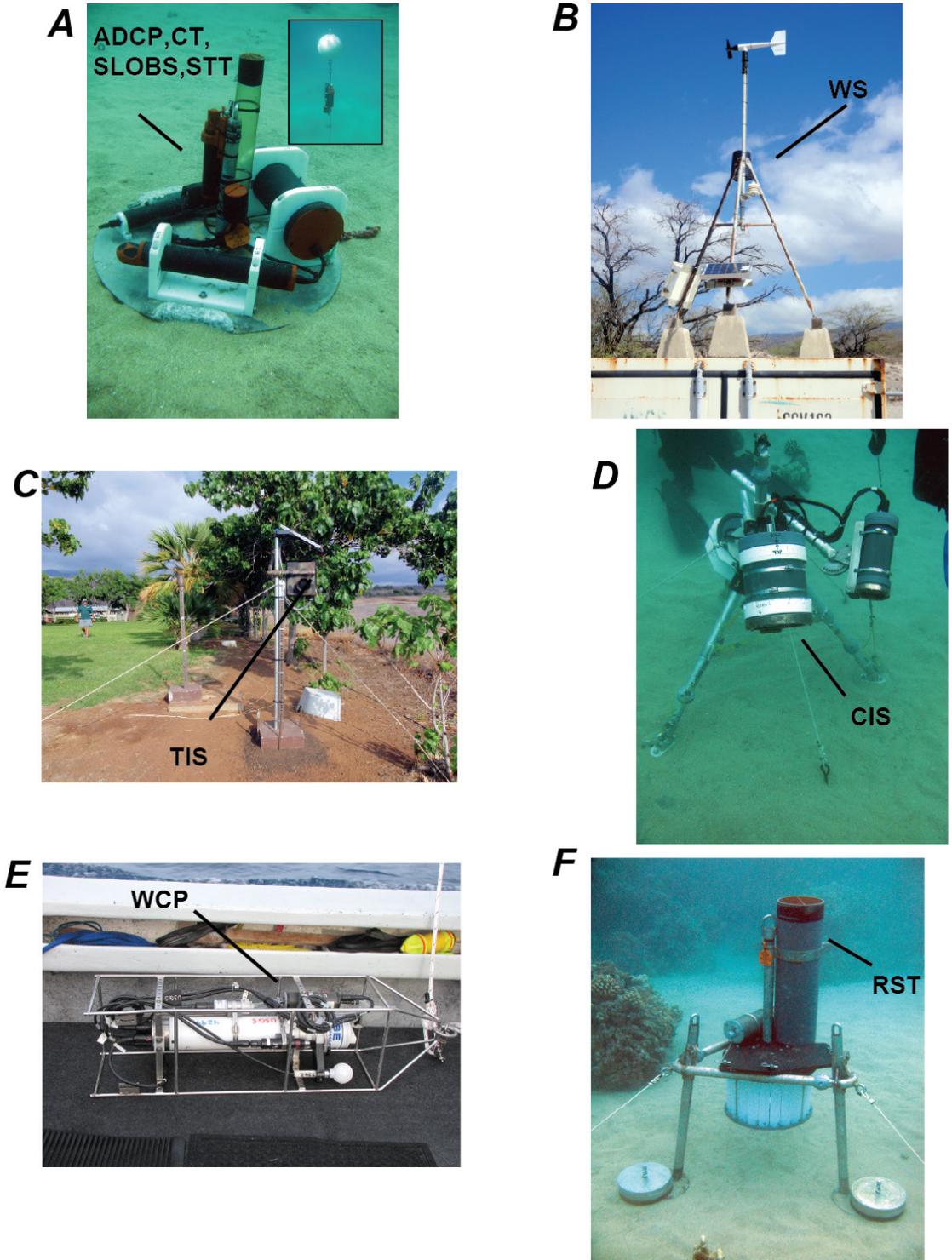
Figure 2. Photographs of the equipment used in the 2010-2011 winter experiment. *A,* Underwater photograph of a MiniProbe with acoustic Doppler current profiler (ADCP), conductivity and temperature (CT) sensor, self-logging optical backscatter sensor (SLOBS), and simple tube trap (STT) along the 5-m isobath at the Central 5-m site; inset, underwater photograph of a mooring with CT and SLOBS at the Central 5-m site. *B,* Weather station (WS) on the USGS storage facility. *C,* Terrestrial Imaging System (TIS) located above Pelekane Bay at the NPS headquarters. *D,* Coral Imaging System (CIS) at the Central 5-m site. *E,* Water-column profiler (WCP). *F,* Rotary sediment trap (RST) at the Central 5-m site.

Conductivity and Temperature (CT) Sensors

Four conductivity and temperature (CT) sensors collected and averaged four samples every 5 min to measure water temperature (°C) and conductivity (S/m), from which salinity in Practical Salinity Units (PSU) was calculated (PSU; fig. 2*A*). The rapid sampling rate was established in an attempt to record internal tidal bores, non-linear internal waves, and transient freshwater plumes and/or submarine groundwater discharge that may have been advected past the instruments. Two conductivity and temperature sensors (fig. 2*A*, inset) were deployed at the top of the moorings along the 5-m and 15-m isobaths in a cross-shore array to examine the dispersion of any freshwater plumes generated by stream flow into the bays. The other two CT sensors were mounted just above the sea floor at the Central 5-m and South 5-m MPs (fig. 2*A*). The sensor locations are listed in table 3; complete sensor and processing information is listed in appendix 2.

Turbidity Sensors (SLOBS)

Eight self-logging optical backscatter sensors (SLOBS) collected 8 samples every 5 minutes to measure turbidity in Nephelometric Turbidity Units (NTU). The SLOBSs were mounted on all of the MPs above the ADCPs (fig. 2*A*) so that the turbidity data could be correlated with co-located ADCP acoustic backscatter data using the methodology described in Storlazzi and Jaffe (2008). The SLOBSs on the 5-m and 15-m moorings were mounted at the same depth as the CT sensors to correlate the two data sets (fig. 2*A*, inset). The sensor locations are listed in table 3; complete sensor information is listed in appendix 3.

Weather Station (WS)

A weather station (WS) was deployed approximately 3 m above ground on top of a storage container in the YMCA yard at Kawaihae Harbor to quantify the influence of meteorologic forcing on circulation and water-column properties in Pelekane and Kawaihae Bays (fig. 2*B*). The WS recorded 25-min averages of barometric pressure (mb), air temperature (°C), precipitation (mm), wind speed (m/s), and wind direction (°True) every 30 min. The instrument's location is listed in table 3; complete sensor information is listed in appendix 4.

Terrestrial Imaging System (TIS)

Imagery of surface waters in Pelekane and central Kawaihae Bays was collected using the USGS Terrestrial Imaging System (TIS). The system consists of a 10.1-megapixel digital SLR camera, a control unit, and battery in a waterproof housing with an external solar panel. Both the housing and the solar panel were mounted on a vertical pole just above Pelekane Bay near the Puukohola Heiau National Historic Site (NPS-PUHE) offices (fig. 2*C*). This system was used to collect a time series of images to provide information on the natural frequency and duration of visually-observable processes impacting Pelekane Bay (for example, stream discharge, freshwater plumes, and sediment plumes). The TIS took images every hour during the morning and every other hour until dark (07:00, 08:00, 09:00, 10:00, 11:00, 13:00, 15:00, and 17:00, Hawaii Standard Time [HST]) throughout the deployments. The sensor location is listed in table 3; complete sensor information is listed in appendix 4.

Coral Imaging System (CIS)

The USGS Coral Imaging System (CIS) was used to collect a time series of seabed images and consists of a 6.3-megapixel digital SLR camera with a 24-mm lens, an external TTL strobe, a control unit, and batteries that are mounted on a tetrapod (fig. 2D). The CIS was deployed in a patch of sand at the Central 5-m site, and the camera and strobe were angled to record images of the adjacent reef and seabed. The CIS provided data on the natural frequency and duration of sediment deposition and resuspension on an actual coral surface. The CIS took images every four hours throughout the day (00:00, 04:00, 08:00, 12:00, 16:00, and 20:00 HST). The sensor location is listed in table 3; complete sensor information is listed in appendix 4.

Water-Column Profiler (WCP)

Surveys of water properties throughout the water column were made using a water-column profiler (WCP) with conductivity, temperature, depth, optical backscatter, light transmission, and chlorophyll sensors (fig. 2E). The surveys were conducted on 6 November 2010 (2010 year day [YD] 310) and 10 March 2011 (2010 YD 434), from north of Kawaihae Harbor south to Puako. During each cast, the sensors collected data at 4 Hz and the data were binned at 0.5-m depth intervals in order to examine variations in water properties throughout the water column. The WCP location and depth information are listed in table 4; complete sensor information and individual cast acquisition logs are listed in appendixes 5–7.

Stream Gauge (SG)

A simple water-level (stream) gauge, consisting of a pressure sensor in a perforated steel pipe set into concrete, was deployed in the lagoon landward of the sand bar that separated Pohaukole Gulch from Pelekane Bay (table 3). The purpose of this sensor was to measure water levels in the lagoon, provide some insight on the relative magnitude of discharge from Pohaukole Gulch, and give some information on the presence or absence of the sand bar at the mouth of the gulch.

Simple Tube Traps (STT), Rotary Sediment Trap (RST), and Seabed Sediment Samples

Two types of sediment traps collected suspended sediment from the water column in the bays. Simple tube traps (STT), consisting of a clear plastic tube 30-cm long, with an internal diameter of 6.7 cm, were deployed with their openings 0.4 m above the seabed at the 6 main instrument sites (fig. 2A). A baffle was placed in the top of each tube trap to reduce turbulence and minimize disturbance by aquatic organisms (see Bothner and others, 2006). A programmable rotary sediment trap (RST) was deployed with its opening 1.4 m above the seabed at the central 5-m site (fig. 2F). The RST consisted of a 20-cm internal-diameter, 75-cm-long cylinder equipped with a funnel in the lower 15 cm of the cylinder to direct settling sediment into one of 21 plastic bottles (500 ml). Sampling bottles were mounted on a carousel that rotated a new bottle under the funnel approximately every 5 days. Both types of sediment traps were employed in this study to obtain a relative measure of suspended sediment collection rates and sufficient

quantity of suspended material for physical and chemical characterization. Because of the energetics of the insular shelf environment, the traps did not measure net vertical sediment flux to the coral reef surface. This is because material falling into the trap has a much lower potential for resuspension than the same material settling on the adjacent reef surface (Bothner and others, 2006). The traps were also likely to preferentially collect coarser particle sizes because of their higher settling velocities than finer particles. Particles with slow settling velocities relative to the circulation and exchange of water contained in the trap can be underrepresented in the collected samples (for example, Gardner and others, 1983; Baker and others, 1988). The average daily trap collection rate for both the STTs and RST was calculated by measuring the total mass of sediment in the trap or bottle and dividing by the trap cross-sectional area and the collection period. Because the STTs were deployed with their openings 0.4 m above the seabed, compared to the RSTs' opening 1.4-m above the seabed, the average daily trap collection rate for the STTs was much greater (even orders of magnitude greater) than the RST (Storlazzi and others, 2011). In addition to these trapped-sediment samples, divers collected seabed-sediment samples by hand by in March 2011 at the instrument sites using 15-cm diameter by 25-cm long acrylic tubes with delrin caps.

The relatively small volumes of sediment collected in some of the RST bottles were due to their short (~5 day) sampling intervals; thus sediment grain-size and composition analyses were made only on selected RST samples with sufficient sample volume. All of the STT samples contained enough sample material to be processed. Sediment grain-size analysis was conducted on wet aliquots of the trap and seabed samples using sieving and Coulter Counter® techniques described by Poppe and others (2000). Total carbon and carbonate carbon measurements were made using a Perkin Elmer CHN analyzer and a UIC coulometer, respectively. Organic carbon (C) was determined by difference between total carbon and carbonate carbon. Critical shear stresses for the different types of sediment were calculated using the modified Shield parameter methodology of Madsen (1999).

Topographic/Bathymetric Survey

A topographic survey of the beach and nearshore portions of Pelekane Bay was conducted on 11-12 March 2011 (2010 YD 435-436). A continuously-recording GPS receiver acquired raw satellite data, at 1 Hz, while the investigators walked or boated throughout the survey area. The acquired data was then post-processed against a concurrently-running GPS base station to obtain preliminary coordinates of the track lines (appendix 8.1). Replicate (stationary) points and points not suitable for generating the topographic surface (for example, transit points) were removed, resulting in a final set of topographic points. In order to reference this survey to a true tidal datum, a GPS static survey was conducted between the survey base station and a National Ocean Service (NOS) tidal benchmark located at Kawaihae Harbor, approximately 1 km from the survey site (National Ocean Service, National Oceanographic and Atmospheric Administration). The NOS tidal benchmark used for this static occupation was "161 7433 B" (NGS PID DK3434).

Topographic elevations are expressed as both ellipsoid heights and orthometric heights (derived by subtracting the Geoid09 undulation values from the ellipsoid heights). In order to reference the Pelekane topographic/bathymetric survey to a tidal datum, the GPS-derived heights had to be adjusted by an amount equivalent to forcing the tidal benchmark ellipsoid height onto the tidal height of the tidal datum of choice. In other words, to render the topographic survey into a surface relative to mean lower-low water (MLLW), 20.967 m (23.207 m – 2.240 m) would

have to be subtracted from each ellipsoid height to obtain the corresponding MLLW height value. A separate GPS receiver was set up on a boat in the Kawaihae Small Boat Harbor near the NOS tide gage. This receiver was allowed to record water elevations at 1 Hz. The GPS receiver file was downloaded and post-processed against the base station data that was collected concurrently. The resulting coordinate ellipsoid elevations were adjusted to MLLW according to the NAD83 (1993) to MLLW offset value listed above (20.967 m). Additionally, NOS data from the tide station at Kawaihae was downloaded from the NOS/Center for Operational Oceanographic Products and Services (CO-OPS) website (National Ocean Service, National Oceanographic and Atmospheric Administration) for the same time period.

Historical bathymetric data were taken from the 1928 U.S. Coast and Geodetic Hydrographic Survey #5007 (appendix 8.2). The resolution of the historical 1928 survey was ±1/6 fathom (±1 ft or ±0.3 m). In order to place the digital map into a frame of reference, the 1970 U.S. Coast and Geodetic Hydrographic Survey #9018 that was in the Old Hawaii Datum was referenced to the 1928 survey using both graticule tics and known benchmark latitudes and longitudes at both the Kawaihae Light and Puako. The georeferencing of 1970 survey map matched fairly well (root mean square, RMS error = 3.93080 m spatially) and aligned with the currently available coastline. The match between the georeferencing of the 1970 survey map and the harbor boundary of the coastline was good. Any differences along the coastline itself were most likely due to different tidal ranges during interpretation. The historical 1928 survey was then rubber-sheeted to the 1970 survey using the Kawaihae Light mark, latitudes and longitudes graticules, and prominent landmarks along the coastline (RMS, error = 12.58580 m). U.S. Coast and Geodetic Hydrographic Survey soundings within the area of interest were digitized and recorded as noted using both fathoms (2 fathoms and greater) and fathoms plus feet (when less than 2 fathoms).

In addition to aligning the historical map with the recently-collected data in horizontal, or coordinate space (georeferencing), it was aligned vertically with respect to depth so that the two datasets can be compared. The 1928 survey soundings were fixed to MLLW that was calculated from concurrent readings at a portable tide gage established at Kawaihae during the survey, and by comparison with observations at Honolulu during the same period of the survey, according to the report accompanying the chart. The USGS 2011 topographic/bathymetric survey was adjusted to the 2001 tidal epoch. The historical data were then transformed to that same tidal datum. Unfortunately there are no tidal data at Kawaihae prior to 1960. Data are available from Honolulu, but due to isostatic loading on the sea floor between the island of Hawaii (in a depression), and Oahu (on a bulge), the tidal data are not comparable. It would be beyond the scope of this calculation to model or account for the isostatic differences. According to the National Ocean Service data (National Ocean Service, National Oceanographic and Atmospheric Administration, n.d.), there is a 0.51-ft difference in mean sea level (MSL) at Kawaihae between the 1960-1978 tidal epoch and the 1983-2001 tidal epoch, which was added to the historical soundings to bring them into a comparable plane of reference.

A raster-interpolation inverse-distance weighting (IDW) method was used to create a raster for both the historical 1928 survey and the USGS 2011 topographic/bathymetric survey. The USGS 2011 survey data were then subtracted from the historical 1928 survey data in order to generate a map of gain in elevation (sedimentation) or decrease in elevation (erosion) between the surveys.

Sediment Coring

A series of seven short ("SC", ~15-cm long) and three long ("PC", ~50-cm long) sediment cores, 15.2 cm in diameter, were collected in Pelekane Bay during March 2011 (fig. 3, table 5). The 15.2-cm core barrels (fig. 3, inset) were used because they greatly diminish the effects of compaction during core collection and allow for a large interval sample size. Of note is that coring occurred both before and after a series of large but diminishing tsunami waves generated from the catastrophic 2011 Japanese Tohoku earthquake in Japan. These tsunamigenic waves lasted several days, effectively pumping seawater into and out of Pelekane Bay several times each day, causing widespread and prolonged sediment resuspension. Core sites were selected based on observations of an intact sediment/water interface, low degree of infaunal bioturbation, and ubiquity of fine-grained sediment. As will be shown, tsunamigenic shear and resuspension did affect the sediment/water interface in many of the post-tsunami cores. Cores were carefully collected and immediately extruded in the field from the top down into 1-cm and 2-cm intervals. The sectioned sediment slices were sealed in plastic bags and kept chilled for transport to the laboratory in Santa Cruz, CA. Based on weight loss after drying at 60 °C for 48 hours, water content (and thus porosity) of the wet sediment was determined and used to derive cumulative mass depths (g/cm^2). Dried samples were then transferred into 10-ml plastic vials,

Figure 3. Map showing the location of short (green) and long (orange) cores (15.2-cm diameter tube) in Pelekane Bay. Locations of cores PC5 and PC6 are not shown. Inset photograph showing one of the long cores with about 65 cm of mud.

equilibrated for 3 weeks to account for radon (Rn) ingrowth, and subsequently analyzed by ultra-low background, gamma spectrometry.

Radionuclides

Three radionuclides (^{210}Pb, ^{137}Cs, and ^{7}Be) were analyzed by non-destructive gamma spectrometry. The uranium-series radioisotope ^{210}Pb ($t_{1/2}$= 22.2 years; 46.5 keV) and the nuclear fission product ^{137}Cs ($t_{1/2}$= 30.2 years; 661.62 keV) are used as complementary sediment chronometers, while cosmogenic ^{7}Be ($t_{1/2}$ = 53.2 days; 477.56 keV) is used to potentially trace flood-induced sedimentation. In the atmosphere, ^{210}Pb occurs as a decay product of the noble gas ^{222}Rn, and falls back to Earth's surface in precipitation and dry fall out. In the oceans, ^{210}Pb is rapidly adsorbed onto sediment particles, and so where sedimentation is occurring there is more ^{210}Pb than would be present from only atmospheric deposition. This "excess" amount of ^{210}Pb is directly related to the sedimentation rate, and may be determined by comparing down-core total ^{210}Pb activity to the activity of the radiogenic parent, ^{226}Ra ($t_{1/2}$= 1600 y; 351.99 and 609 keV).

A fallout radionuclide from nuclear weapons testing and nuclear accidents, ^{137}Cs does not occur naturally. The first observations of appreciable ^{137}Cs activities in the atmosphere occurred in the early 1950s, and peak quantities were released in 1963–1964. Like ^{210}Pb, ^{137}Cs is washed out of the atmosphere by wet and dry precipitation and accumulates and also decays in sediment after burial. Theoretically, down-core profiles of ^{137}Cs will exhibit a pronounced peak that corresponds to the 1963 atmospheric maximum. Secondary ^{137}Cs peaks may resolve the 1986 Chernobyl accident, and most recently, the 2011 Japanese nuclear accident at Fukushima.

Radionuclide activities were measured in the radioisotope laboratory at the USGS Pacific Coastal and Marine Science Center in Santa Cruz, California, using ultra-low-background, high-purity germanium (HPGe) positive-voltage (P-type) well detectors that are routinely calibrated with the International Atomic Energy Association (IAEA). RGU-1, RGTH-1 and IAEA 300 standards. Each standard is prepared to the same geometry as the sample.

Electrical Resistivity

Electrical resistivity surveys of Pelekane Bay were conducted using a multi-channel system. An external switching box controlled the flow of current along a 56-electrode (2-m electrode spacing), stationary cable that is 112 m long. In stationary (land-based) mode, current potentials are measured in a distributed array, with array geometry (for example, dipole: dipole) defined by the user. For every resistivity measurement (~1 per second), the system injects an optimized current, reverses the polarity, and then re-injects the current again to cancel spontaneous voltages that may occur down-cable. This process is typically repeated and if the recorded error is less than a pre-determined threshold value (for example, 5 percent), then the next reading advances. Replicate measurements provide a means to assess electronic noise or other artifacts. Each survey consisted of more than 600 readings and was completed in approximately 25 min. Resistivity measurements were subsequently processed using a user-defined inverse modeling routine. Resolution was optimized using a starting model with the apparent-resistivity pseudo-section, and a best-fitting layered model was then developed using an iterative, least-squares, smooth-model-inversion method.

A series of 8 lines, or electrical resistivity surveys, were conducted in Pelekane Bay (fig. 4) to cover the full extent of the bay. The position and orientation of these lines within the bay was optimized for sea floor coverage and expected electrical signal contrasts. Whenever possible, resistivity data were collected only when the cable was exposed subaerially. Relative electrode elevations per line were manually obtained with the high-precision GPS system used for the topographic/bathymetric survey. Concurrent with the GPS work, a rough approximation of depth-to-bedrock per electrode was established using a simple probing rod.
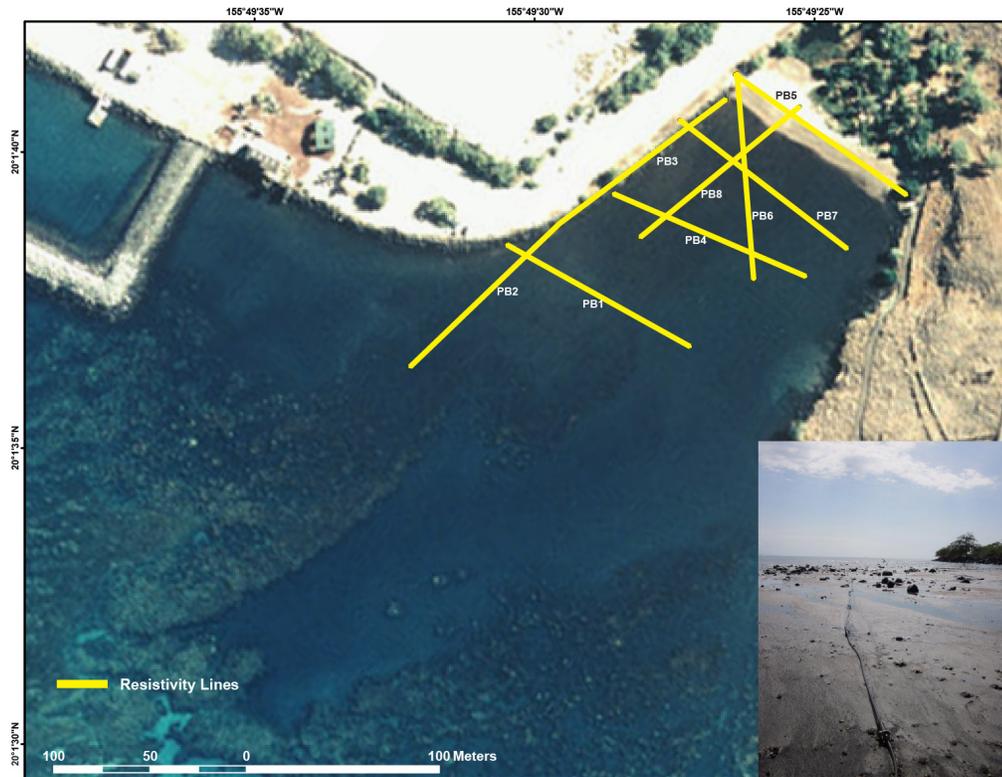
Figure 4. Map showing the position of the eight electrical resistivity lines in Pelekane Bay. Inset photograph was taken from the terminal sand bar, close to the intersection of lines PB8 and PB5 and looking down-cable along line PB8, across the bay. Note the scattered, fluvial rock debris exposed on the seabed as the tide approached low stage.

Miscellaneous Data Sources

Navigation equipment for deployment, recovery, and survey operations included hand-held WAAS-equipped DGPS units and a computer with positioning and mapping software. The positioning and mapping software enabled real-time DGPS data to be combined with previously-collected, high-resolution images of SHOALS color-coded lidar, shaded-relief bathymetry, 5-m isobaths, and aerial photographs of terrestrial portions of the maps (fig. 1).

Data Acquisition and Quality

Data were acquired for 120 days during the period between 6 November 2010 and 6 March 2011 (2010 YD 310–430). More than 2 million data points were recorded by the ADCPs, CTs, SLOBSs, and WS; more than 8,000 data points were recorded by the WCP. The raw data

were archived and copies of all the data were post-processed for analysis. The ADCPs, CTs, SLOBSs, WS, TIS, SG, and WCP data generally appeared to be of high quality. The ADCP at the Central 2-m site was damaged, and as a result, the current data were not of sufficient quality to be included in this report. A series of large-wave events in late January to early February 2011 moved and/or buried some of the instruments deployed on the seabed, reducing the quality of some of the pressure, wave, current, and conductivity data. The CIS was dislodged from its anchors and deposited on its side during one of these events, rendering the photos unusable after the January 2011 wave event. In addition, some of the SLOBSs' optical sensors began to foul because of biologic growth and wiper failure toward the end of the deployment. The RST's main funnel was plugged with sediment in January 2011 and thus there was no sediment collected in the remaining 7 bottles. For these reasons, the range of data included for the analyses presented in this report is limited from 6 November 2010 to 4 February 2011 (2010 YD 310–390).

The quality of the topographic/bathymetric survey of Pelekane Bay was determined by comparing the GPS-derived water levels to the NOS tidal elevations. Ideally, the NOS tidal elevations should match up and superimpose themselves on the GPS-derived water surface elevations. Although the signal from the GPS base station was very noisy, near the end of the occupation, the NOS heights were typically lower than the GPS-derived elevations. It is difficult to determine the magnitude of this offset, but it may be as much as 0.2 m. At this time, there is not enough information to determine whether the ellipsoid to tidal datum corrections are accurate or if the difference shown above is a function of ellipsoid/datum problems, smoothing of the NOS tide data to a 6-min interval, or an undetermined source of error.

Results

General Meteorology

The study period from 2010 YD 310–390 covered the wet winter season in Hawaii. The general meteorology of the study area, including barometric pressure, air temperature, precipitation, and stream depth, was recorded by the USGS weather station (WS) and stream gage (SG) (fig. 5). The barometric pressure ranged from 1005.56 to 1017.75 mb, with a mean and standard deviation of 1012.95±1.99 mb (table 6). The barometric pressure was relatively stable throughout the deployment, except during the large-wave events that occurred towards the end of the deployment (fig. 5A). The air temperature ranged from 17.69 ºC to 31.06 ºC, with a mean temperature ± one standard deviation of 24.36±2.24ºC (table 6). The air temperature fluctuated on the order of 5 °C daily, with a slight decreasing trend in temperature over the period of study (fig. 5B). The precipitation ranged from 0 to 24 mm during the 25-min sampling intervals, with a mean rainfall ± one standard deviation of 0.05±0.83 mm (table 6). The rainfall was episodic, with heavy rainfall often occurring over short periods of time (fig. 5C). The data from the SG deployed in the lagoon landward of the sand bar that separated Pohaukole Gulch from Pelekane Bay ranged in height from 0.00 m to 1.00 m, with a mean depth ± one standard deviation of 0.14±0.13 m (table 6). The SG showed little fluctuation prior to the large rainfall event on 19 November 2010 (2010 YD 323). After the breach of the sand bar by fluvial discharge in mid-November 2010, the SG was able to measure the propagation of the higher high tides into the lagoon (fig. 5D).
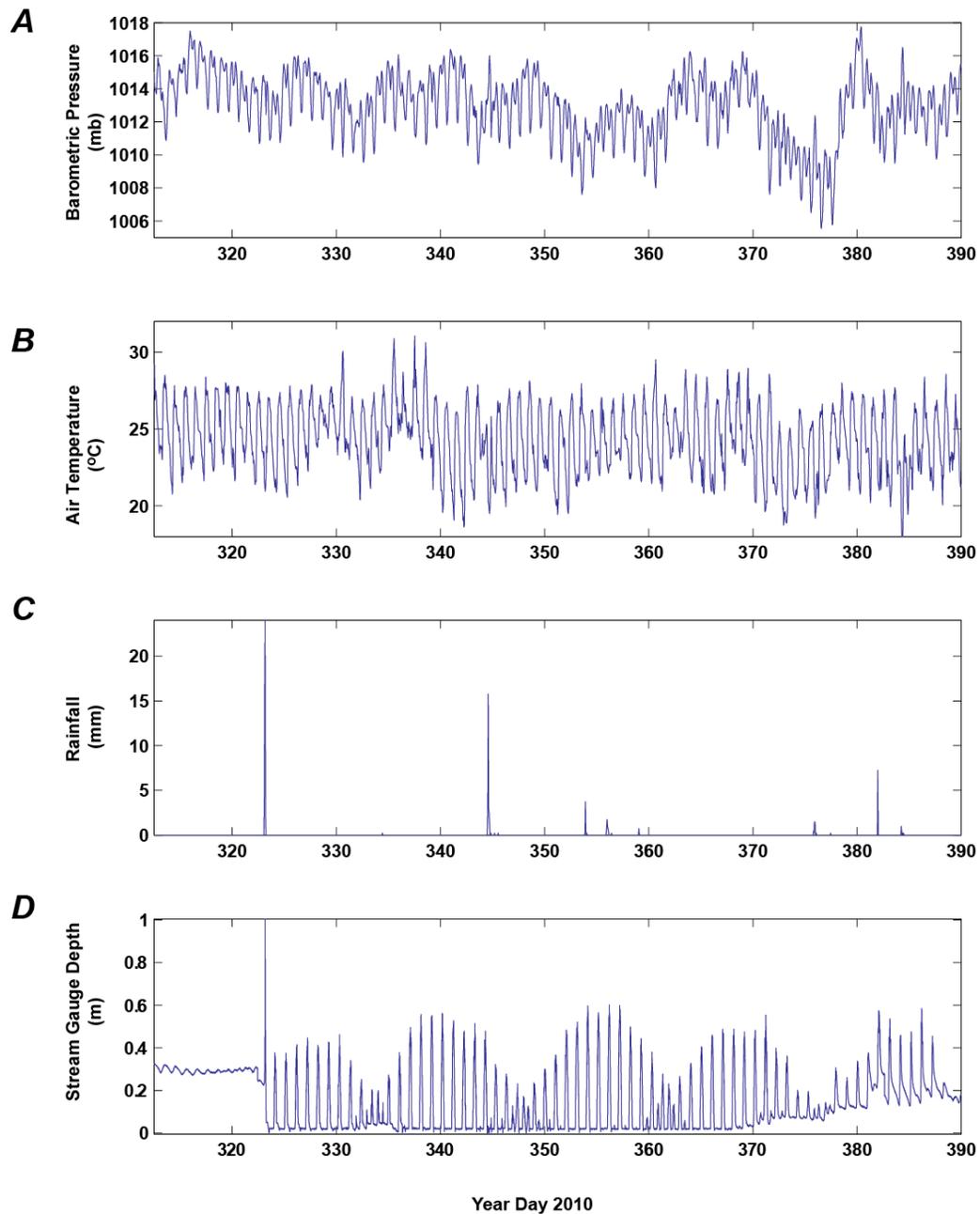
Figure 5. Time-series plots of meteorological data from the USGS weather station (WS) during the 2010–2011 winter experiment. *A*, Barometric pressure, in millibars, showing relatively stable pressure except during low-pressure systems. *B*, Air temperature, in degrees Celsius, showing the approximately 5° change every day. *C*, Rainfall, in millimeters, showing the episodic and short-term events during the winter experiment. *D*, Stream height, in meters, showing fluvial and tidal components to the signal inshore of the sand bar.

Tides

The study period encompassed more than five complete spring-neap tidal cycles (fig. 6*A*). The tides in Pelekane and Kawaihae Bays are typical for the Hawaiian Islands: microtidal, mixed, semidiurnal with two uneven high tides and two uneven low tides per day; so the tides
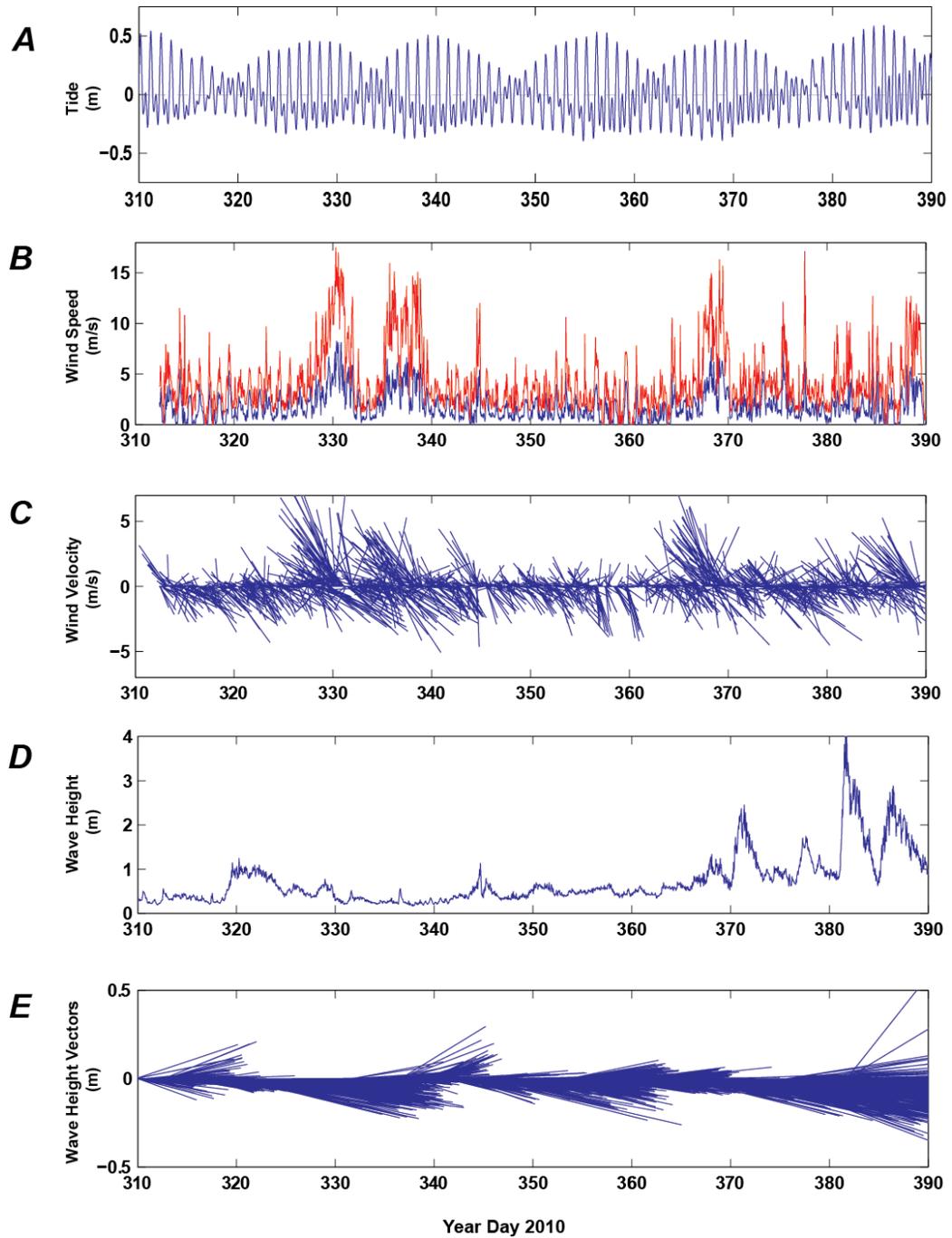
Figure 6. Time-series plots of meteorologic and oceanographic forcing during the 2010–2011 winter experiment. *A,* Tidal height, in meters, showing the semi-diurnal nature of the tides. The study period encompassed 5 spring-neap tidal cycles. *B,* Wind speed, in meters per second, with mean speed in black and peak speed in red. *C,* Wind velocity, with direction given in degrees clockwise from true north and speed in meters per second, showing that the winds were predominantly from the northwest and southeast due to trade-wind interaction with island topography. *D,* Wave height, in meters, showing the relatively low wave energy during the winter, with a few periods of elevated wave activity toward the end of the deployment. *E,* Wave vectors, with direction from true north and height in meters, showing that the waves were predominantly from the northwest either due to trade winds or the north Pacific swell.

change approximately every 6 hours. The mean daily tidal range was approximately 0.6 m, while the minimum and maximum daily tidal ranges were 0.4 m and 1.0 m during neap and spring tides, respectively.

Winds

The mean wind speeds at the weather station (WS) ranged from 0 to 8.25 m/s, with a mean speed ± one standard deviation of 1.83±1.45 m/s during the deployment. The mean wind direction ± one standard deviation during the deployment was 197°±99°(table 6). The daily fluctuations in winds due to heating and cooling of the land (thus, land breeze and sea breeze) were fairly consistent throughout the deployment, with a few periods of strong winds from the southeast (figs. 6*B, C*), likely during the passage of storms through the study area.

Waves

The directional wave gage at the Central 15-m site provided time-series information about the size and direction of waves that impacted Kawaihae and Pelekane Bays during the course of the experiment (figs. 6*D, E*). Significant wave heights at this site ranged from 0.16 m to 4.12 m (maximum wave heights exceeded 6 m), with a mean significant height ± one standard deviation of 0.72±0.57 m. Dominant wave periods varied from 2.8 to 14.7 s, with a mean dominant period ± one standard deviation of 7.4±2.6 s. The mean wave direction ± one standard deviation was 276°±7° (table 7). The time-series wave data for all of the sites are shown in appendixes 9.1–9.6. The mean wave direction for all of the instrument sites was predominantly from the west, with the largest mean wave heights located in the central part of the experiment area, at the Central 5-m and 15-m sites and the South 5-m site (fig. 7).

Currents

The mean current speeds at the shallow (depth~5 m) sites (depth ~5 m) averaged 0.02±0.06 m/s close to the surface and 0.01±0.04 m/s close to the sea floor (table 8). The range in current speeds was 0.00-0.84 m/s near the surface and 0.00-0.58 m/s near the bed. The mean current speeds at the deeper sites (depth~15 m) averaged 0.02±0.04 m/s close to the surface and 0.01±0.02 m/s close to the sea floor (table 8). The range in current speeds at these deeper sites was 0.00-0.35 m/s near the surface and 0.00-0.19 m/s near the bed. The time-series data for each ADCP are shown in appendixes 10.1–10.5. The mean and variability of near-surface and near-bed current speeds and directions for the entire deployment period (YD 310–390) for the ADCPs at each site are shown in figures 8 and 9. The mean near-surface currents were strongest in the central part of the experiment area, at the Central 5-m and 15-m sites and the South 5-m site. The mean near-surface current speeds at the North 15-m and South 15-m sites were significantly weaker than the other instrument sites (fig. 8). The near-surface currents were predominantly oriented offshore, except at the North 15-m and Central 15-m sites. The near-bed mean currents were also strongest in the central part of the experiment area, at the Central 15-m and South 5-m sites (fig. 9). The dominant near-bed current direction was to the south and onshore at all of the sites except the South 5-m site. This may be the result of the instrument at this site being deployed in a channel where offshore-directed bottom flow may have balanced the wave-driven onshore flow over the adjacent bathymetric highs (fig. 9).
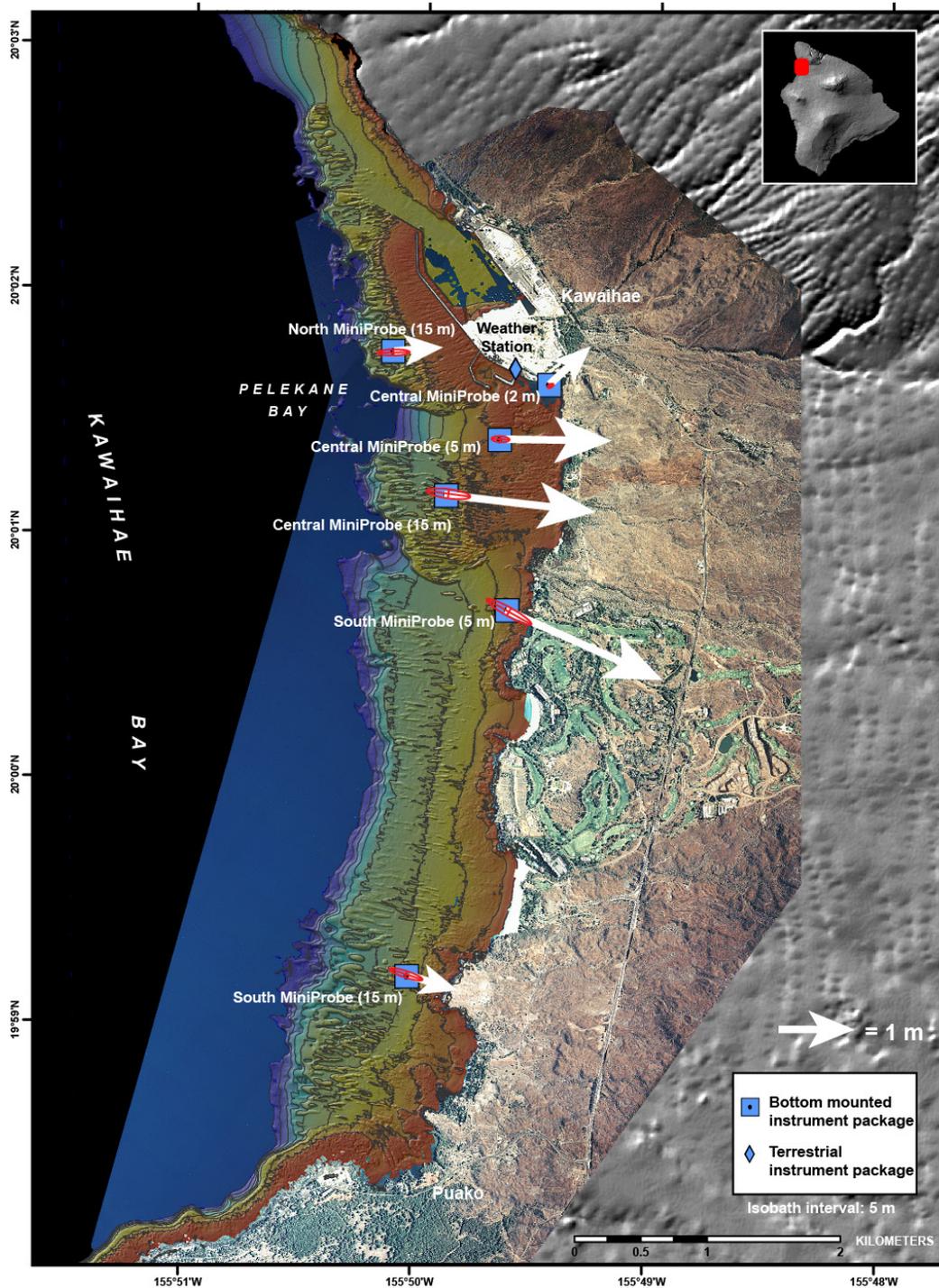
Figure 7. Map showing the mean (white arrows) and variability (red ellipses) of wave directions and heights, in meters, during the 2010–2011 winter experiment for the Central 15-m, Central 5-m, Central 2-m, North 15-m, South 15-m, and South 5-m sites. All of the sites showed a predominant wave direction from the northwest, with the largest wave heights measured in the more-exposed central portion of the bay.
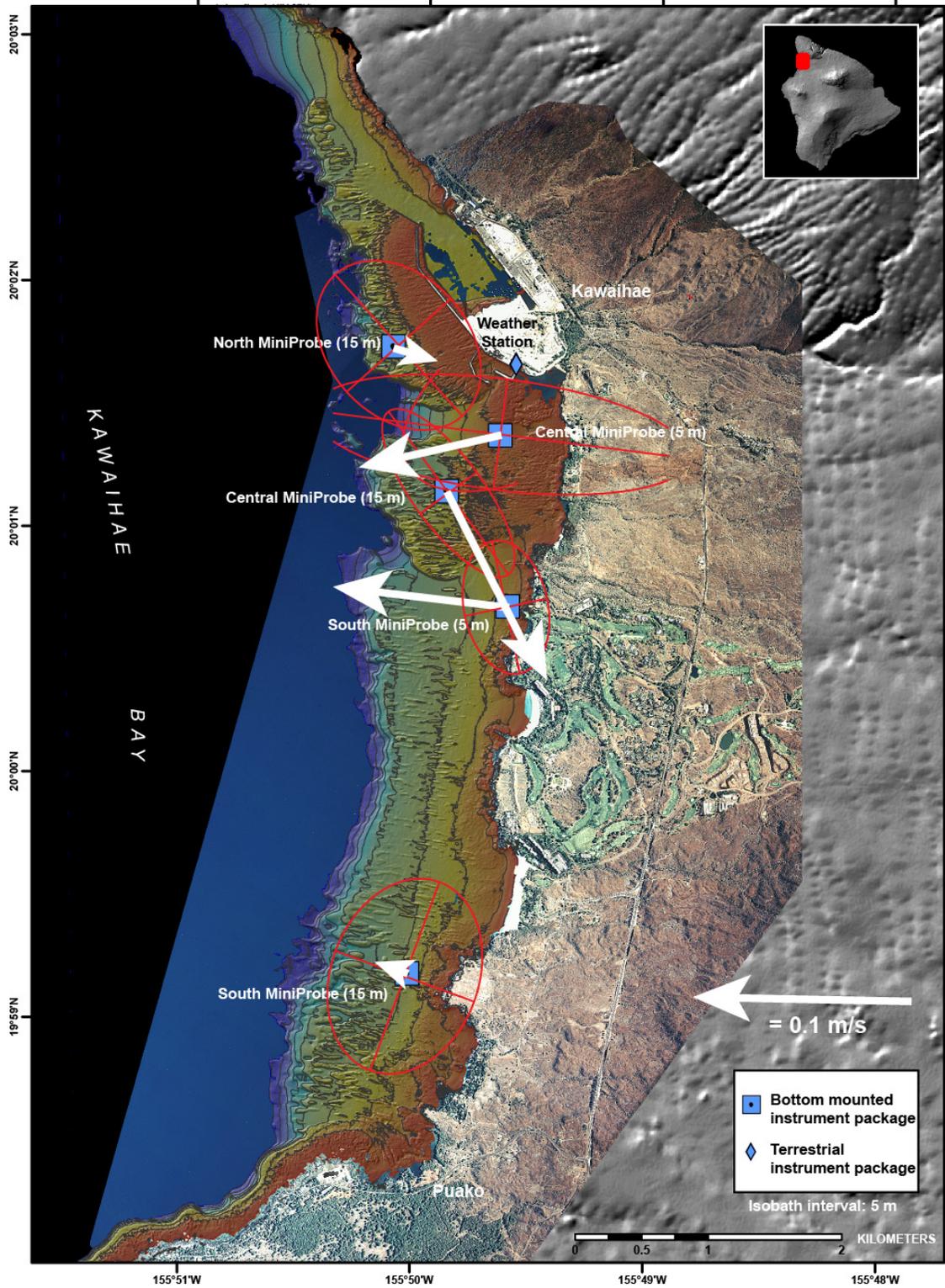
Figure 8. Map showing the mean (white arrows) and variability (red ellipses) of near-surface current directions and speeds, in meters per second, near the surface for the 2010–2011 winter experiment. Currents speeds and directions in the bays varied due to local bathymetry and exposure to wind and waves.
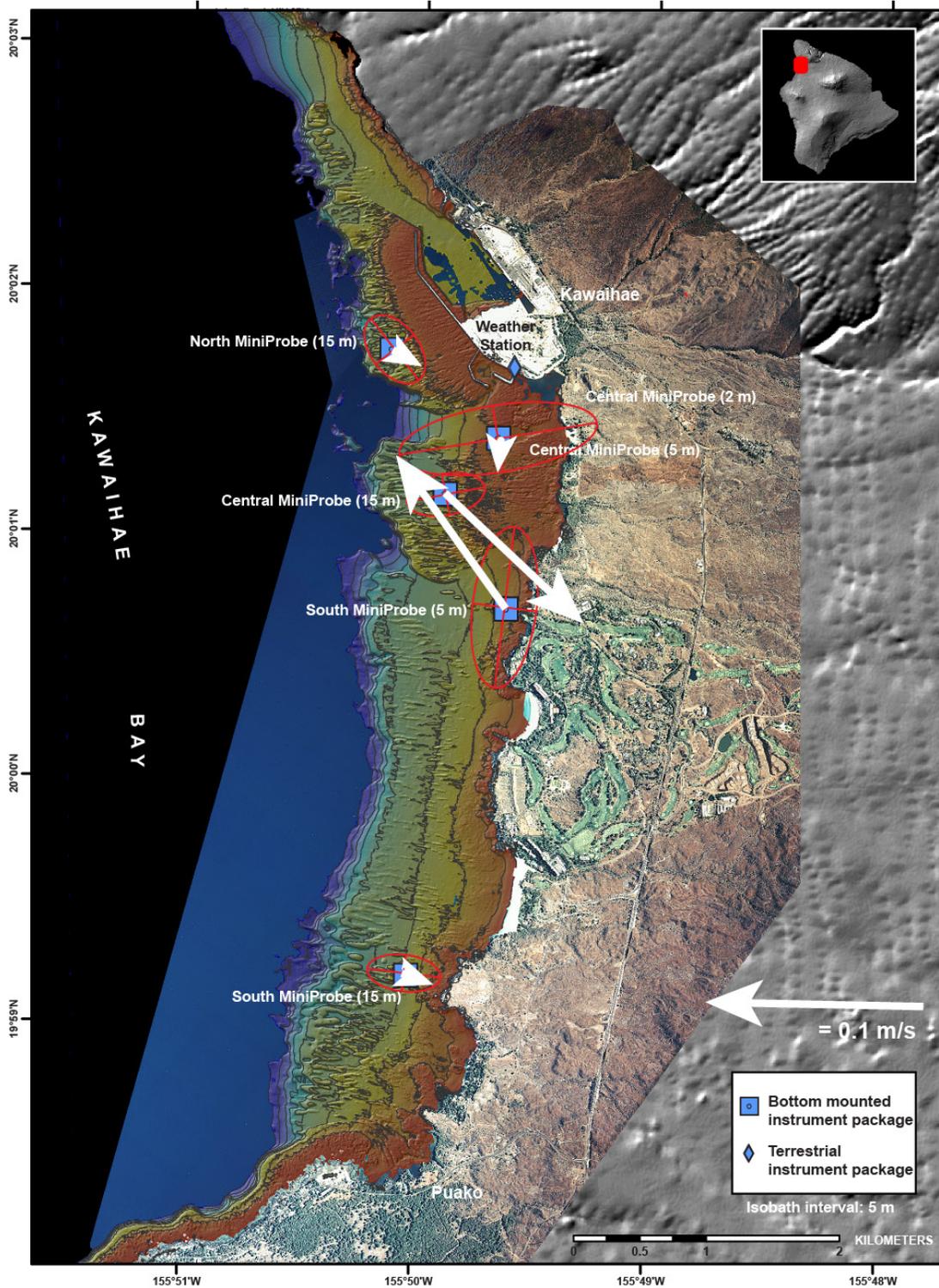
Figure 9. Map showing the mean (white arrows) and variability (red ellipses) of near-bed current directions and speeds, in meters per second, near the bed for the 2010–2011 winter experiment. Near-bed current directions in the bay were variable, with more cross-shore flow than in the near-surface currents. The current speeds were greatest in the more-exposed central part of the bay.
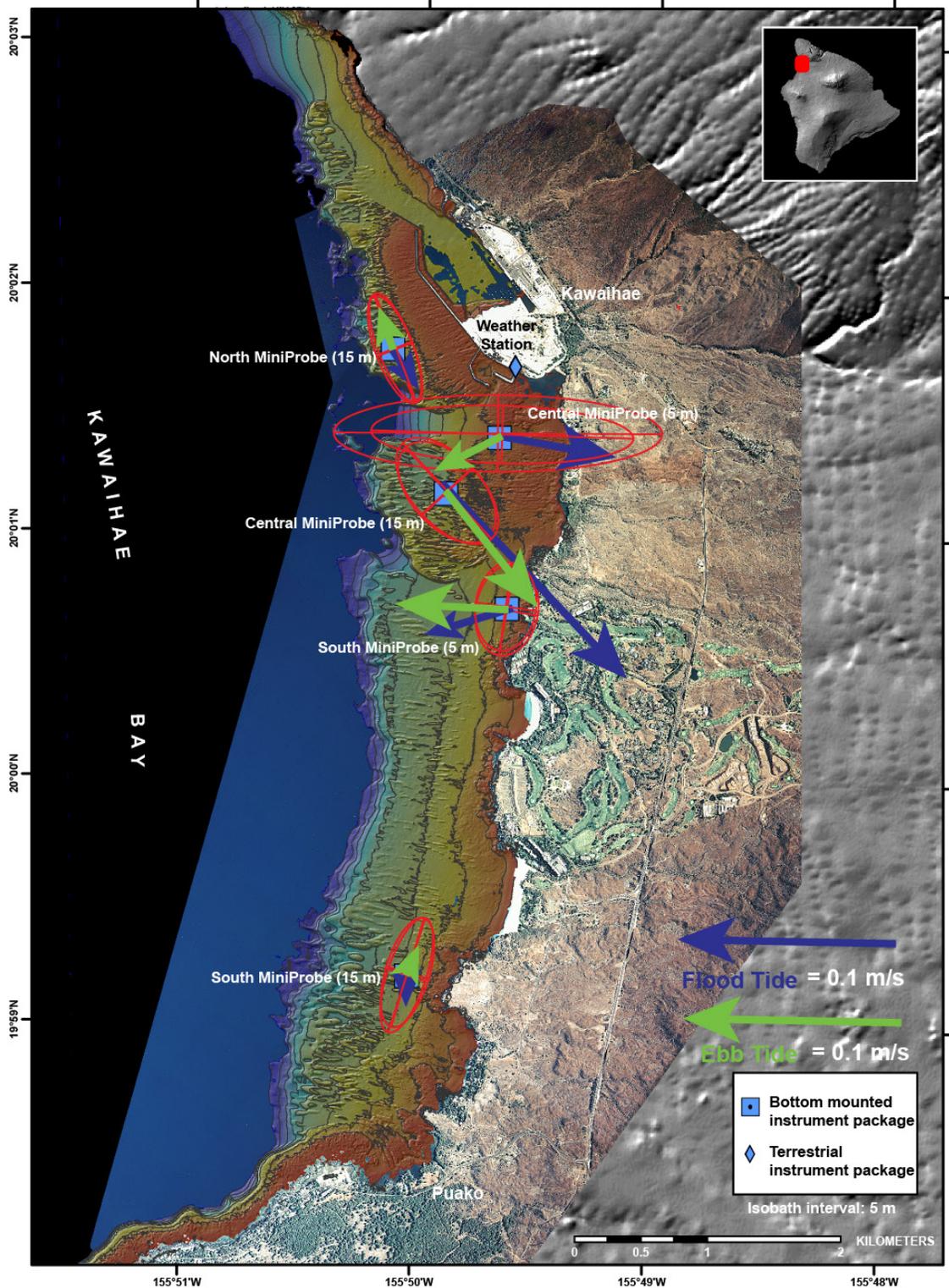
Figure 10. Map showing the mean (blue and green arrows) and variability (red ellipses) of current directions and speeds, in meters per second, during flood and ebb tides for the 2010–2011 winter experiment. Flood-tide current directions (blue arrows) in the bay were predominantly to the south and onshore. Ebb-tide current directions (green arrows) in the bay were more variable.

The tidal currents measured at mid-water depth at the instrument sites also provide insight into the general nature of flow under ebb- and flood-tidal conditions (fig. 10). The flood-tidal currents at all of the instrument sites were primarily to the south and onshore, with speeds of 0.10 m/s or less (fig. 10, blue arrows). The ebb-tidal currents were generally more to the north, offshore, and weaker than the flood-tidal currents (fig. 10, green arrows).

Temporal Variations in Water-Column Properties

The water-column properties that were measured by the CTs and SLOBSs included temperature (ºC), salinity (PSU), and turbidity (NTU). These measurements were made to address the temporal variability in water-column properties during the experiment and to provide additional information about the physical controls on the hydrography of the bays.

Temperature

Water temperatures in Pelekane and Kawaihae Bays ranged from 23.91 to 29.03 °C, with a mean temperature ± one standard deviation of 25.91±0.58 °C (table 9) during the deployment (2010 YD 310–390). On average, the coolest temperatures were at the Central 15-m mooring (depth ~2 m), as it was more exposed to cooler oceanic waters. The warmest average temperatures were measured at the Central 2-m site, which was the shallowest, most restricted location and may have been subject to the greatest solar heating (table 9). The water temperature at all the sites showed daily cooling and heating on the order of 1–2 °C, with the largest variations at the Central 2-m site, and an overall decreasing trend in temperature throughout the experiment (appendix 11.1*A*).

Salinity

Salinity in Pelekane and Kawaihae Bays ranged between 24.99 and 35.21 PSU, with a mean salinity ± one standard deviation of 34.05±0.29 PSU (table 10). The highest average salinity was measured at the Central 15-m mooring, most likely due to the influence of more saline oceanic water (table 10). The lowest average salinity was located at the Central 2-m site, probably due to fluvial discharge (this site was close to Pohaukole Gulch) or submarine groundwater discharge, known to be prevalent in this region (table 10). Overall, the salinity signal was fairly stable throughout the deployment at Central 5-m site, Central 5-m mooring, and Central 15-m mooring, with small, short-lived decreases due to freshwater inputs (appendix 11.1*B*).

Turbidity

Turbidity in the bays ranged between 0 and 1524.30 NTU, with a mean turbidity ± one standard deviation of 8.07±15.59 NTU (table 11). The turbidity statistics were calculated from 2010 Year Day 310–390, omitting days 340–370.5 due to biofouling of the optical sensors or other instrument problems. The mean turbidity and variability were lowest (1.67±2.95 NTU) at the Central 15-m mooring for the deployment period (table 11). The mean turbidity was greatest (20.71 NTU) at the Central 5-m mooring for the deployment period (table 11). Appendix 12.1 shows the time-series plots of turbidity for all of the instruments deployed in Pelekane and

Kawaihae Bays, with the period that was excluded from the statistics due to poor data quality (2010 YD 340–370.5) shaded gray.

Spatial Variations in Water-Column Properties

Spatial variability of water-column properties in Pelekane and Kawaihae Bays was measured using the WCP at the beginning of the experiment on 6 November 2010 (2010 YD 310) and the end of the experiment on 10 March 2011 (2010 YD 434), with cast locations shown in appendix 13.1. The water-column properties that were measured by the WCP included temperature (ºC), salinity (PSU), turbidity (NTU), light transmission (percent) and fluorescence (mg/m^3) as measured by the chlorophyll sensor. The cast location identification information is listed in table 4, and the WCP logs are listed in appendixes 6 and 7. The mean and standard deviation statistics for the measured parameters are listed in tables 12 and 13. The surveys were conducted to place the spatially-limited time-series instrument measurements made at the main study sites in the context of the greater southern Kohala region.

Temperature

The mean temperature in Pelekane and Kawaihae Bays ranged from 26.44 °C to 26.93 °C during the November 2010 survey and from 25.05 °C to 26.50 °C during the March 2011 survey (tables 12 and 13). Overall, the temperatures were warmer in November 2010 than March 2011 due to seasonal cooling through the winter months, which was also observed in the time-series data collected by the CT sensors (appendix 11.1). In November, the warmest and most variable temperatures were located close to shore in Pelekane Bay (appendix 13.2); this area is very shallow and appears to have restricted wave-driven mixing and circulation due to shadowing by the Kawaihae Harbor breakwaters. The coolest temperatures were measured in the southern part of the study area near Puako (appendix 13.2); these cooler temperatures may have been a result of unobstructed mixing with cooler, offshore oceanic waters. The warmest temperatures measured during the March 2011 water-column surveys were located close to shore in Pelekane Bay (appendix 13.3). Temperatures were cooler in the southern part than the northern part of the study area; the coolest temperatures were measured in the southern part of the study area during the March 2011 survey (appendix 13.3).

Salinity

The mean salinity in Pelekane Bay and the surrounding area ranged from 33.80 to 35.09 PSU during the November 2010 survey and from 33.73 to 34.60 PSU during the March 2011 survey (tables 12-13). Overall, the salinity values were lower during the March 2011 survey, likely due to increased surface runoff and/or submarine groundwater discharge resulting from rainfall over the winter. The spatial variability in salinity during the November 2010 survey showed the lowest salinity values close to shore in Pelekane Bay near Pohaukole Gulch (appendix 13.4). Outside of this area, the salinity was fairly uniform, with higher salinities and low variability up and down the coast, except near Honokoa Gulch just to the north of Kawaihae Harbor, which was discharging water and sediment during this survey. The spatial variability during the March 2011 survey also showed the lowest salinities near the shore in Pelekane Bay, where the Pohaukole stream discharges (appendix 13.5).

Turbidity

The mean turbidity in Pelekane Bay and the surrounding area ranged from 0.40 to 4.72 NTU during the November 2010 survey and from 0.32 to 20.24 NTU during the March 2011 survey (tables 12-13). Although the mean turbidity values during the November 2010 and March 2011 surveys were greater close to shore in Pelekane Bay, overall the mean turbidity values were generally low in the surrounding area (appendixes 13.6 and 13.7).

Turbidity in Pelekane Bay was also measured in percent light transmission, with higher percentages indicating clearer water and lower percentages indicating more turbid water. The mean percent light transmission in Pelekane Bay ranged from 69.86 to 96.51 percent during the November 2010 survey and from 44.79 to 96.13 percent during the March 2011 survey (tables 12 and 13). The lowest light transmission (or most turbid water) measured was located inshore in Pelekane Bay for both the November 2010 and March 2011 surveys (appendixes 13.8-13.9). The slightly lower mean percentages during the March 2011 surveys may have been a result of the input of terrigenous sediment during the November 2010 flood (which occurred after the November 2010 WCP measurements).

Fluorescence

The mean values of fluorescence in Pelekane Bay ranged from 0.56 to 1.96 mg/m^3 during the November 2010 survey and from 0.19 to 1.77 mg/m^3 during the March 2011 survey (tables 12 and 13). Fluorescence was highest and most variable close to shore during both surveys and generally near areas of infrastructure and freshwater input. Overall, the November 2010 survey had more areas of higher fluorescence, potentially due to land-derived inputs of nutrients. The spatial variability in fluorescence during the November 2010 survey showed elevated fluorescence in areas off the potential point sources of Honokoa Gulch and Pohaukole Gulch, and off Kaunaoa Beach to the south of Pelekane Bay (appendix 13.10). The fluorescence values generally decreased with distance from shore and away from gulches or stream mouths. The spatial variability in fluorescence during the March 2011 survey showed elevated fluorescence near Pelekane Bay and off Kaunaoa Beach to the south of Pelekane Bay (appendix 13.11). The fluorescence quickly decreased to the south, away from the stream input. The rest of the study area was characterized by low fluorescence both close to shore and farther offshore (appendix 13.11).

Seabed and Sediment Trap Grain Size, Composition, and Collection Rates

The simple tube trap (STT) average trap collection rates ranged from 156.70 milligrams per cubic centimeter per day (mg/cm^2/d), at the mouth of Pelekane Bay (Central 2-m site), to 537.24 mg/cm^2/d, at the South 5-m site (table 14). Although the Central 2-m site had the lowest average trap collection rate, the material collected in the trap was predominantly mud-sized (silt+clay) material by mass (93.29 percent, fig. 11, table 15); this sediment was composed of almost exclusively (93.28 percent) terrigenous material (fig. 12, table 15). The other STTs collected predominantly carbonate (76.01–94.31 percent), sand-sized (80.74–95.59 percent) material by mass (table 15). The south 5-m site off Waiulaula Gulch had the second-highest percentage of terrigenous material by mass (23.99 percent)—after the Central 2-m site at the

mouth of Pelekane Bay—showing a clear relationship between the terrigenous component of the sediment in the near-bed water column to the proximity of onshore sediment sources (for example, Pokuhoale and Waiulaula Gulches).

The mean trap accumulation rates at the rotary sediment trap (RST) ranged from 0.01 mg/cm^2/d, just before the small-wave event and November 2010 flood (2010 YD 319–323), to 12.91 mg/cm^2/d during the large-wave events in January 2011 (YD 2010 380–390), as shown in figure 13 and tables 14 and 15. The sediment collected in the RST was primarily terrigenous clayey silt of volcanic origin in the first half of the deployment, becoming coarser and predominantly carbonate in origin by the end of the deployment; these trends were more rapid during the large-wave events in January 2011.

The seabed samples collected from the instrument sites in March 2011 at the end of the experiment were predominantly sand-sized material by mass (fig. 14, tables 16 and 17). The sediment composition at the instrument sites was also predominantly carbonate (>90 percent), except at the Central 2-m and South 5-m sites, where the composition was approximately half terrigenous and half carbonate (fig. 15, tables 16–17). Similar to the sediment trap samples, the large percentage of terrigenous material at these two sites was likely due to their proximity to terrestrial sediment sources. Overall, the seabed samples had a higher percentage of sand-sized carbonate sediment than the trap samples. This may have been a result of the timing of the sample collection after the large-wave events in January 2011, which likely resuspended the fine, silty, terrigenous sediment deposited in Pelekane Bay during the November 2010 flood and advected it out of the bays.
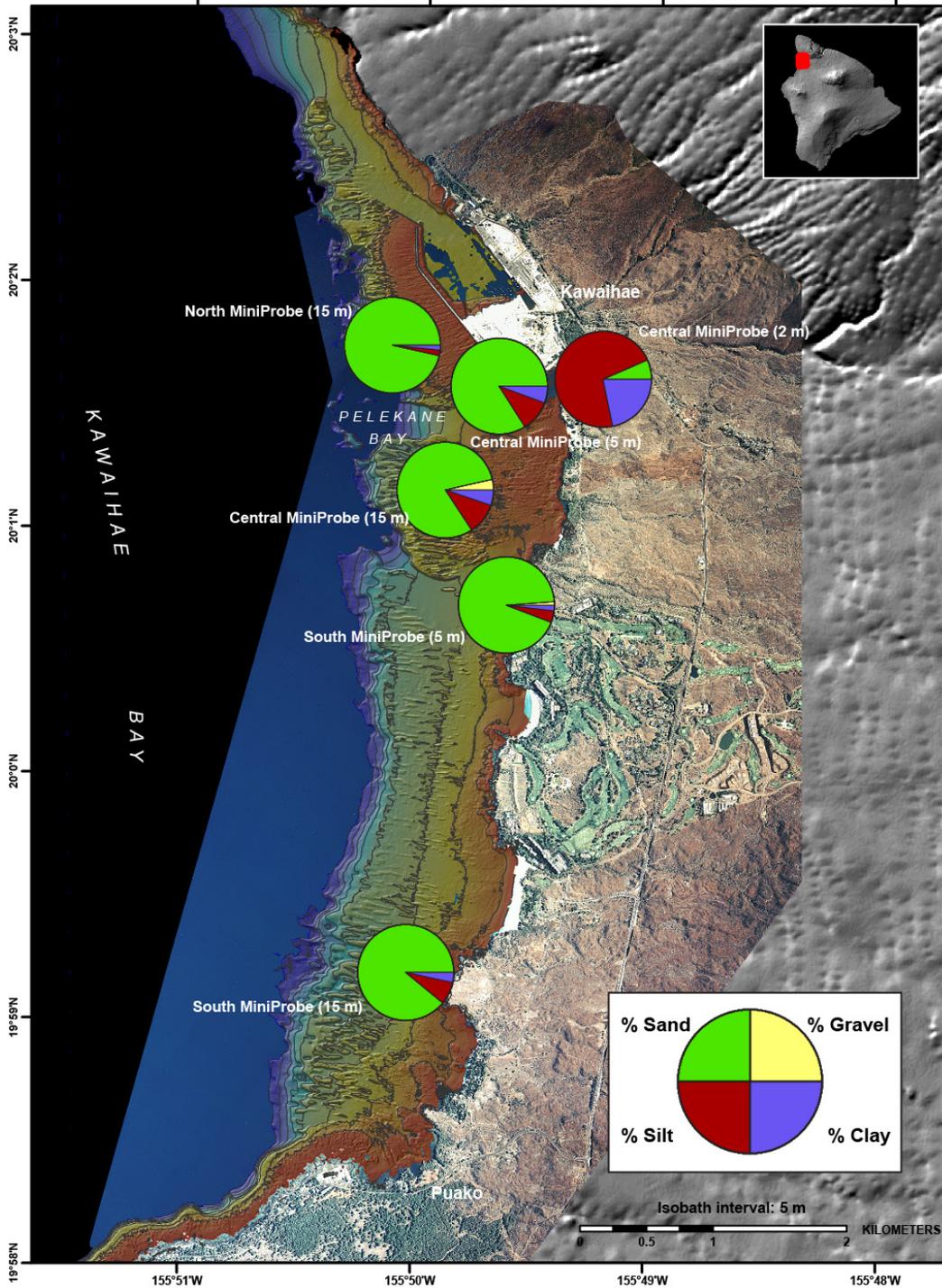
Figure 11. Map showing the spatial variability of sediment grain size collected by the simple tube traps (STTs) at the instrument sites. The STTs primarily collected sand-sized material except at the Central 2-m site, at the mouth of Pelekane Bay, which was primarily mud (silt and clay).
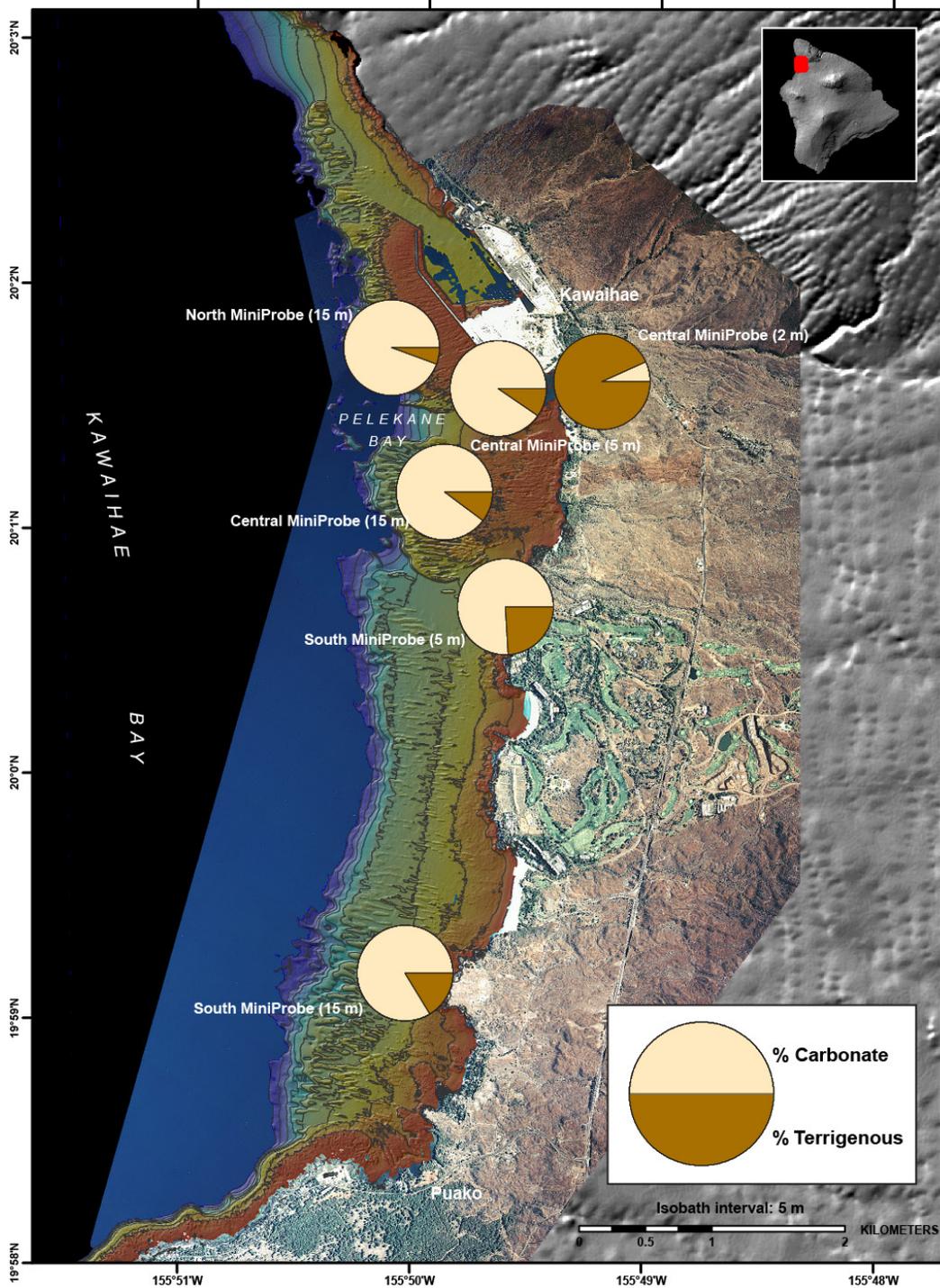
Figure 12. Map showing the spatial variability of sediment composition collected by the simple tube traps (STTs) at the instrument sites. The STTs primarily collected carbonate material except at the Central 2-m site, at the mouth of Pelekane Bay, which was primarily terrigenous material. Although the South 5-m site off Waiulaula Gulch was predominantly carbonate material, it had almost twice the percentage of terrigenous material as the rest of the sites (except for the Central 2-m site).
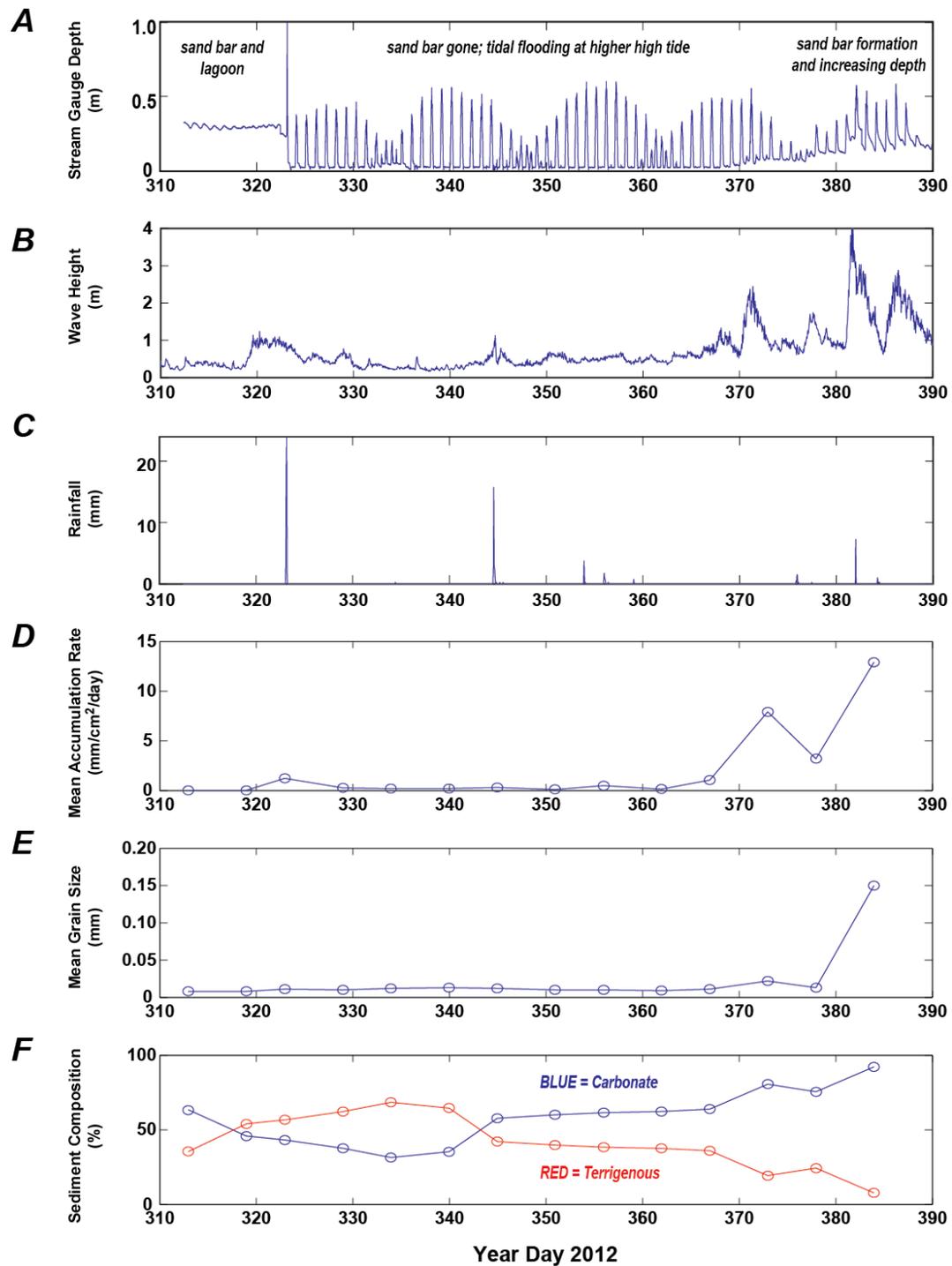
Figure 13. Time-series plots of weather and hydrologic data in Pelekane Bay (various instrument sites, as noted) and the corresponding data from the rotary sediment trap (RST) at the Central 5-m site. *A*, Stream gage depth, in meters. *B*, Wave height, in meters, measured at the Central 15-m site. *C*, Rainfall, in millimeters per 25 minutes, measured at the weather station. *D*, Mean accumulation rate of material collected in the RST, in milligrams per square centimeter per day. *E,* Mean grain size, in millimeters, of material collected in the RST. *F*, Bulk composition of material collected in the RST, in percent by mass, with red and blue denoting the terrigenous (volcanic) and carbonate material, respectively. The November 2010 flood was concurrent with an increase in trap accumulation and finer-grained terrigenous material collected in the RST; during the January 2011 large-wave events there were much higher trap accumulation rates of coarser-grained carbonate sediment than following the flood.
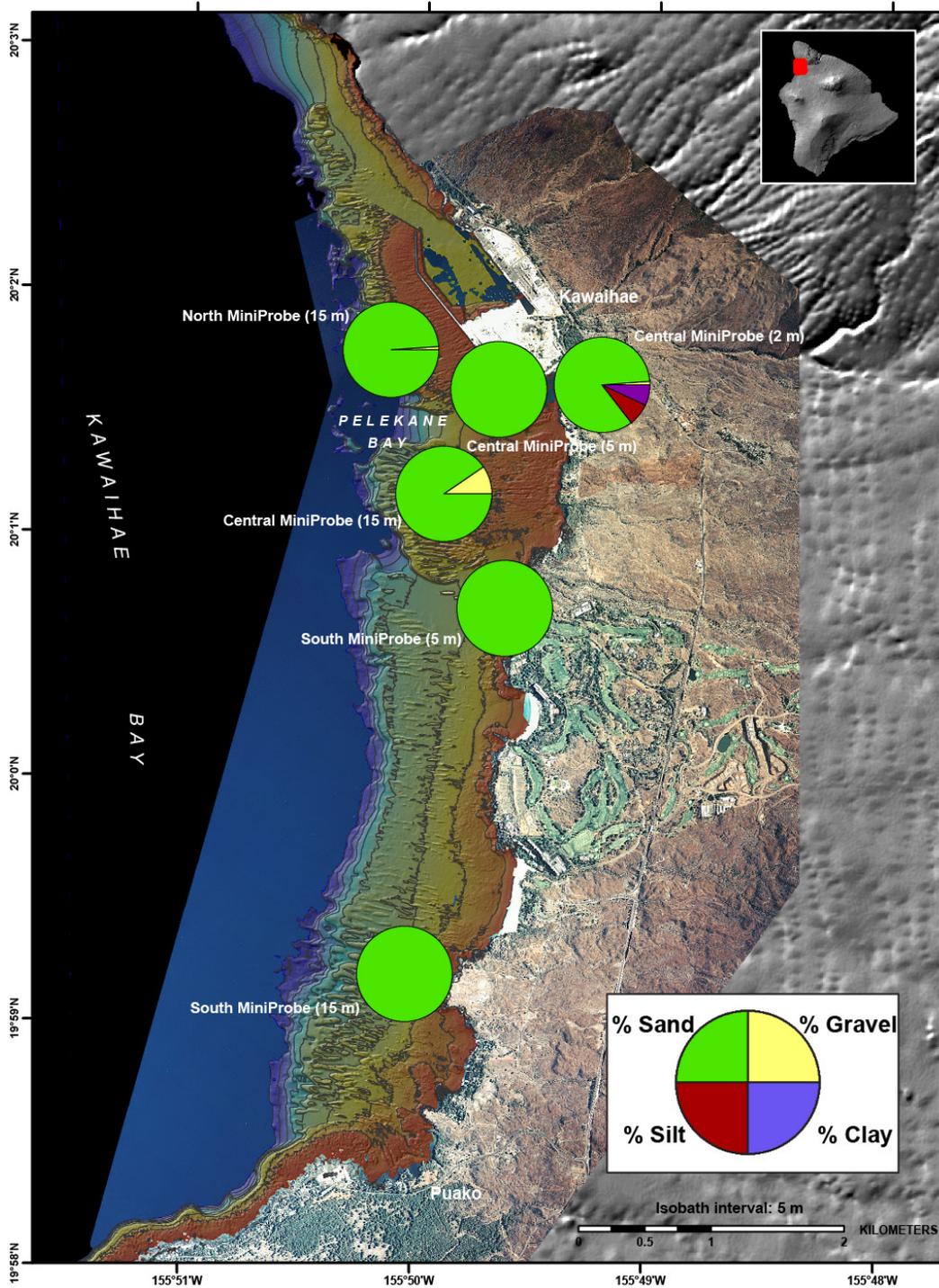
Figure 14. Map showing the spatial variability of mean sediment grain size on the seabed at the instrument sites, March 2011. All of the seabed samples collected from the instrument sites were predominantly sand-sized, except for the small percentages of silt and clay at the Central 2-m site.
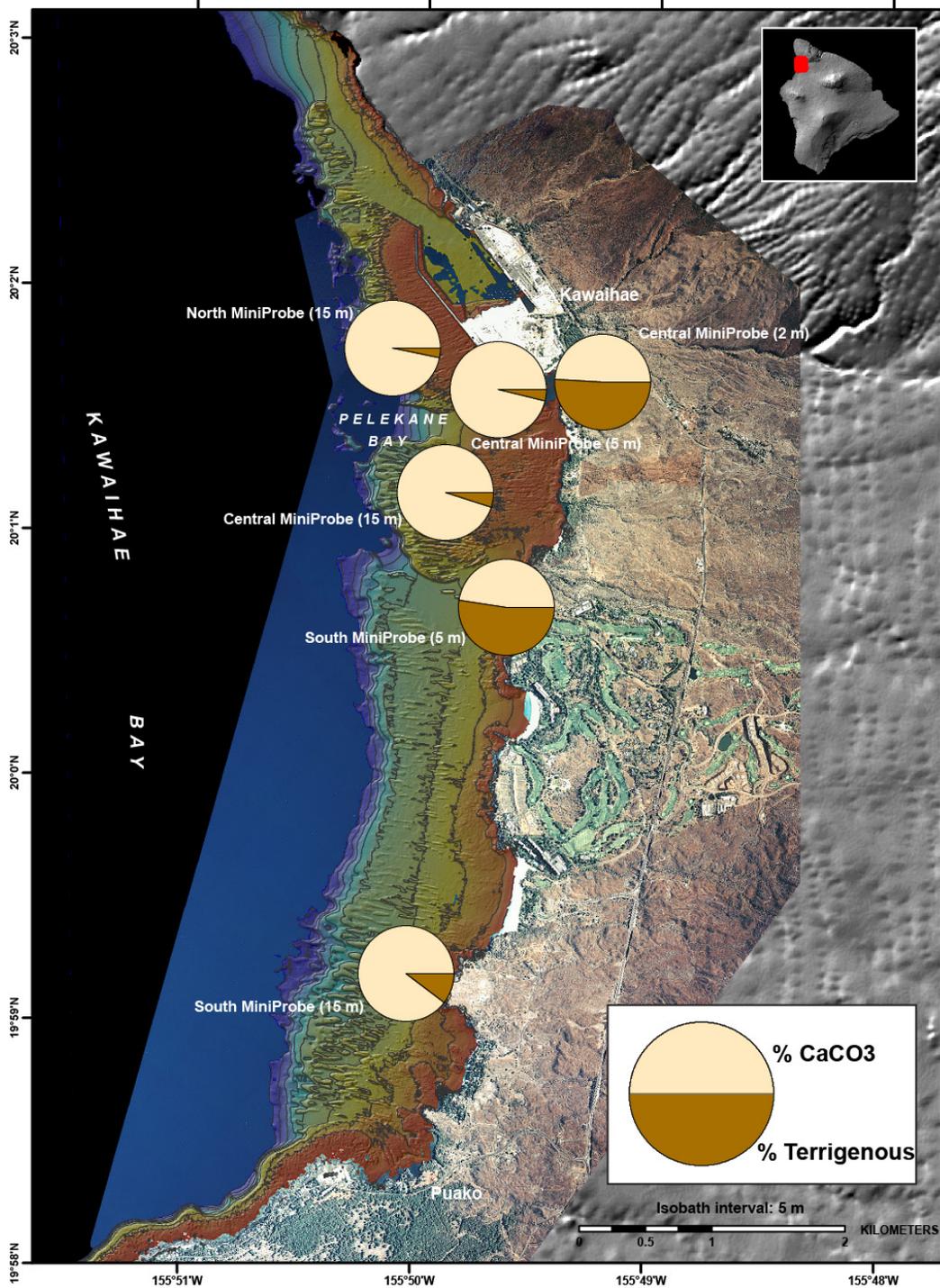
Figure 15. Map showing the spatial variability of sediment composition on the seabed at the instrument sites. The composition of the seabed samples was predominantly carbonate, with the exception of Central 2-m site and South 5-m site. This may be a result of their proximity to onshore terrestrial sediment sources.

Topographic/Bathymetric Survey of Pelekane Bay

In order to visualize the changes in elevation between the 1928 and 2011 surveys, contour lines at 0.25-m intervals were generated. Since the resolution of the historical 1928 survey was ±1/6 fathom (±1 ft or ±0.3 m), the error of measure is ±0.3 m. To accommodate this error for visualization, the range of change in depth between -0.25 and +0.25 m was colored green on the map to acknowledge that changes in this range are within the error of measurement (fig. 16). A gain in elevation implies net sedimentation on the seabed; a decrease in elevation implies erosion between the surveys. Based on the range in survey and datum error, overall the bay became 0.41 m to 0.61 m shallower, due to the accumulation of 22,500 to 37,500 m^3 of sediment above the sea floor mapped in the historical 1928 survey.
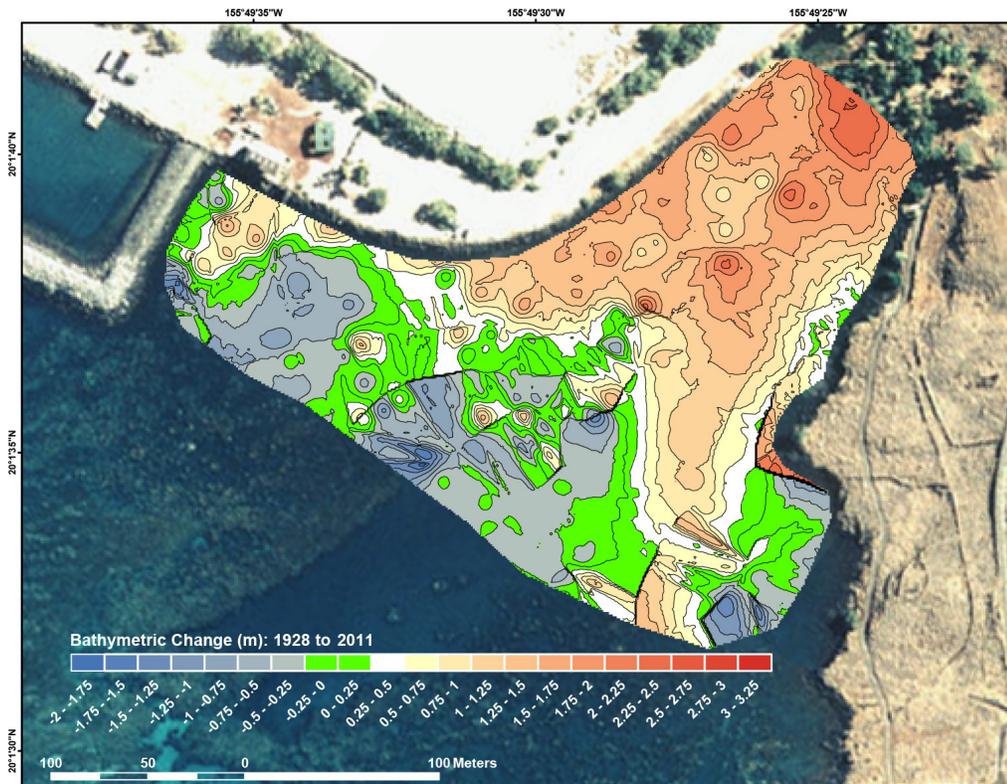
Figure 16. Map of bathymetric change, in meters, in Pelekane Bay between 1928 and 2011. The red colors denote areas that became shallower due to sediment accumulation, and the blue colors denote areas that became deeper due to erosion. Areas colored green represent depth changes between -0.25 m and +0.25 m, which are within the error of measurement and thus potentially not real.

Sedimentation Rates in Pelekane Bay

In Pelekane Bay sediment, the down-core distribution of excess ^{210}Pb ($^{210}Pb_{xs} = {}^{210}Pb_{tot} - {}^{214}Pb$) followed exponential decreases (fig. 17) below the bioturbated layer (depths >10–15 cm). Bioturbation effectively mixes all geochemical signals; the onset of burial or accumulation, t_0, must consequently be defined to the bottom of this biologically mixed layer. Such $^{210}Pb_{xs}$ profiles can be interpreted by a steady-state advection-decay model, assuming that fluxes of sediment and ^{210}Pb are constant at a given location. Thus, influx of $^{210}Pb_{xs}$ by precipitation at the
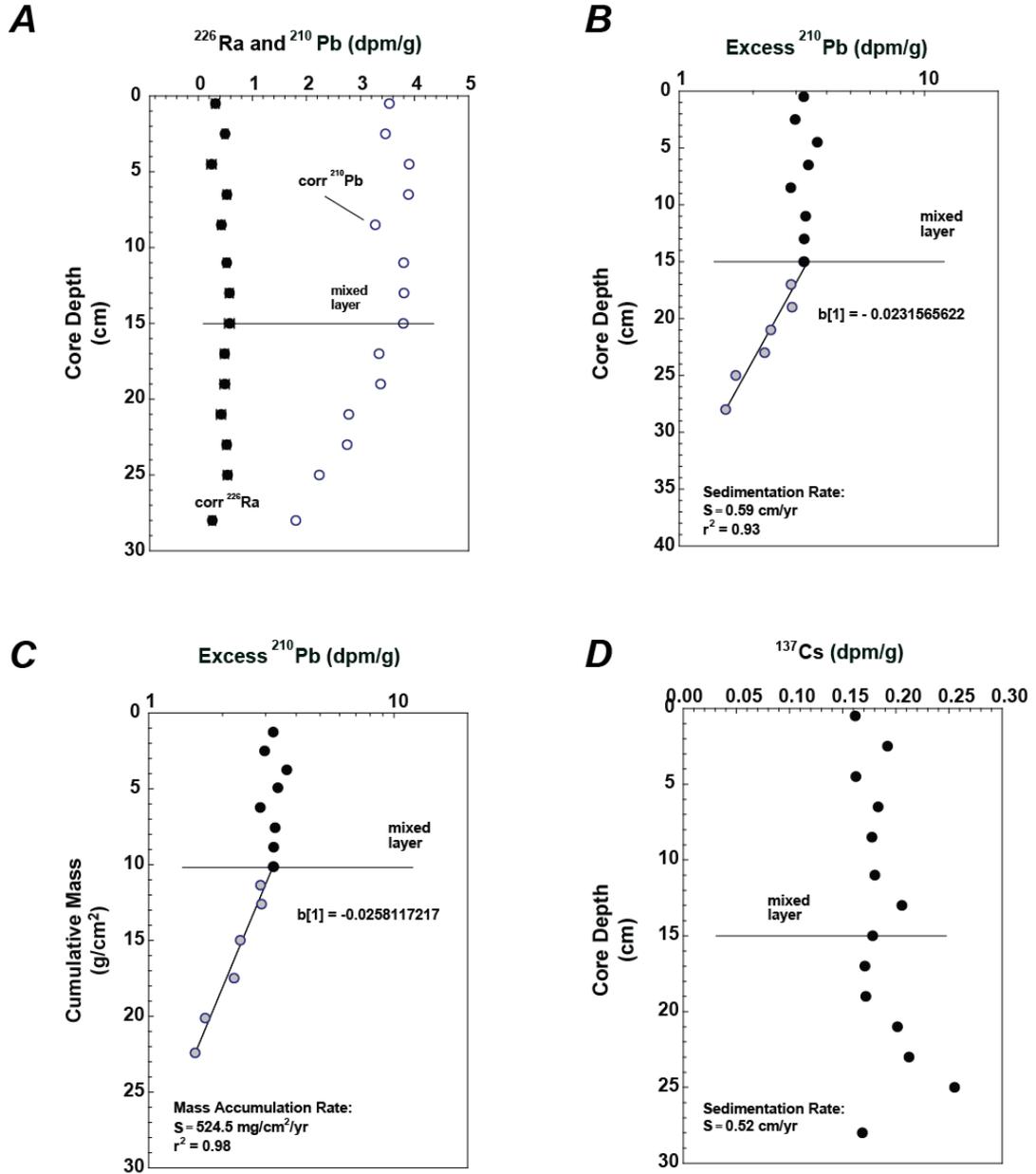
Figure 17. Plots showing down-core profiles from core PC3 of *A*, [226]Ra and total [210]Pb. *B*, Excess ^{210}Pb as a function of linear depth, and the best-fit line, corresponding to sedimentation rate, which is represented by the slope, S, given in centimeters per year (cm/yr). *C*, Excess ^{210}Pb as a function of cumulative depth, and the corresponding best-fit line, corresponding to a mass accumulation rate, represented by the slope, S, given in milligrams per square centimeter per year (mg/cm^{2}/yr), and *D*, [137]Cs.

sediment/water interface must be balanced by radioactive decay following deposition and burial. The down-core distribution of $^{210}Pb_{xs}$ must therefore be invariable with time and can be described as:

$$(^{210}Pb_{xs})_z = (^{210}Pb_{xs})_0 \, exp^{(-\lambda/S)},$$

where $(^{210}Pb_{xs})_0$ and $(^{210}Pb_{xs})_z$ are excess ^{210}Pb activities at the sediment/water interface and at some depth z, respectively, λ is the ^{210}Pb decay constant (0.03114/yr), and S is the sedimentation rate. The slope of a regression line ($-\lambda/S$) defines either a linear sedimentation rate (cm/yr) or a mass accumulation rate (g/cm^2/yr), depending on whether an apparent depth (cm) or a cumulative mass (g/cm^2) is used as the depth variable. The radionuclide data were also modeled using the classic constant rate of supply (CRS) age model, following Appleby and Oldfield, 1978 (table 18). The age models produced using these two approaches yielded consistent results.

Activities of the radionuclides are reported in disintegrations per minute per gram, dpm/g, where 60 dpm = 1 Becquerel (Bq) = 27.027 pCi. Activities of ^{226}Ra were generally low (<1 dpm/g) and did not change dramatically either down-core or from one core to the next. In contrast, corrected total ^{210}Pb activities were typically about 3–4 dpm/g or more in the upper-most sediment layers, and then decreased systematically to background (thus, ^{226}Ra) values at depth. Bomb-produced ^{137}Cs activities were usually low (<0.3 dpm/g), but did show a defined subsurface peak in some cores that could be used to develop a secondary geochronology. ^{7}Be has a high affinity for aerosols and is thus delivered to the Earth's surface via wet and dry deposition. In aqueous environments, it becomes quickly associated with particles and colloids by cation exchange reactions. Because of this rapid scavenging of ^{7}Be onto particle surfaces once introduced into aqueous environments, this radioisotope may be useful for assessing particle movement, including deposition and resuspension. In Pelekane Bay, where annual rainfall rates are very low, ^{7}Be activities in the surface sediment were expectedly low and did not reveal clear systematic trends (fig. 18).
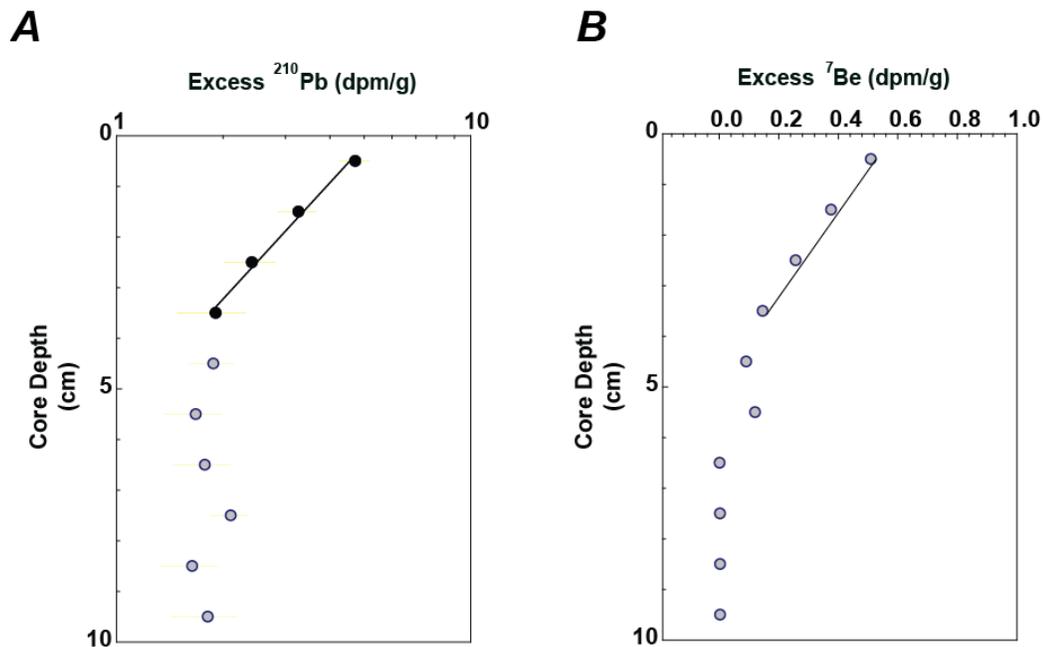
Figure 18. Plots showing down-core profiles of excess ^{210}Pb and ^{7}Be from core SC7.

In Pelekane Bay sediment, ^{210}Pb-based sedimentation rates (PC3 = 0.59 cm/yr) agree reasonably well with those estimated from the subsurface ^{137}Cs peak (1963–1964; 0.52 cm/yr), and the penetration depth of ^{137}Cs (1950s) was beyond the bottom of the sediment column collected in core PC3. The mass accumulation rate of core PC3 was 524.5 mg/cm^2/yr (fig. 17C).

This suggests that in Pelekane Bay, sediment profiles of such particle-reactive radionuclides as ^{210}Pb and ^{137}Cs are controlled principally by syndepositional processes and that post-depositional processes (for example, reversible sorption, redox-mediated transport, preferential mobility) are less important. These physio-chemical processes do not rule out biologically mediated post-depositional transport in the upper sediment column since the upper 10-15 cm of the ^{210}Pb profiles suggest active bioturbation.

Radionuclide inventories per whole core (dpm/cm^2) can be computed using the cumulative mass depths, and when assessed against local atmospheric fallout rates, can provide an estimate of sediment focusing or winnowing. Here, as sediment resuspension was event driven by the recurring tsunami waves, the radionuclide inventories can be used to determine tsunamigenic resuspension and sediment movement.

Various components of sedimentary carbon in core PC3 are shown in Figure 19. Of note is that the total carbon (TC) content was elevated for such an arid coastal system and likely reflected recent high watershed inputs. While the down-core TC profile varied consistently between 6 and 7 percent, the total inorganic carbon (TIC) and total organic carbon (TOC) components fluctuated with depth. TOC was maintained at about 5 percent beyond a depth of 30 cm, while at those depths, the TIC decreased to less than 2 percent. Percent calcium carbonate (CaCO$_3$) followed the down-core profile of TIC and ranged between 15 and 30 percent.
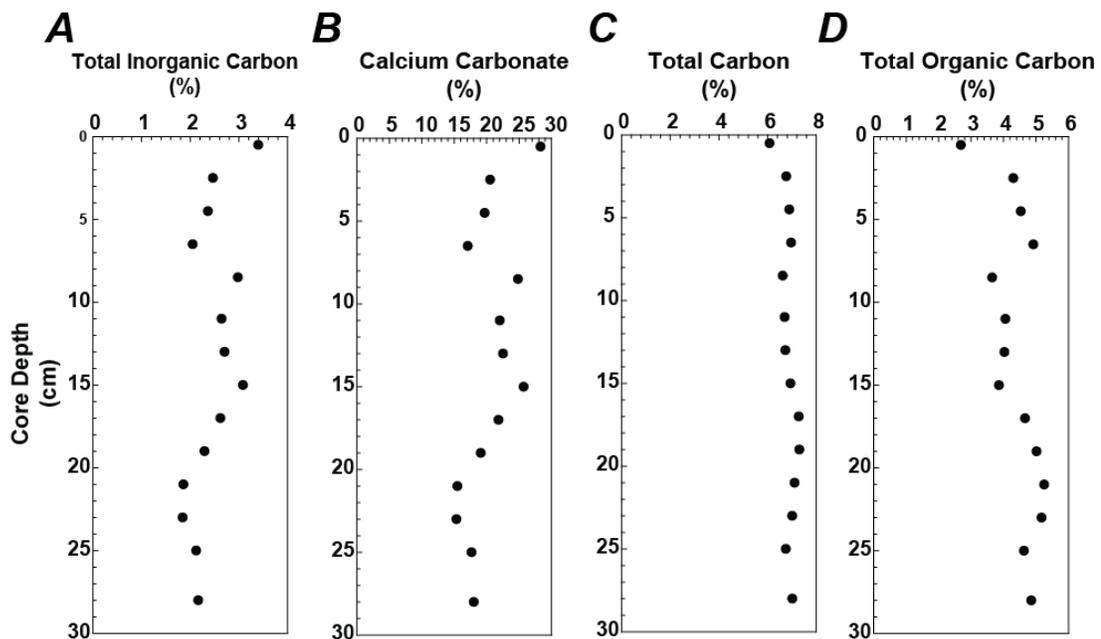
Figure 19. Plots showing down-core profiles from core PC3 of *A,* Percent total inorganic carbon (TIC). *B,* Percent carbonate. *C,* Percent total carbon (TC). *D,* Percent total organic carbon (TOC). Note that total carbon (TC) in core PC3 exceeds 6 percent, which is surprisingly high for such a dry coastal system.

Electrical Resistivity Values in Pelekane Bay

Two-dimensional (2D) electrical resistivity surveys were conducted to estimate the subsurface electrical resistivity distribution along the survey lines. Each measurement requires electrical current to be injected into the sediment through two current-producing electrodes while voltage readings are conducted at two potential electrodes spaced at some variable distance down

the cable. An apparent resistivity is then calculated using the injected current, the measured voltage, and a geometric factor defined by the electrode arrangement (in this case, dipole-dipole). The maximum exploration depth for this technique depends on the spacing of the current-injecting electrodes. Sampling different depths is accomplished by changing the electrode spacing. Individual measurements are taken along a survey line using pre-determined combinations of electrodes and spacings to produce a cross section of apparent resistivity. Apparent resistivity is an averaged value with contributions from both horizontal and vertical directions.

Apparent resistivity data are then inverted into an electrical resistivity model that increases the resolution and allows interpretation of the subsurface structure and stratigraphy (de Groot-Hedlin and Constable, 1990; Oldenburg and Li, 1999; Loke, 2001). Many factors, including the sediment type, the amount of water in the subsurface, and the salinity of the pore fluid, affect the apparent resistivity. Electrical resistivity inversion models are used to identify, delineate, and map subsurface features such as electrically conductive contamination plumes, bedrock fracture zones, the saltwater/freshwater interface, the vadose zone, and electrically conductive lithologic units such as clays and silts (Behiry and Hanafy, 2000; Benson and others, 1997).

Electrical resistivity is reported here in Ohm-meters (Ω•m). In all but one of the 8 lines collected from Pelekane Bay, values of apparent electrical resistivity were typically less than 10 Ω•m, except for the most landward Line 5, where values ranged up to approximately 25 Ω•m (fig. 20). Such resistivity values are indicative of mixed lithologies (Swarzenski and others, 2009; Dimova and others, 2012). Based on the 8 resistivity lines collected in Pelekane Bay, values of apparent electrical resistivity typically increased with depth, while the sharpest contact appeared at about 13 m below the sediment surface. This electrical-resistivity contact possibly defines a transition from volcanic basement rock to the overlying carbonate reef structure (figs. 20–21).

Discussion

The winter 2010–2011 experiment conducted by the USGS in Pelekane and Kawaihae Bays coincided with three different sets of meterologic and oceanographic forcing conditions that characterize sediment dynamics on many Hawaiian fringe reefs: trade-wind conditions, a heavy rainfall event that generated a flood, and large-wave events (for example, Storlazzi and Jaffe, 2008). The TIS and CIS captured these events qualitatively from above and below the water surface, respectively, providing a visual photographic context (figs. 22–23) to the time-series instrument data. Trade winds, terrestrial flooding, and large-wave events are all important controls on circulation and sediment dynamics in the bays.

Trade Winds

Trade-wind conditions in the Hawaiian Islands occur approximately 50 percent of the time during the winter months and are characterized by consistent winds from the northeast at 5–10 m/s, stable weather patterns and barometric pressure, and little rainfall (Moberly and Chamberlain, 1964). The winds in Pelekane and Kawaihae Bays, as measured by the USGS weather station, generally showed wind speeds on average of 3–5 m/s from the northwest
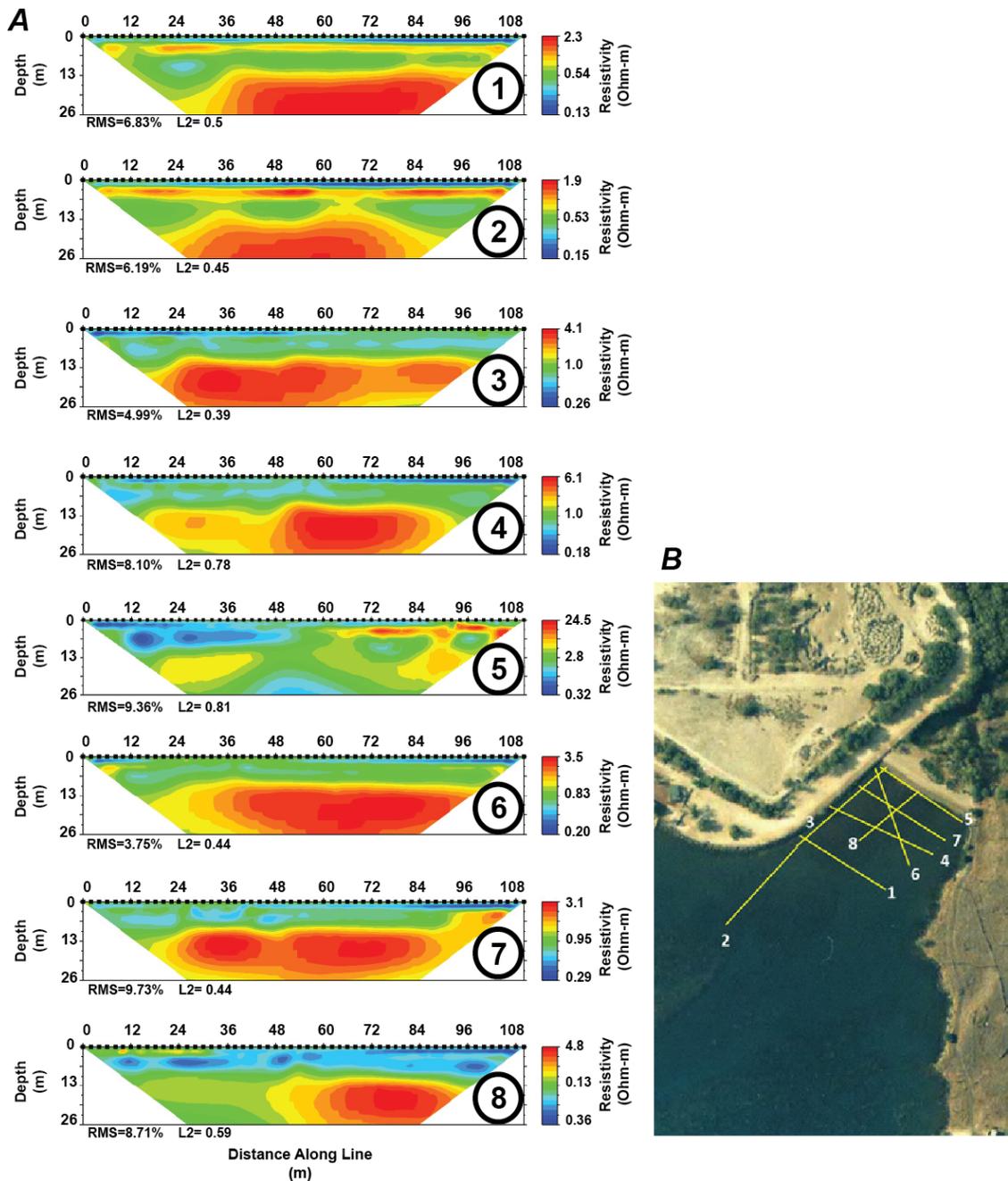
Figure 20. View of the electrical resistivity lines in Pelekane Bay. *A*, Cross-sectional plots of all 8 multi-channel electrical resistivity lines from Pelekane Bay. *B,* Inset photograph showing numbered locations of electrical resistivity lines in Pelekane Bay. A resistivity value, given in Ohm-meters (Ohm-m) reflects both pore fluid and sediment resistivity and is affected by such physical parameters as porosity and temperature. Hotter colors indicate more resistive values, which correspond to lower porosity and colder temperatures (note that the resistivity scale was maximized for each image). Several lines show a sharp electrical resistivity contact at a depth of about 13 m, which may represent the transition from the volcanic basement rock to the overlying carbonate reef structure.

Resistivity (Ohm-m)

| 0.135 | 0.37 | 1.00 | 2.72 | 7.39 | 12.18 |
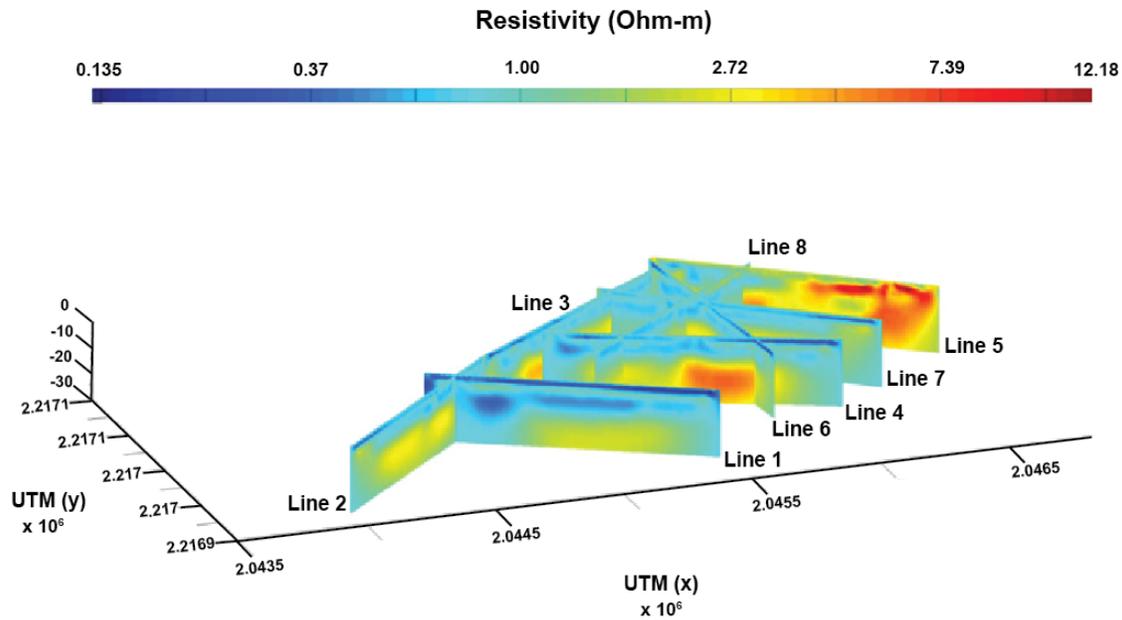
Figure 21. Plot showing a pseudo-three dimensional rendering of the 8 resistivity lines, normalized to a single color scale. The horizontal scale is expressed as Universal Transverse Mercator (UTM) easting (x) and northing (y) coordinates; the vertical scale is depth in meters, where zero is the surface. The volcanic bedrock that outcrops on the northeastern corner of the bay is clearly evident in the hotter colors of Line 5. From these resistivity lines, a shallow transition zone that separates finer from coarser material appears to be approximately 2–3 meters thick, although the resolution of the 56-electrode cable makes it difficult to obtain more quantitative estimates.

direction. These northwesterly winds, divergent from the regional northeasterly winds, were likely due to the orographic steering of the air around Kohala Volcano. Two time periods, 2010 YD 317–320 (before the flood) and 2010 YD 340–360 (after the flood), showed consistent winds from the northwest, small waves, and stable barometric pressure; these time frames were used to examine currents, turbidity, critical shear stresses, and sediment flux during trade-wind conditions (figs. 5 and 6).

The near-surface current speeds and directions measured by the instruments showed stronger currents at the Central 5-m, South 5-m, and Central 15-m sites than at the North 15-m and South 15-m sites (fig. 24). The near-surface currents were faster and directed to the southeast in the central part of the bay (Central 15-m and Central 5-m sites), although rarely exceeding 0.05 m/s, and were to the north-northeast and slower at the North 15-m and South 15-m sites. The near-bed currents at the instrument sites had current speeds and directions similar to those near the surface, suggesting little vertical velocity shear through the water column, likely in part due to the weak wind forcing and slow currents (fig. 25).

The turbidity levels at the instrument sites during trade-wind conditions were, on average, the lowest for any period during the entire experiment. The highest mean turbidity during the trade-wind period (1.65 NTU) was measured at the Central 5-m MP (table 11). This was expected, as its location was near the seabed and closest to the area of terrigenous sediment accumulation in Pelekane Bay offshore from Pohaukole Gulch. The lowest mean turbidity values were measured at the Central 15-m mooring. This was also expected, as it was deployed approximately 2 m below the surface in clear water and away from possible terrestrial sediment sources (appendix 12).

Figure 22. Photographs from the Terrestrial Imaging System (TIS) showing surface conditions in the study area. *A,* Pre-flood trade-wind conditions. *B,* Flood conditions in November 2010. *C,* Post-flood trade-wind conditions. *D.* Large-wave conditions in February 2011. The images showed the differences in surface turbidity in the bays resulting from these different conditions. Note the return to clear, blue surficial water after the November flood due to calm trade-wind conditions.

The critical shear stress levels necessary for resuspending terrigenous (volcanically derived) coarse silt and clay due to currents, waves, and the combination of waves and currents is shown in appendixes 14.1–14.2. During trade-wind conditions (2010 YD 317–320 and 340–360), the shear stresses from currents alone rarely exceeded the threshold needed to suspend terrigenous coarse silt or clay at most of the instrument sites (table 19; appendixes 14.1–14.2, green shaded area). Very few wave events occurred during these time periods, and consequently there was little sediment resuspension from shear stresses due to waves at the instrument sites. Only at the South 5-m site were the wave shear stresses and combined wave-current shear stresses high enough during trade-wind conditions to resuspend terrigenous coarse silt and clay for brief periods of time (appendix 14.2, green shaded area). The weak combined shear stresses resulted in little terrigenous (silt and clay) and/or carbonate (sand-sized) sediment being resuspended and contributing to turbidity recorded by the SLOBS.
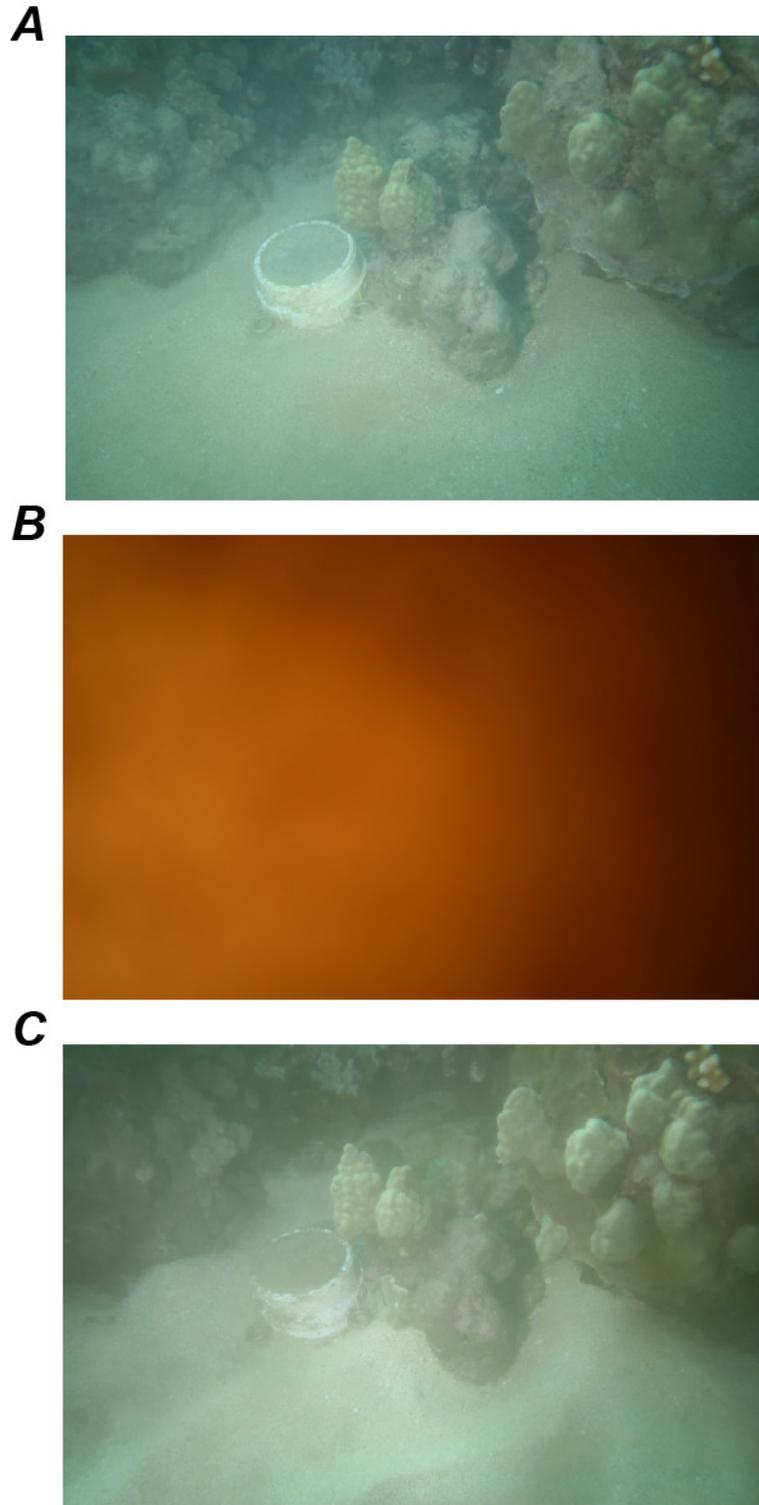
Figure 23. Photographs from the Coral Imaging System (CIS) showing underwater conditions at the Central 5-m site. *A,* Pre-flood trade-wind conditions. *B,* Flood conditions in November 2010. *C.* Post-flood trade-wind conditions. There were no photos taken during the large-wave conditions in February 2011, as the large waves knocked over the CIS. These images showed the differences in turbidity and sediment accumulation resulting from these different conditions.
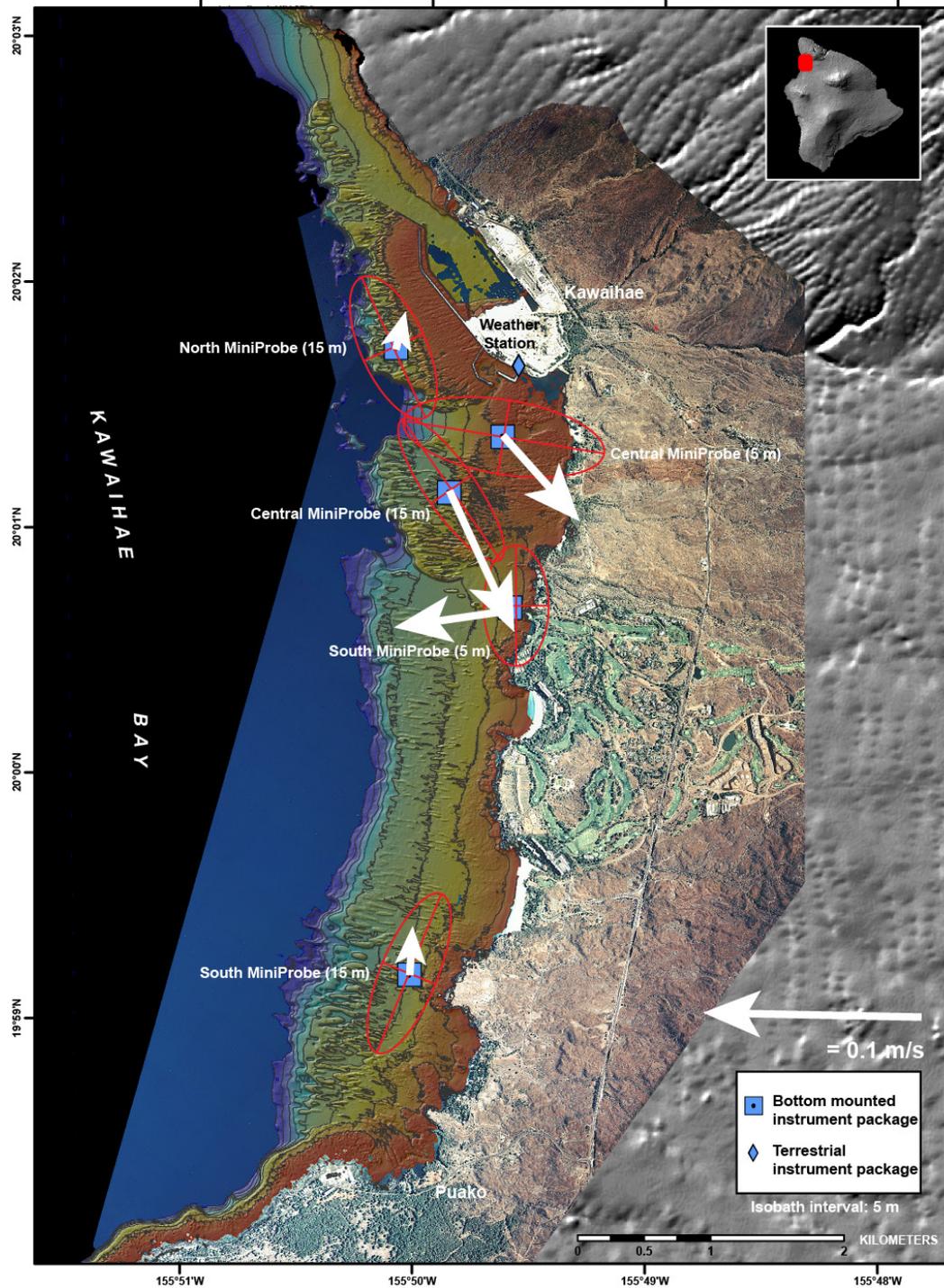
Figure 24. Map showing the mean (white arrows) and variability (red ellipses) of near-surface current directions and speeds, in meters per second, during trade-wind conditions for the 2010–2011 winter experiment. In the central part of the bay, currents were stronger and in the direction of the winds. At the North 15-m and South 15-m sites, currents were weaker and to the north.
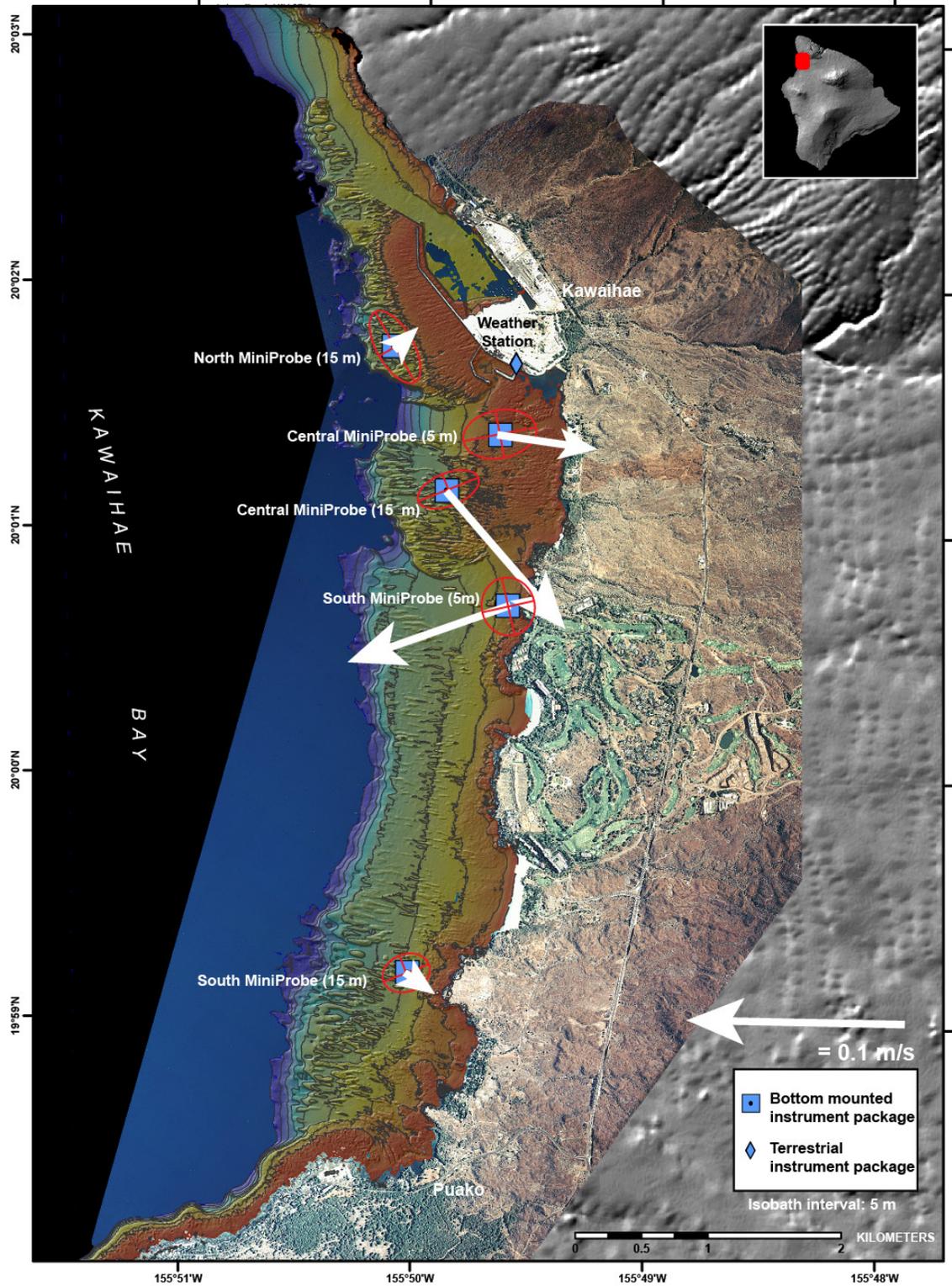
Figure 25. Map showing the mean (white arrows) and variability (red ellipses) of near-bed current directions and speeds, in meters per second, during trade-wind conditions for the 2010–2011 winter experiment. The currents were strongest in the central part of the bay, with variable directions, and weakest at the North 15-m and South 15-m sites, with onshore directions.

Suspended-sediment flux was calculated using turbidity values from the SLOBSs and current speed and direction from the ADCPs at co-located depths to examine where and how much sediment was transported through Pelekane and Kawaihae Bays area during the pre-flood trade-wind conditions (2010 YD 317–320; fig. 26). The suspended-sediment flux measured over the 3-day period near the seabed was directed to the south at the northern sites and to the north at the southern sites. The largest suspended-sediment flux was measured at the South 5-m site, as the currents and shear stresses were largest at this site. The smallest suspended-sediment flux was measured at the North 15-m site, where the currents and turbidity values were low (fig. 26). Overall, the suspended-sediment flux during trade-wind periods was the lowest of the deployment period, as little sediment was resuspended into the water column and transported by weak trade-wind currents (table 20).

Qualitatively, the TIS showed blue, clear water at the surface during pre-flood trade-wind conditions (fig. 22*A,* photo taken 11 November 2010 at 11:00 HST). The CIS at the Central 5-m site also showed clear water during this period (fig. 23*A,* photo taken 16 November 2010 at 17:00 HST). These photographs suggest that the few times critical shear stresses were sufficient to resuspend sediment from the seabed, the hydrodynamics were not sufficient to advect it high enough above the seabed to be imaged by either the TIS or CIS systems, and it must have been constrained to a thin near-bed nepheloid layer.

Flood

The heavy rainfall event on 19 November 2010 (2010 YD 323) flooded Pohaukole Gulch and delivered large quantities of both freshwater and sediment to Pelekane Bay. This was the heaviest rainfall event of the study period, with 49 mm recorded in 2 hours at the WS. High discharge from Pohaukole Gulch resulted in the breaching of the sand bar that separated the lagoon at the base of the gulch from Pelekane Bay (fig. 5). This single rainfall event contributed approximately half the rainfall that was measured over the entire 80-day study (YD 2010 310–390). The winds during this event were predominantly from the northwest at 3–5 m/s, similar to trade-wind conditions (fig. 6). A small-wave event (significant wave heights <2 m) from the northwest was measured by the ADCPs during the time of the flood (fig. 6). The data from 18-21 November 2010 (YD 2010 322–325) were analyzed to describe the circulation, turbidity, critical shear stresses, and suspended-sediment flux resulting from the rainfall and subsequent flood.

The near-surface currents during the flood event (0.08–0.10 m/s) were stronger than those measured during trade-wind conditions and directed offshore, to the west, at the Central 5-m, Central 15-m, and South 5-m sites. The near-surface currents at the North 15-m and South 15-m sites (~0.03 m/s) were slower than in the central portion of Kawaihae Bay and oriented to the north (fig. 27). The near-bed currents (~0.10 m/s) were also stronger at the Central 5-m, Central 15-m, and South 5-m sites than those measured at the North 15-m and South 15-m sites (~0.02 m/s), although the directions of flow were not consistent at any of the sites (fig. 28). The turbidity at the instrument sites was slightly elevated prior to the flood on 19 November 2010 (YD 2010 323) due to a small-wave event from the northwest. The greatest increases in turbidity were measured at the Central 2-m and 5-m sites (>100 NTU) and coincided with the flood (appendix 12.1). The other instrument sites recorded much smaller increases in turbidity during this time, possibly as a result of sluggish circulation in the area (figs. 27–28).
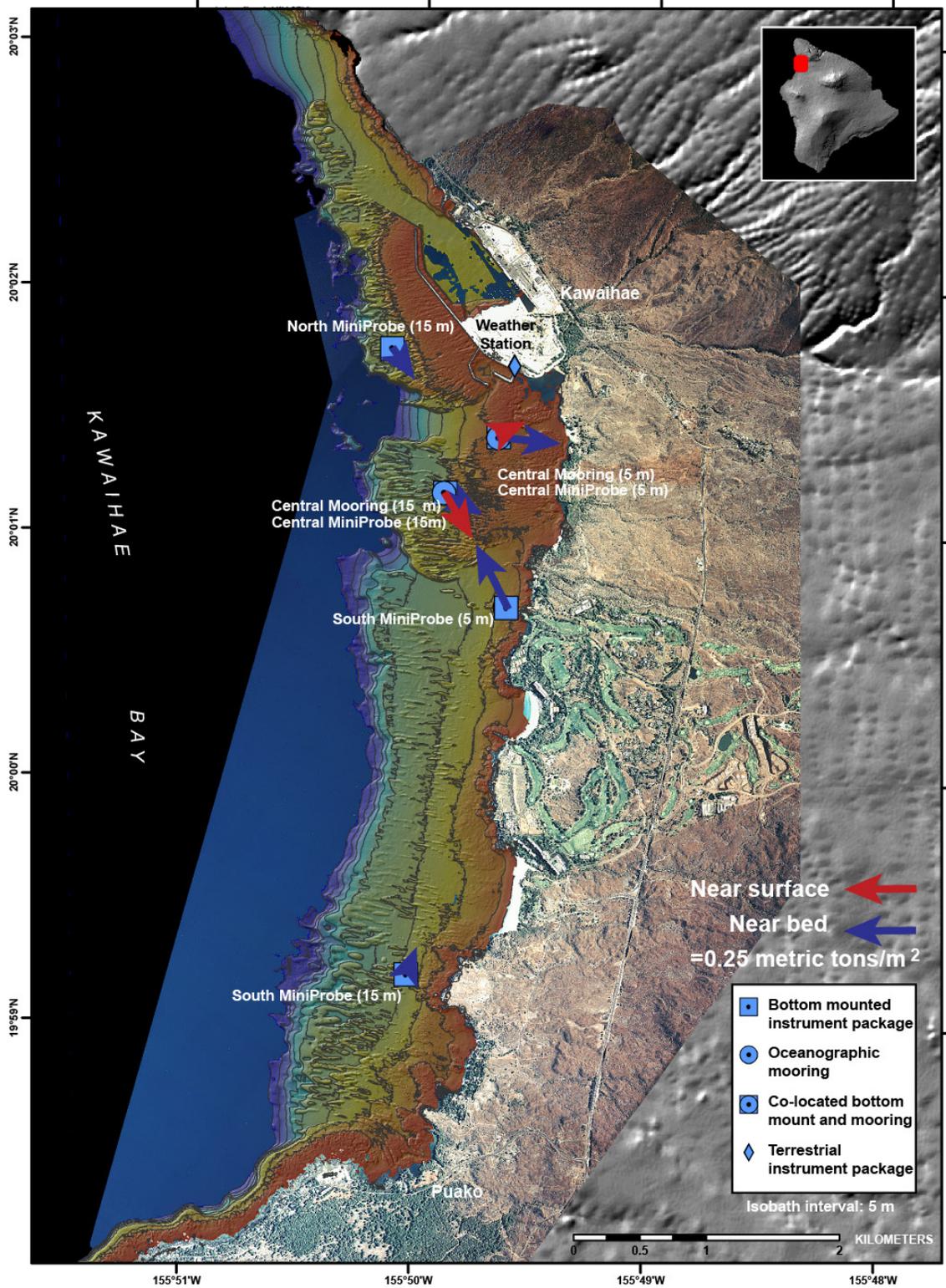
Figure 26. Map showing the mean daily near-surface (red arrows) and near-bed (blue arrows) suspended-sediment flux, in metric tons per square meter, during trade-wind conditions for the 2010–2011 winter experiment. Suspended-sediment flux was small at all of the instrument sites due to low turbidity and weak, variable currents.
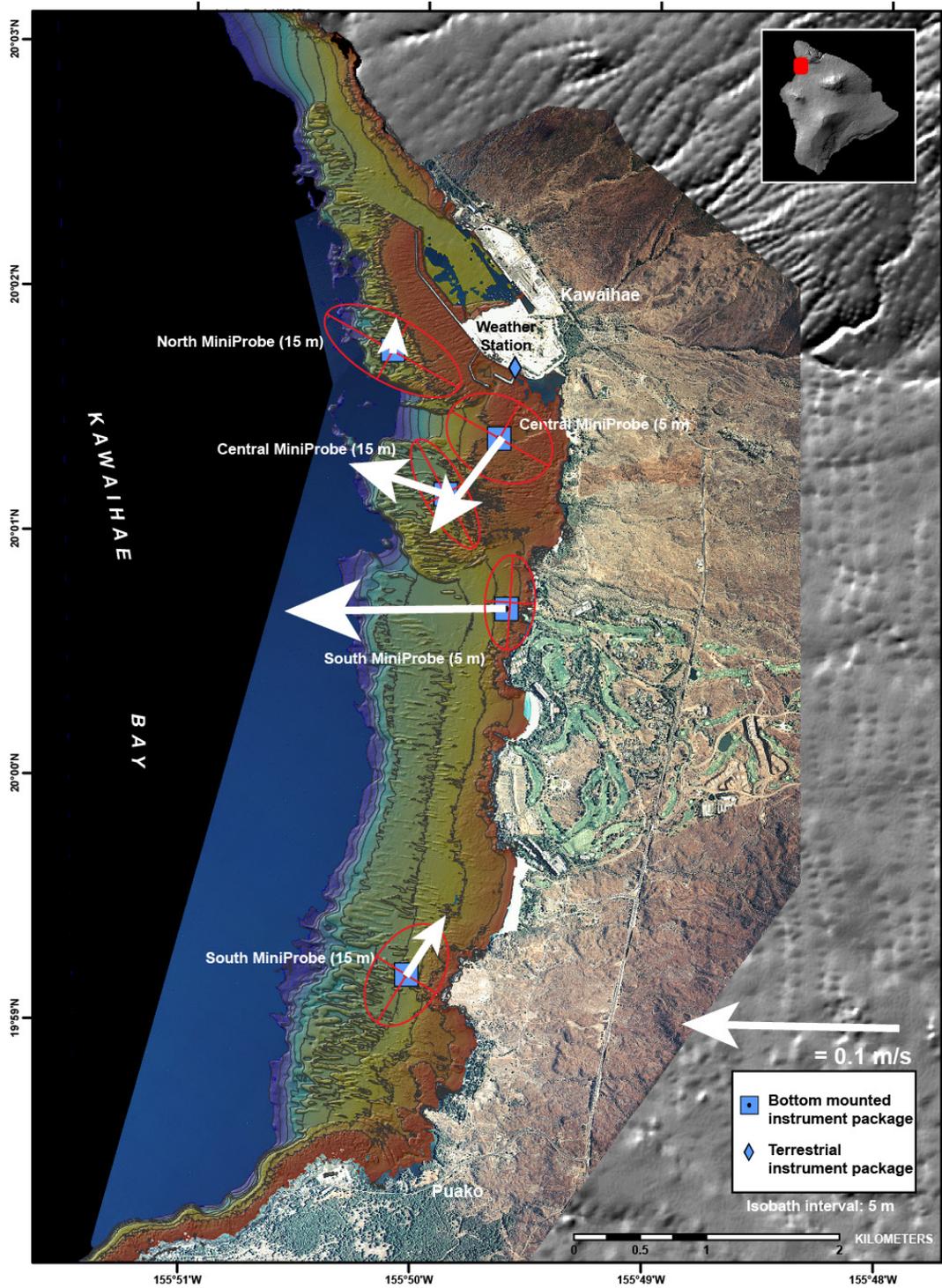
Figure 27. Map showing the mean (white arrows) and variability (red ellipses) of near-surface current directions and speeds, in meters per second, during flood conditions for the 2010–2011 winter experiment. The strongest currents were located in the central part of the bay, with offshore directions. The currents at the North 15-m and South 15-m sites were weaker and directed to the north.
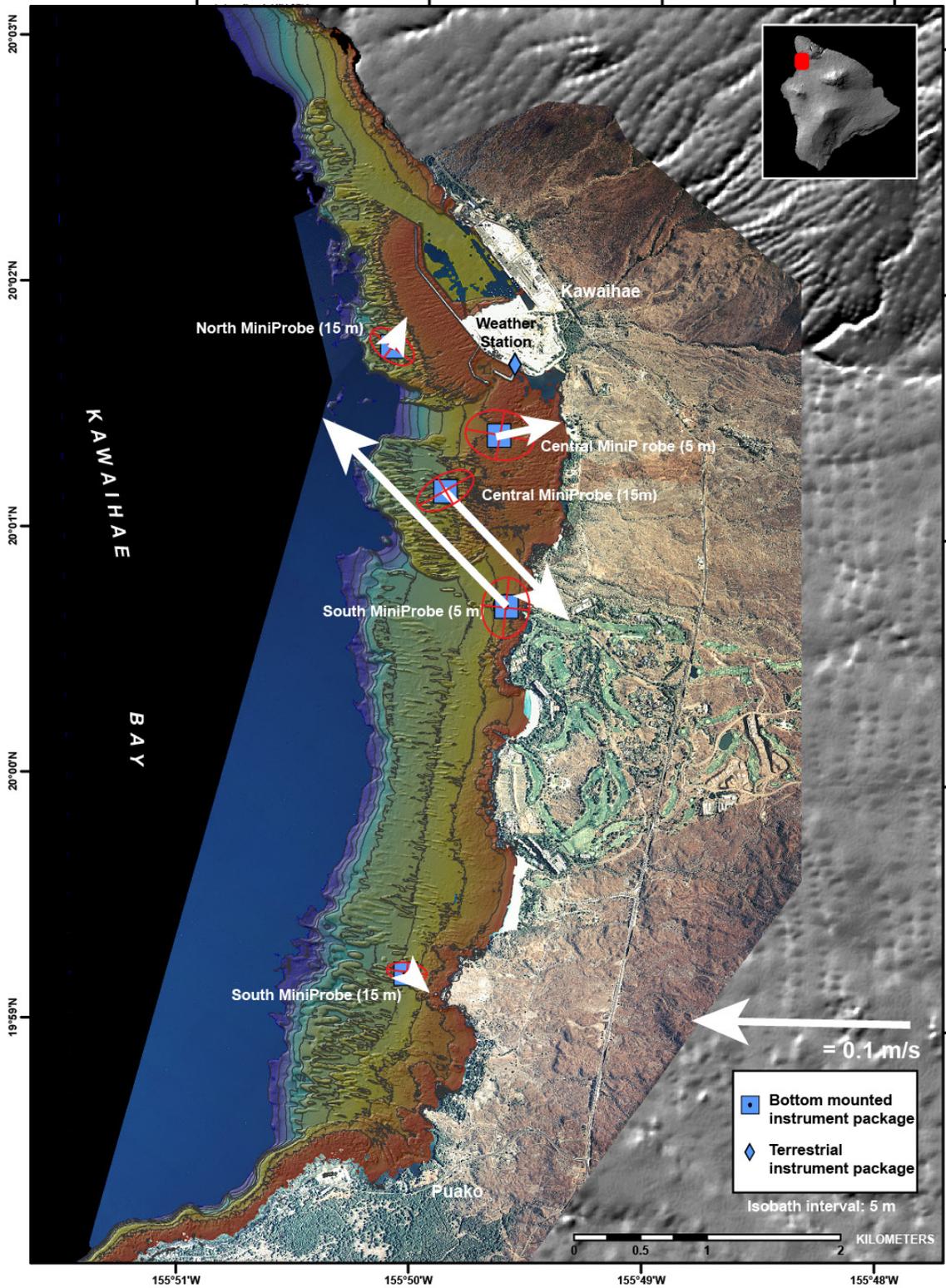
Figure 28. Map showing the mean (white arrows) and variability (red ellipses) of near-bed current directions and speeds, in meters per second, during flood conditions for the 2010–2011 winter experiment. The near-bed currents were primarily onshore at all sites except the South 5-m site.

44

The shear stresses due to currents alone were small and below the threshold for the resuspension of terrigenous clay- and silt-sized particles at all of the instrument sites (table 19; appendixes 14.1–14.2, orange shaded area). The small-wave event, however, generated enough wave-driven stress that the threshold for both of these particle sizes was exceeded at the majority of instrument sites.

The suspended-sediment flux during the flood event was four times greater than during the trade-wind conditions at the Central 5-m and South 5-m sites, due to stronger currents and higher turbidity (fig. 29; table 20). The other instrument sites showed relatively little increase in suspended-sediment flux due to the weak currents and relatively low turbidity. The orientations of suspended-sediment flux near the seabed were predominantly onshore and to the south (fig.29, blue arrows); the near-surface suspended-sediment fluxes at the Central 5-m and Central 15-m moorings were small in magnitude and varied in direction (fig. 29, red arrows). The calculated shear stresses and suspended-sediment fluxes suggest that even though a large input of sediment entered the system due to the flood at Pohaukole Gulch, the sediment fluxes were small due to relatively weak currents, likely resulting in much of the flood material being deposited on the seabed inshore of the Central 5-m and South 5-m sites.

Visually, the flood event delivered a large volume of terrigenous sediment to the bays, as recorded by the TIS and CIS. The TIS photo taken on 19 November 2010 at 13:00 HST (fig. 22*B*) showed red, terrigenous sediment throughout Pelekane Bay and the inner portion of Kawaihae Bay. The turbidity caused by the flood sediment was so great at the Central 5-m site that it blocked all surface light from reaching the CIS only 4 m below the water surface (fig. 23*B*, photo taken 19 November 2010 at 11:00 HST). The TIS and CIS also captured the rapid return of relatively clear water to the water column (fig. 22*C*, photo taken 20 November 2010 at 08:00 HST) due to rapid settling of the flood material and the deposition of the red, terrigenous sediment on the adjacent coral reef and sea floor (fig. 23*C*, photo taken 21 November 2010 at 08:00 HST).

Large Waves

Large waves impacted Kawaihae and Pelekane Bays from 15-25 January 2011 (YD 2010 380–390). The mean significant wave heights exceeded 4 m and the maximum wave heights exceeded 6 m; these waves were from the northwest at 12–14 s (figs. 6*D,* 6*E*). During this event, the winds were moderate (fig. 6*B*), and minor rainfall was measured at the WS (fig. 5*C*). The fast current speeds (figs. 30, 31) and large waves generated high shear stresses that resulted in high turbidity values and generated large suspended-sediment fluxes during this time period (fig. 32). The suspended-sediment fluxes during the large-wave events were the greatest of all the time periods analyzed at all of the instrument sites during the experiment (table 20). The mean direction of suspended-sediment fluxes during the large-wave events was variable at the instrument sites.

Near-surface currents during the large-wave events were the fastest measured during the deployment, exceeding 1.0 m/s and directed offshore at the Central 5-m and South 5-m sites. Moderate onshore flow was measured at the North 15-m, Central 15-m, and South 15-m sites (fig. 30). The near-bed currents were also vigorous (>1 m/s) during this time period, with offshore flow at the Central 5-m site and northerly flow at the South 5-m site. The other sites exhibited primarily weaker onshore flow (fig. 31). The fast currents directed offshore and to the north at the 5-m MP sites may have been due to circulation cells or return flows that were likely

generated by large gradients in wave-driven set-up, resulting from the complex morphology of the reef in this area.

The turbidity values during these large-wave events were the highest on average at all of the sites except the Central 2-m site (appendix 12.1). The turbidity at the Central 2-m site was lower during the wave events than during the flood event, likely due to the large waves dissipating most of their energy by breaking further offshore; relatively small waves were measured at the shallow Central 2-m site at that time. The wave shear stresses and combined wave-current shear stresses during these large-wave events were the highest measured for all of the instrument sites and greatly exceeded the threshold for the resuspension of terrigenous clay- and silt-sized material for the majority of the 15-25 January 2011 (YD 2010 380-390) time period spanning 15–25 January 2011 (YD 2010380–390) (table 19; appendix 14, blue shaded area). Only at the Central 5-m and 15-m sites did the current shear stress alone exceed the threshold for the resuspension of terrigenous clay- and silt-sized material. The current shear stress exceeded the silt threshold for resuspension at the South 5- and 15-m sites for the duration of the large-wave events (appendix 14, blue shaded area). The largest suspended-sediment fluxes occurred at the Central 5-m mooring and Central 5-m site; these were predominantly oriented offshore (fig. 32). Onshore suspended-sediment flux was measured at the Central 15-m mooring, the Central 15-m site, and North 15-m site. Wave asymmetry during shoaling likely drove the currents and resultant suspended-sediment fluxes onshore at these sites, which was balanced by offshore-directed return flow through the large paleo-stream channel in the reef at the Central 5-m site. The TIS captured the large-wave events that impacted Pelekane and Kawaihae Bays in January 2011 (fig. 22*D*, photo taken 16 January 2011 at 11:00 HST). The normally quiescent Pelekane Bay was turbid due to dark, resuspended terrigenous sediment (not new flood material); the lighter color of the turbid water in Kawaihae Bay may have been due to either more wave-breaking-induced bubbles or resuspended seabed carbonate material diluting the darker terrigenous material. The CIS did not capture the turbidity from the wave events, as it was damaged at the arrival of the first of the large waves and did not take usable photos afterwards.
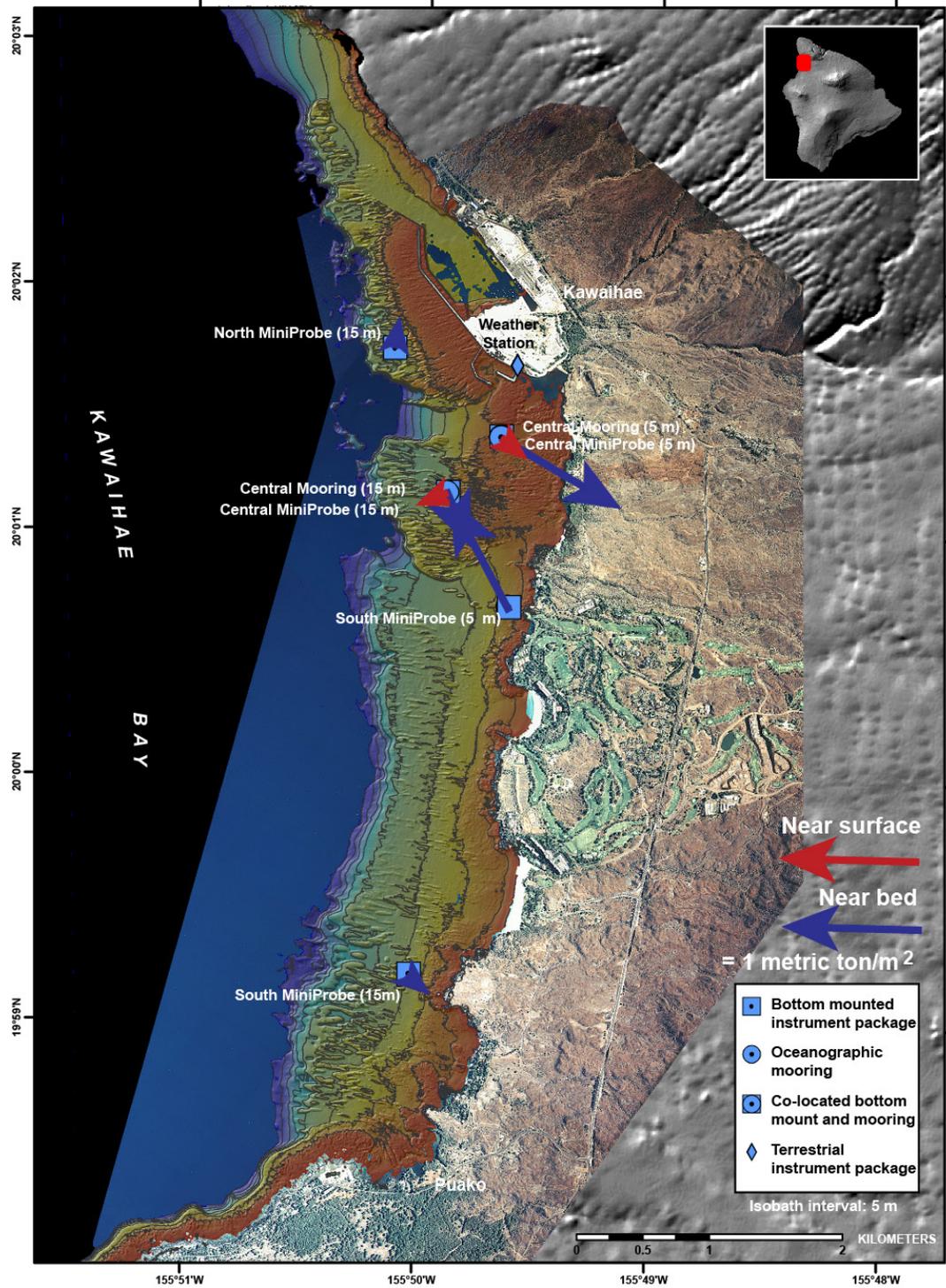
Figure 29. Map showing the mean daily near-surface (red arrows) and near-bed (blue arrows) suspended-sediment flux, in metric tons per square meter, during flood conditions for the 2010-2011 winter experiment. The near-surface suspended-sediment flux in the central part of the bay was variable and smaller than the near-bed suspended-sediment flux. Suspended-sediment flux near the seabed was primarily onshore.
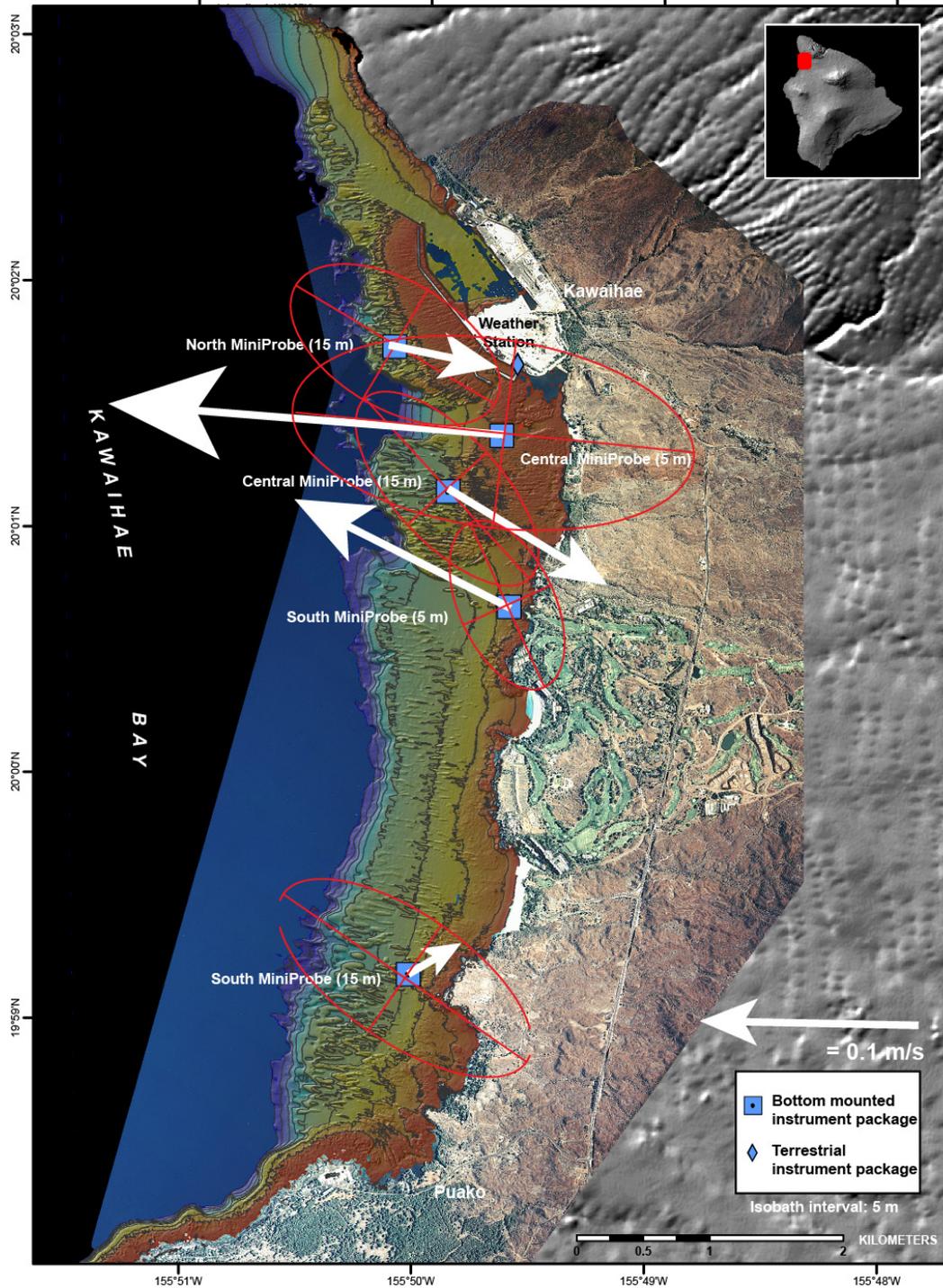
Figure 30. Map showing the mean (white arrows) and variability (red ellipses) of near-surface current directions and speeds, in meters per second, during large-wave events for the 2010–2011 winter experiment. The near-surface currents were onshore at the North 15-m, Central 15-m, and South 15-m sites, and offshore at the Central 5-m and south 5-m sites. The current speeds were highest of the entire deployment during this time period.
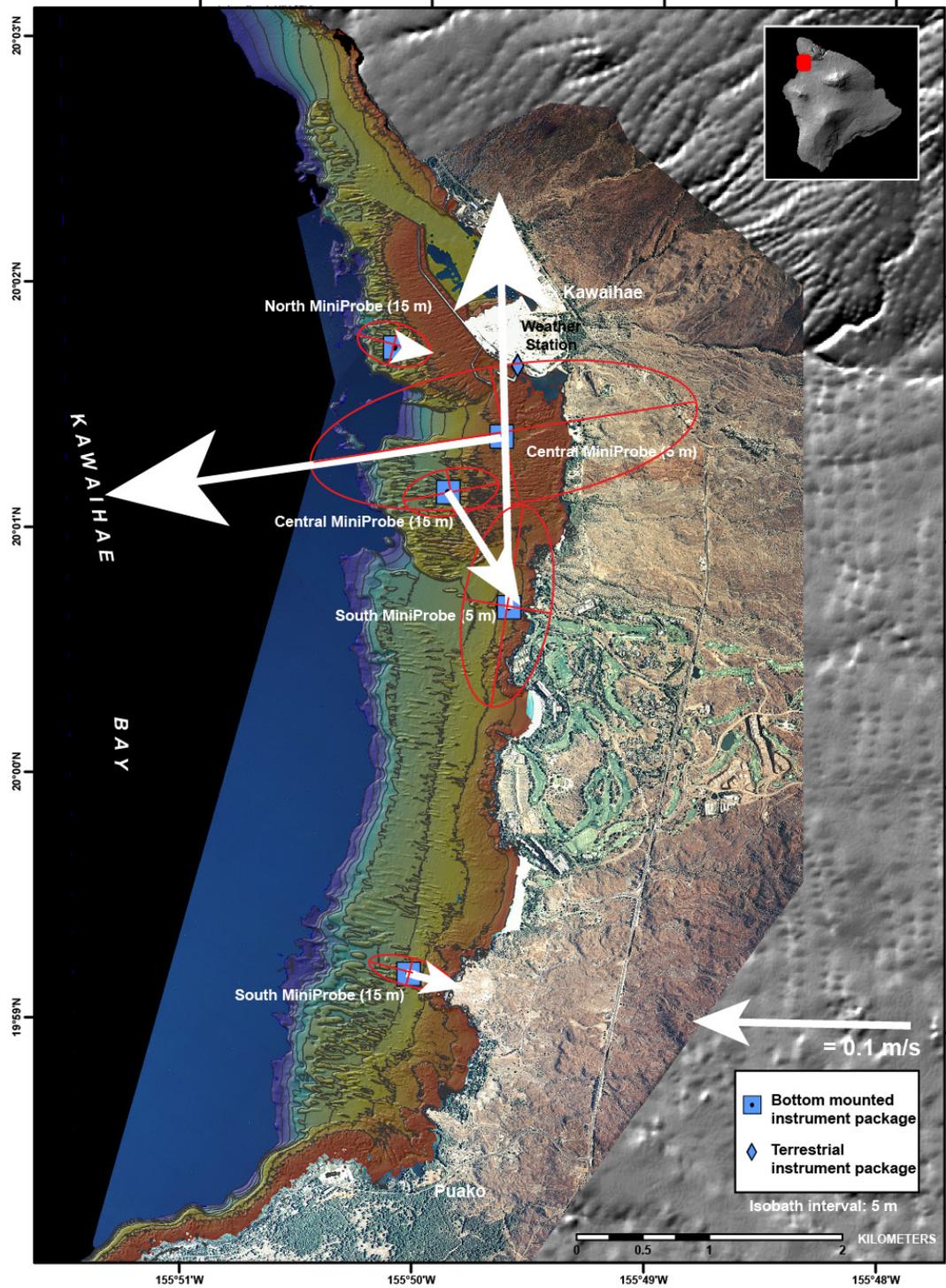
Figure 31. Map showing the mean (white arrows) and variability (red ellipses) of near-bed current directions and speeds, in meters per second, during large-wave events for the 2010–2011 winter experiment. The near-bed current speeds at the South 5-m and Central 5-m sites were higher during the large-wave events than any other time during the deployment.
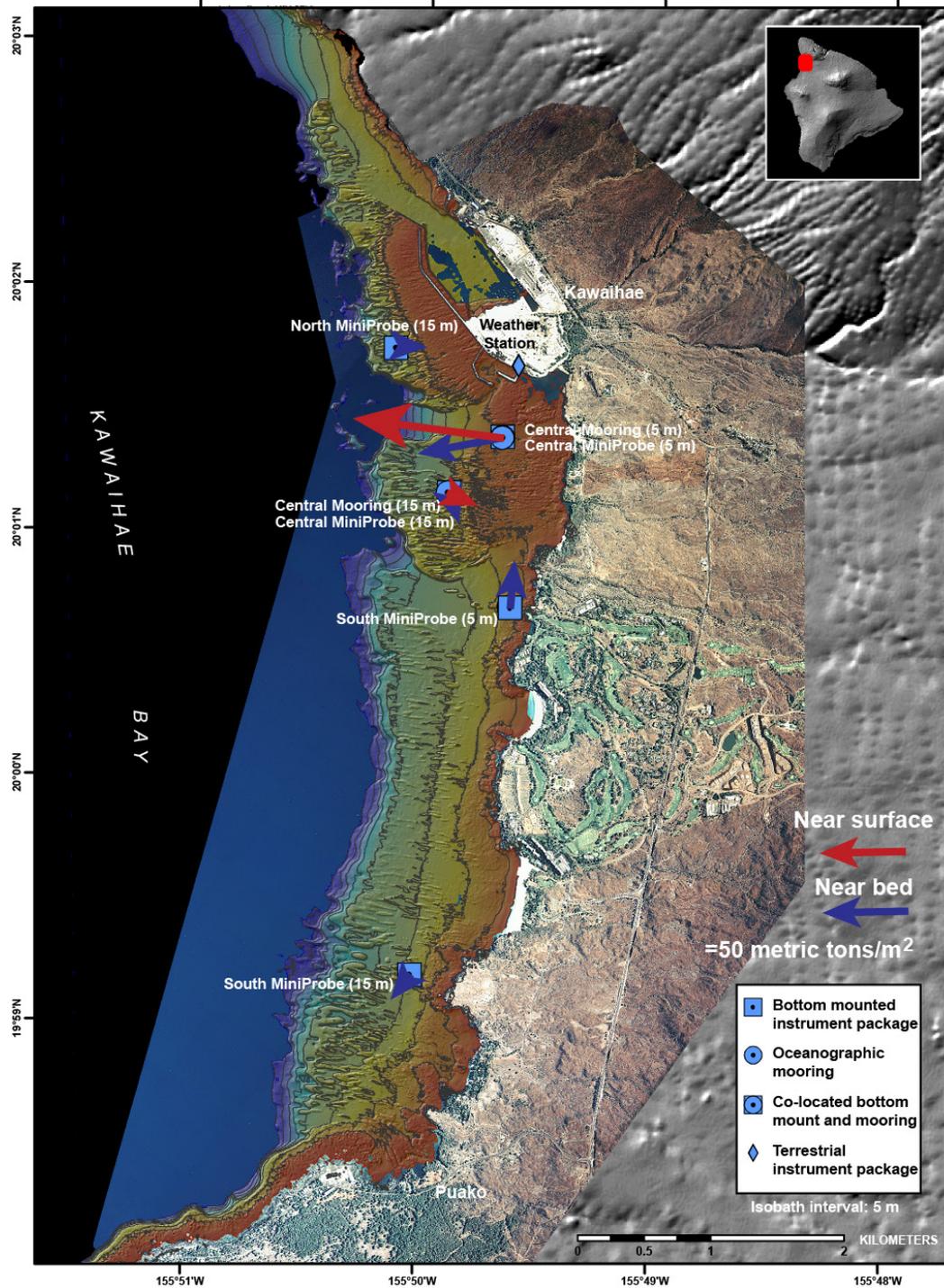
Figure 32. Map showing the mean daily near-surface (red arrows) and near-bed (blue arrows) suspended-sediment flux, in metric tons per square meter, during large-wave events for the 2010-2011 winter experiment. The suspended-sediment flux was highest during the deployment at the Central 5-m site due to the strong currents and high turbidity; the flux was predominantly directed offshore throughout the water column at this location. Elsewhere, the suspended-sediment flux was smaller and predominantly directed onshore or alongshore.

Circulation and Sediment Dynamics

The instrument measurements and sediment-trap data presented here indicate that sediment transport processes in Pelekane and Kawihae Bays result from a combination of (1) relatively common, longer-duration, low-intensity processes such as tides and trade winds and (2) episodic, short-term, energetic processes such as floods and large-wave events (fig. 33). The 19 November 2010 flood (2010 YD 323) breached the sand bar that separated Pohaukole Gulch from Pelekane Bay and delivered terrigenous material to Pelekane Bay (fig. 33*A,G*). This resulted in elevated turbidity levels that were highest close to shore but extended across the reef (fig. 33*D-F*). During the subsequent trade-wind period (2010 YD 330–365), some of this terrigenous sediment was mobilized by moderate waves and tidal currents and slowly advected at low levels out to the upper forereef (fig. 33*E*) and, to a lesser extent, the lower fore reef (fig. 33*F*) during falling tides. The impact of the large-wave events during 15-25 January 2011 (2010 YD 380–390) to nearshore Pelekane Bay appears to have been relatively minor compared to the fore reef. This was likely a result of depth-induced breaking of the large waves on the fore reef, which dissipated most of the energy and left the inner reef flat relatively quiescent (but still more energetic than during trade-wind periods). These larger-than-normal waves in Pelekane Bay during January 2011 resuspended terrigenous flood sediment at low levels—although lower than measured during the November 2010 flood—suggesting that much of the mobile, fine-grained terrigenous material delivered by the flood had already been slowly advected out to the fore reef at low levels by moderate waves and tidal currents under trade-wind forcing. The large-wave shear stresses on the exposed fore reef during January 2011 resuspended not only the terrigenous flood sediment but also large quantities of carbonate seabed material (fig. 33*G*).

It appears that episodic floods from Pohaukole Gulch deposit much of their sediment in Pelekane Bay. In addition, it appears that some of the sediment is advected during the flood out and over the fore reef (fig. 22*B*), causing high turbidity (fig. 33*D–F*), low light penetration (fig. 23*B*), and temporary deposition on the upper fore reef (fig. 23*C*). During relatively low-energy trade-wind conditions, a small amount of fine-grained terrigenous sediment was resuspended from the reef flat and advected out over the fore reef into Kawaihae Bay (fig. 33), where it can decrease photosynthetically available radiation (PAR) and potentially desorb nutrients and/or contributing toxicants. Quiescent conditions (as observed during trade-wind conditions) can result in temporary accumulation of fine-grained terrigenous sediment on the fore reef, potentially settling on corals or at potential sites for new coral recruitment. Large waves appear to be very effective at resuspending terrigenous flood material on the fore reef and advecting it offshore to the insular shelf. Thus the phasing of sediment-injection events (for example, floods) relative to resuspension and advection events (for example, large-wave events) is critical to the residence time of sediment on the reef flat and fore reef. If floods are coincident with or closely followed in time by energetic oceanographic conditions, the residence time for the terrigenous flood sediment is lower relative to other scenarios. This suggests that early spring (or summer) floods during the transition to summer trade-wind conditions are more likely to result in longer residence times for terrigenous sediment on the reefs of these bays than floods that occur in the winter, when energetic wave conditions are more common.
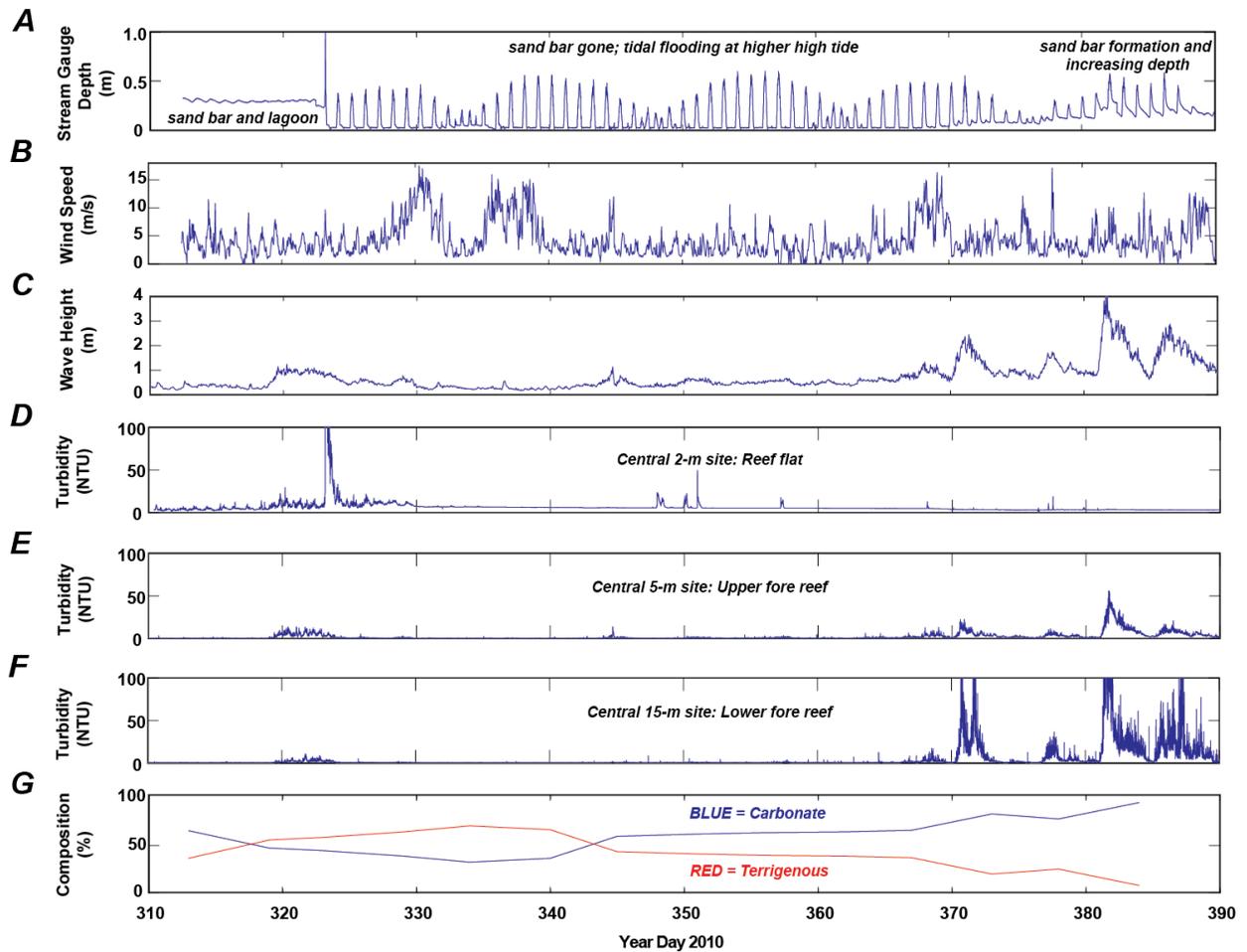
Figure 33. Time-series plots of oceanographic conditions and sediment dynamics during the 2010–2011 winter experiment. *A*, Stream gauge depth, in meters. *B*, Wind speed, in meters per second, measured at the USGS weather station. *C*, Wave height, in meters, measured at the Central 15-m site. *D*, Turbidity, in Nephelometric Turbidity Units (NTU), at the Central 2-m site. *E*, Turbidity, in Nephelometric Turbidity Units (NTU), at the Central 5-m site. *F*, Turbidity, in Nephelometric Turbidity Units (NTU), at the Central 15-m site. *G*, Rotary sediment trap bulk composition, in percent by mass, with red and blue lines denoting the terrigenous (volcanic) and carbonate components, respectively.

On average, about 50 cm (41–61 cm) of sediment has accumulated in Pelekane Bay between the 1928 topographic/bathymetric survey and the 2011 survey (fig. 16). This average accumulation rate (50 cm in 83 years = 0.6 cm per year) is consistent with the accumulation rate derived from excess ^{210}Pb activities (0.59 cm per year). Based on a constant-rate-of-supply (CRS) model of the excess ^{210}Pb down-core profile, sediment accumulation rates in core PC3 from Pelekane Bay have increased through recent time (table 18). It is likely that the expansion of the small craft breakwater on the southwest side of the harbor in the 1970s has impacted sediment accumulation rates in Pelekane Bay by restricting flow and reducing the propagation of wave energy into the bay. It is also possible that other external forcing factors such as climatic shifts and/or recent watershed impacts have affected trends in sediment accumulation. The observed shear stresses imparted by waves and currents during normal trade-wind conditions (table 19), which characterize most of the year (for example, Fletcher and others, 2002), are generally insufficient to resuspend the fine-grained terrigenous sediment in the bay. Although the

52

shear stresses imparted by waves and currents during episodic large-wave events are sufficient to resuspend the fine-grained terrigenous sediment in the bay (table 19), the historical accumulation of sediment and apparent recent increase in accumulation rates (table 18) suggest the rate of new sediment delivery to the bay from the adjacent watersheds is exceeding the ability of infrequent large-wave events to resuspend and transport the terrigenous material out of the bay.

Conclusions

In all, more than 2 million measurements of meteorologic and oceanographic conditions and water-column properties were made between November 2010 and March 2011 to assess circulation and sediment dynamics in Pelekane and Kawaihae Bays. Key findings from these measurements and subsequent analyses include:

1. The salinity values were consistently lower closer to shore due to runoff and possibly submarine groundwater discharge and increased offshore and away from Pelekane Bay. The temperatures were warmest in shallow Pelekane Bay and were cooler offshore and downcoast. The highest turbidity values were observed in Pelekane Bay; turbidity decreased to the south, away from Pelekane Bay, and offshore. The fluorescence in the region was highest close to shore and was variable alongshore, generally greater closer to human development and stream inputs.

2. Based on the range in bathymetric survey and considering datum error, overall the bay became 0.41 m to 0.61 m shallower between 1928 and 2011, due to the accumulation of 22,500 m^3 to 37,500 m^3 of sediment above the sea floor mapped in the 1928 survey.

3. Trade winds occurred during most of the deployment. Suspended-sediment transport during trade-wind conditions was limited due to sluggish currents and low shear stresses in Pelekane Bay, resulting in little to no sediment resuspension from the seabed or the capability to transport it.

4. The heavy rainfall and resulting flood event on 19 November 2010 occurred during relatively quiescent conditions, with average wind speeds and small waves. Suspended-sediment transport in Kawaihae Bay during the flood was minimal due to these weak forcing conditions. The data from the in situ oceanographic instruments and imagery (both terrestrial and underwater) indicate that although there was a large input of sediment into the coastal system, most of it remained in Pelekane Bay and the inner portion of Kawaihae Bay (inshore of the 15-m isobath), where it settled out of suspension and accumulated on the seabed.

5. The large-wave events that impacted the region in January and February 2011 were responsible for the highest turbidity values and sediment flux in the bays during the experiment. Based on the data from the in situ oceanographic instruments and imagery (both terrestrial and underwater), it appears that these large-wave events resuspended large quantities of terrigenous sediment that had been delivered to the system during the November 2010 flood, as well as carbonate sand resuspended from the seabed. The strong wave-driven currents transported large quantities of resuspended sediment from the inner portion of the reef offshore to the insular shelf, effectively removing sediment delivered by the November 2010 flood from portions of the reef.

6. It appears that floods from Pohaukole Gulch deposit much of their sediment in Pelekane Bay. Although some of the fluvial sediment was advected seaward over the fore reef during the flood, causing high turbidity and low light penetration, most of the sediment was temporarily deposited on the reef flat in Pelekane Bay. During relatively low-energy trade-wind conditions, low-levels of fine-grained terrigenous sediment were resuspended from the reef flat in Pelekane Bay and advected seaward over the fore reef in Kawaihae Bay, resulting in the temporary accumulation of this material on the fore reef. Large-wave events appear to be effective at resuspending terrigenous flood material on the fore reef and advecting it offshore to the deeper, outer portions of the fringing reefs where there is currently high coral coverage.

7. Short-lived radionuclides (for example, ^{210}Pb, ^{137}Cs) were measured to estimate recent sediment geochronologies. Based on the down-core excess ^{210}Pb and ^{137}Cs profiles, the linear sedimentation rate at site PC3 was approximately 0.6 cm/yr, which corresponds to a mass accumulation rate of 524.5 mg/cm^2/yr. The measured whole-core inventory of excess ^{210}Pb was 49.3 dpm/cm^2, and assuming a latitudinally corrected atmospheric deposition rate of about 0.9 dpm/cm/yr, the expected sediment inventory would amount to ~30 dpm/cm^2. This suggests that Pelekane Bay has effectively retained the majority of sediment that is delivered to the bay. This sequestered sediment is then also prone to repeat resuspension events, driven by large-wave events or tsunami waves.

Coastal circulation and sediment dynamics in Pelekane and Kawaihae Bays are complex in nature. Our results provide specific information on the physical oceanographic processes and sediment transport within the bays during winter conditions that can be applied to understanding their relation to coral reef health.

Acknowledgements

References Cited

Appleby, P.G., and Oldfield, F., 1978, The calculation of lead-210 dates assuming a constant rate of supply of unsupported ^{210}Pb to the sediment: Catena, v. 5, p. 1–8.

Baker, E.T., Milburn, H.B., and Tennant D.A., 1988, Field assessment of sediment trap efficiency under varying flow conditions: Journal of Marine Research, v. 46, p. 573–592.

Behiry, M.G., and Hanafy, S.M., 2000, Geophysical surveys to map the vertical extension of a sinkhole—a comparison study, *in* Proceedings of the Symposium on the Application of Geophysics to Engineering and Environmental Problems (SAGEEP-2000): Denver, Colo., Environmental and Engineering Geophysical Society, p. 341–350.

Benson, A.K., Payne, K., and Stubben, M.A., 1997, Mapping groundwater contamination using DC resistivity and VLF geophysical methods—A case study: Geophysics, v. 62, p. 80–86.

Bothner, M.H., Reynolds, R.L., Casso, M.A., Storlazzi, C.D., and Field, M.E., 2006, Quantity, composition, and source of sediment collected in sediment traps along the fringing coral reef off Molokai, Hawaii: Marine Pollution Bulletin, v. 52, p. 1034–1047.

de Groot-Hedlin, C., and Constable, S., 1990, Occam's inversion to generate smooth, two-dimensional models from magnetotelluric data: Geophysics, v. 55, p. 1613–1624.

Dimova, N.T., Swarzenski, P.W., Dulaiova, H., and Glenn, C., 2012, Utilizing multichannel electrical resistivity methods to examine the dynamics of the freshwater–saltwater interface in two Hawaiian groundwater systems: Journal of Geophysical Research, v. 117, C02012. doi:10.1029/2011JC007509

Fletcher, C.H., Grossman, E.E., Richmond, B.M., and Gibbs, A.E., 2002, Atlas of natural hazards in the Hawaiian coastal zone: U.S. Geological Survey Geologic Investigations Series I–2761, 182 p. [*http://pubs.usgs.gov/imap/i2761/*, last accessed June 25, 2012].

Gardner, W.D., Richardson, M.J., Hinga, K.R., and Biscaye, P.E., 1983, Resuspension measured with sediment traps in a high-energy environment: Earth and Planetary Science Letters, v. 66, p. 262–278.

Group 70 International, Inc. and Oceanit Center, 2007, Pelekane Bay watershed sediment runoff analysis: Report prepared for the U.S. Army Corps of Engineers, Honolulu Engineer District, 112 p.
[*http://www.csc.noaa.gov/digitalcoast/_/pdf/PelekaneBayWatershedSedimentRunoffAnalysis_FinalReport2007.pdf*, last accessed June 25, 2012].

Hoover, D.J., and Gold, C., 2006, Assessment of coastal water resources and watershed conditions at Puʻukoholā Heiau National Historic Site, Hawaiʻi: Denver, Colo., National Park Service [Technical Report NPS/NRWRD/NRTR–2006/359].

Loke, M.H., 2001, Tutorial—2-D and 3-D electrical imaging surveys: available online at [*http://www.geoelectrical.com*, last accessed June 10, 2011].

Madsen, O.S., 1999, Coastal sediment transport processes: American Society of Civil Engineers Short Course, Coastal Sediments '99 Conference, New York.

Moberly, R.M., and Chamberlain, T., 1964, Hawaiian beach systems: Honolulu, University of Hawai'i, [Hawaii Institute of Geophysics Report HIG 64–2] 177 p.

National Ocean Service, National Oceanographic and Atmospheric Administration [n.d.], Tide data for Kawaihae Harbor, Hawaii, CO-OPS ID 1617433: [*http://tidesandcurrents.noaa.gov/data_menu.shtml?stn=1617433%20Kawaihae,%20HI&type= Tide%20Data*, last accessed June 25, 2012].

Oldenburg, D.W., and Li, Y., 1999, Estimating depth of investigation in DC resistivity and IP surveys: Geophysics, v. 64, p. 403–416.

Poppe, L.J., Elaison, A.H., Fredericks, J.J., Rendigs, R.R., Blackwood, D., and Polloni, C.F., 2000, Grain-size analysis of marine sediments—Methodology and data processing, *in* USGS east-coast sediment analysis—Procedures, database, and georeferenced displays: U.S. Geological Survey Open-File Report 00–358, available online at http://pubs.usgs.gov/of/2000/of00-358/ (last accessed June 25, 2012).

Storlazzi, C.D., and Jaffe, B.E., 2008, The relative contribution of processes driving variability in flow, shear, and turbidity over a fringing coral reef—West Maui, Hawaii: Estuarine, Coastal and Shelf Science, v. 77, no. 4, p. 549–564.

Storlazzi, C.D., Field, M.E., and Bothner, M.H., 2011, The use (and misuse) of sediment traps in coral reef environments—Theory, observations, and suggested protocols: Coral Reefs, v. 30, p. 23–38.

Swarzenski, P.W., Izbicki, J.A., Grossman, E.E., Glenn, C.R., Plath, C.A., and Kelly, J.L., 2009, A multi-proxy tracer approach to submarine groundwater discharge studies—Examples from Santa Barbara, CA and Maunalua Bay, HI [abs.]: Geochimica et Cosmochimica Acta, v. 73, no. 13 suppl., p. A1299.

Tissot, B.N., 1998, Changes in the marine habitat and biota of Pelekane Bay, Hawaii over a 20-year period: Honolulu, Hawaii, U.S. Fish and Wildlife Service, 34 p.

Thornberry-Ehrlich, T., 2011, Puʻu-koholā Heiau National Historic Site—Geologic resources inventory report: Ft. Collins, Colo., National Park Service [Natural Resource Report NPS/NRPC/GRD/NRR–2011/386].

Additional Digital Information

For additional information on the instrument deployments, please see:
http://walrus.wr.usgs.gov/infobank/a/a510bi/html/a-5-10-bi.meta.html
http://walrus.wr.usgs.gov/infobank/a/a111bi/html/a-1-11-bi.meta.html

For more information on the U.S. Geological Survey Western Region's Coastal and Marine Geology Team, please see:
http://walrus.wr.usgs.gov/

For more information on the U.S. Geological Survey's Coral Reef Project, please see:
http://coralreefs.wr.usgs.gov/

Direct Contact Information

Regarding this report:
Curt D. Storlazzi (USGS Pacific Coral Reef Project chief):   cstorlazzi@usgs.gov

Table 1: Experiment personnel.

Person	Affiliation	Responsibilities
Michael Field	USGS	Co-chief scientist, diver
Curt Storlazzi	USGS	Co-chief scientist, diver
Kathy Presto	USGS	Oceanographer, instrument specialist
Joshua Logan	USGS	Physical scientist, diver
Tom Reiss	USGS	Dive safety officer, surveying specialist
Tim Elfers	USGS	Mechanical technician
Peter Swarzenski	USGS	Core geochemistry, electrical resistivity
Michael Torresan	USGS	Sediment sampling and processing
Susan Cochran	USGS	Sediment sampling and processing
Hank Chezar	USGS	Camera technician
Joe Reich	F/V *Alyce C*	Vessel captain

Table 2: Instrument package sensors.

Site Name	Depth [m]	Sensors
North Pressure Sensor	2	Onset pressure sensor
North 15-m MiniProbe	15	RD Instruments 600 kHz Workhorse Monitor acoustic Doppler current profiler
	15	Aquatec 210TYT turbidity sensor
Central 15-m MiniProbe	15	RD Instruments 600 kHz Workhorse Monitor acoustic Doppler current profiler
	15	Aquatec 210TYT turbidity sensor
Central 15-m mooring	2	Aquatec 210TYT turbidity sensor
	2	Seabird SBE-37SI Microcat conductivity-temperature sensor
Central 5-m MiniProbe	5	Nortek 2 MHz Aquadopp acoustic Doppler current profiler
	5	Seabird SBE-37SI Microcat conductivity-temperature sensor
	5	Aquatec 210TYT turbidity sensor
Coral imaging system (CIS)	5	Canon D60 6.3 MP digital SLR
Rotary sediment trap (RST)	5	USGS programmable, 21-bottle
Central 5-m mooring	5	Aquatec 210TYT turbidity sensor
	5	Seabird SBE-37SI Microcat conductivity-temperature sensor
Central 2-m MiniProbe	2	Nortek 2 MHz Aquadopp acoustic Doppler current profiler
	2	YSI Ecowatch 6600-EDS temperature, salinity, turbidity sensor
South 15-m MiniProbe	13	RD Instruments 600 kHz Workhorse Monitor acoustic Doppler current profiler
	13	Aquatec 210TYT turbidity sensor
South 5-m MiniProbe	5	Nortek 2 MHz Aquadopp acoustic Doppler current profiler
	5	Seabird SBE-37SI Microcat conductivity-temperature sensor
	5	Aquatec 210TYT turbidity sensor
South pressure sensor	2	Onset pressure sensor
Terrestrial imaging system (TIS)	[38]*	Canon EOS Rebel Xti 10.1 MP digital SLR
Stream gage	[1]*	Onset pressure sensor
Weather station (WS)	[3]*	NovaLynx WS-16N-A weather station

*Height, in meters

Table 3: Instrument package location information.

Site Name	Latitude [decimal degrees]	Longitude [decimal degrees]
North 15-m MiniProbe	20.029227	-155.835508
Central 15-m MiniProbe	20.023265	-155.827783
Central 15-m mooring	20.019481	-155.831628
Central 5-m MiniProbe	20.023302	-155.827743
Central 5-m mooring	20.023278	-155.827786
Central 5-m camera (CIS)	20.023265	-155.827783
Central 2-m MiniProbe	20.027089	-155.824247
South 15-m MiniProbe	19.986714	-155.833797
South 5-m MiniProbe	20.011733	-155.827024
South pressure sensor	19.943791	-155.872963
Terrestrial Camera (TIS)	20.026102	-155.820538
Stream gage	20.028547	-155.823369
Weather station	21.287697	-157.719459

Table 4: **Water-column profiler cast locations and depth information.**

Cast Number	Latitude [decimal degrees]	Longitude [decimal degrees]	Depth [m]
1	19.97859	-155.84153	24.15
2	19.97600	-155.83407	6.98
3	19.98144	-155.83188	5.93
4	19.98445	-155.84052	24.65
5	19.98691	-155.83394	10.24
6	19.99203	-155.82839	6.38
7	19.99295	-155.83747	22.04
8	20.00522	-155.83607	24.21
9	20.00453	-155.82692	5.67
10	20.01166	-155.82743	5.95
11	20.01211	-155.83662	23.34
12	20.01755	-155.83576	38.77
13	20.01705	-155.82521	4.58
14	20.01940	-155.83180	16.52
15	20.02311	-155.83645	35.00
16	20.02331	-155.82800	4.78
17	20.02372	-155.82367	2.81
18	20.02490	-155.82394	1.93
19	20.02616	-155.82858	5.27
20	20.02481	-155.83326	22.99
21	20.02633	-155.83400	19.62
23	20.02561	-155.82411	2.48
24	20.02692	-155.82429	1.50
25	20.02902	-155.83192	3.12
26	20.02937	-155.83565	15.62
27	20.02882	-155.83783	43.00
28	20.03530	-155.83806	36.77
29	20.03818	-155.83489	12.37
30	20.04950	-155.84022	9.99
31	20.04800	-155.84302	22.82
32	20.06548	-155.85451	7.95
33	20.06437	-155.85595	29.12
34	19.94436	-155.87297	10.50

Table 5: Sediment core locations.

Core ID	Latitude [decimal degrees]	Longitude [decimal degrees]
PC1	20.0271	-155.8251
PC2	20.0272	-155.8252
PC3*	20.0270	-155.8250
SC1	20.0270	-155.8250
SC2	20.0272	-155.8242
SC3	20.0272	-155.8250
SC4	20.0274	-155.8235
SC6	20.0287	-155.8232
SC7	20.0276	-155.8263

* Core PC3 was used for subsequent geochemical analyses.

Table 6: Meteorological statistics.

[All statistics were calculated for 2010 Year Days 312.5–390; wind direction is "going to"]

Parameter	Mean ± 1 std. deviation	Minimum	Maximum
Barometric pressure [mb]	1012.95±1.99	1005.56	1017.75
Air temperature [^{o}C]	24.36±2.24	17.69	31.06
Precipitation [mm]	0.1±0.8	0	24.0
Wind speed [m/s]	1.83±1.45	0	8.25
Wind direction [^{o}]	196.8±98.9	0.1	359.8
Stream gauge depth [m]	0.14±0.13	0	1.00

Table 7: **Wave statistics.**

[All statistics were calculated for 2010 Year Days 310–390; wave direction is "from"]

Site Name	Parameter	Mean ± 1 std. deviation	Minimum	Maximum
North 15-m MiniProbe	Height [m]	0.52±0.39	0.15	2.92
	Period [s]	10.4±2.3	4.3	18.0
	Direction [º]	263.3±11.5	224.0	309.0
Central 15-m MiniProbe	Height [m]	0.72±0.57	0.16	4.12
	Period [s]	7.4±2.6	2.8	14.7
	Direction [º]	275.6±6.7	217.5	292.3
Central 5-m MiniProbe	Height [m]	0.39±0.22	0.14	1.82
	Period [s]	6.1±1.4	2.9	10.8
	Direction [º]	269.1±15.0	8.2	324.9
Central 2-m MiniProbe	Height [m]	0.18±0.06	0.1	0.61
	Period [s]	4.0±0.7	2.6	7.8
	Direction [º]	224.6±24.8	1.3	342.3
South 15-m MiniProbe	Height [m]	0.57±0.43	0.15	3.00
	Period [s]	9.7±2.6	3.4	18.4
	Direction [º]	286.4±9.6	233.0	337.0
South 5-m MiniProbe	Height [m]	0.80±0.62	0.21	4.29
	Period [s]	7.1±1.4	3.6	11.8
	Direction [º]	291.1±7.6	256.4	320.9

Table 8: Current statistics.

[All statistics were calculated for 2010 Year Days 310–390; current direction is "going to;" N.S. = near surface, N.B. = near bed]

Site Name	Parameter	Depth [m]	Mean ± 1 std. deviation	Minimum	Maximum
North 15-m MiniProbe	Speed [m/s]	2 [N.S.]	0.01±0.04	0.00	0.34
	Direction [º]	2 [N.S.]	106.8±104.8	0.0	359.6
	Speed [m/s]	13 [N.B.]	0.01±0.02	0.00	0.19
	Direction [º]	13 [N.B.]	119.2±103.1	0.0	359.7
Central 15-m MiniProbe	Speed [m/s]	2 [N.S.]	0.03±0.04	0.00	0.32
	Direction [º]	2 [N.S.]	153.2±85.2	0.0	359.9
	Speed [m/s]	13 [N.B.]	0.02±0.02	0.00	0.08
	Direction [º]	13 [N.B.]	133.3±62.6	0.0	359.5
Central 5-m MiniProbe	Speed [m/s]	2 [N.S.]	0.013±0.09	0.00	0.84
	Direction [º]	2 [N.S.]	251.4±89.8	0.0	359.9
	Speed [m/s]	4 [N.B.]	0.01±0.05	0.00	0.58
	Direction [º]	4 [N.B.]	163.4±88.5	0.0	359.5
Central 2-m MiniProbe	Speed [m/s]	1 [N.S.]	N.D.±N.D.	N.D.	N.D.
	Direction [º]	1 [N.S.]	N.D.±N.D.	N.D.	N.D.
	Speed [m/s]	3 [N.B.]	N.D.±N.D.	N.D.	N.D.
	Direction [º]	3 [N.B.]	N.D.±N.D.	N.D.	N.D.
South 15-m MiniProbe	Speed [m/s]	2 [N.S.]	0.01±0.05	0.00	0.35
	Direction [º]	2 [N.S.]	289.6±113.7	0.0	359.9
	Speed [m/s]	11 [N.B.]	0.01±0.02	0.00	0.16
	Direction [º]	11 [N.B.]	110.0±90.8	0.0	359.0
South 5-m MiniProbe	Speed [m/s]	2 [N.S.]	0.02±0.03	0.00	0.25
	Direction [º]	2 [N.S.]	279.0±87.3	0.0	359.9
	Speed [m/s]	4 [N.B.]	0.02±0.04	0.00	0.34
	Direction [º]	4 [N.B.]	324.5±103.0	0.0	359.9

Table 9: Temperature statistics.

[All statistics were calculated for 2010 Year Days 310–390]

Site Name	Depth [m]	Mean ± 1 std. deviation [ºC]	Minimum [ºC]	Maximum [ºC]
Central 15-m Mooring	2	25.78±0.48	24.45	27.01
Central 5-m Mooring	2	25.85±0.54	24.58	27.27
Central 5-m MiniProbe	5	25.81±0.51	24.23	27.08
Central 2-m MiniProbe	2	26.26±0.91	23.91	29.03
South 5-m MiniProbe*	5	25.84±0.47*	24.81*	26.92*

*Statistics were calculated for 2010 Year Days 310–381.

Table 10: Salinity statistics.

[All statistics were calculated for 2010 Year Days 310–390]

Site Name	Depth [m]	Mean ± 1 std. deviation [PSU]	Minimum [PSU]	Maximum [PSU]
Central 15-m Mooring	2	34.91±0.11	34.01	35.16
Central 5-m Mooring	2	34.85±0.12	32.94	35.21
Central 5-m MiniProbe	5	34.74±0.15	32.82	35.08
Central 2-m MiniProbe	2	30.99±0.93	24.99	33.20
South 5-m MiniProbe *	5	34.77±0.16*	32.51*	35.09*

*Statistics were calculated for 2010 Year Days 310-381.

Table 11: Turbidity statistics.

[All statistics were calculated for 2010 Year Days 310–390, removing 2010 Year Days 340.0–370.5 due to biofouling]

Site Name	Depth [m]	Mean ± 1 std deviation [NTU]	Minimum [NTU]	Maximum [NTU]
North 15-m MiniProbe	15	3.38±6.84	0.23	73.21
Central 15-m MiniProbe	15	7.25±14.77	0.12	204.61
Central 15-m Mooring	2	1.67±2.95	0.01	45.49
Central 5-m MiniProbe	5	13.49±21.07	0.36	232.23
Central 5-m Mooring	2	20.71±20.24	0.00	102.12
Central 2-m MiniProbe	2	7.35±30.92	1.60	1524.30
South 15-m MiniProbe	15	7.60±22.46	0.25	441.13
South 5-m MiniProbe	5	3.08±5.49	0.00	55.83

Table 12: **Water-column profiler statistics for the 6 November 2010 survey.**

Station ID	Mean temperature ± 1 std. deviation [^{o}C]	Mean salinity ± 1 std deviation [PSU]	Mean turbidity ± 1 std. deviation [NTU]	Mean light transmission ± 1 std. deviation [percent]	Mean fluorescence ± 1 std deviation [mg/m^3]
1	26.47±0.01	35.07±0.00	0.41±0.12	95.71±4.61	0.91±0.05
2	26.44±0.07	34.89±0.01	1.50±3.73	90.58±14.54	0.60±0.04
3	26.45±0.00	35.00±0.00	0.51±0.02	94.99±0.04	0.82±0.03
4	26.48±0.01	35.06±0.01	0.41±0.15	94.45±0.19	0.92±0.07
5	26.45±0.03	35.03±0.02	2.41±13.45	93.13±10.31	1.08±0.13
6	26.52±0.02	34.97±0.06	0.56±0.06	92.33±5.28	1.39±0.11
7	26.50±0.01	35.06±0.01	0.40±0.11	94.48±9.71	1.18±0.08
8	26.57±0.02	35.07±0.01	0.46±0.06	95.10±0.45	1.15±0.12
9	26.63±0.02	35.03±0.05	0.52±0.09	90.82±2.84	1.96±0.53
10	26.66±0.02	35.06±0.02	0.62±0.31	94.33±6.30	0.59±0.06
11	26.61±0.01	35.09±0.01	0.44±0.03	96.51±3.69	0.65±0.12
12	26.56±0.07	35.06±0.12	0.50±0.10	96.12±2.68	0.80±0.10
13	26.64±0.03	34.90±0.14	4.72±16.93	88.04±14.81	0.94±0.06
14	26.65±0.03	35.02±0.22	0.44±0.07	95.96±1.17	0.75±0.09
15	26.55±0.07	35.05±0.10	1.69±11.13	94.84±9.82	0.86±0.14
16	26.65±0.04	34.93±0.10	0.94±2.03	91.28±14.77	1.06±0.08
17	26.76±0.00	34.73±0.00	1.62±0.04	84.50±4.65	0.63±0.05
18	26.70±0.01	34.67±0.17	1.69±0.37	83.38±9.54	0.58±0.05
19	26.66±0.01	34.90±0.01	0.67±0.06	89.31±15.60	0.82±0.08
20	26.60±0.03	35.04±0.12	0.48±0.10	94.90±6.37	0.88±0.05
21	26.59±0.04	35.01±0.09	2.91±16.24	93.25±11.75	0.91±0.14
23	26.71±0.02	34.19±0.02	4.76±4.08	71.84±0.23	1.39±0.06
24	26.93±0.22	33.80±0.20	3.76±0.28	69.86±1.28	1.36±0.32
25	26.64±0.00	34.81±0.00	0.59±0.05	92.00±6.98	0.80±0.04
26	26.62±0.01	35.06±0.02	0.44±0.25	94.93±3.39	0.86±0.11
27	26.60±0.01	35.07±0.02	0.43±0.07	96.15±6.24	0.86±0.14
28	26.61±0.02	35.06±0.02	0.44±0.10	95.41±8.52	0.94±0.09
29	26.64±0.03	35.00±0.03	0.79±0.18	92.46±8.29	1.14±0.53
30	26.57±0.05	34.58±0.91	1.85±2.17	83.73±5.61	1.46±0.60
31	26.61±0.01	35.02±0.01	0.67±1.83	93.45±6.80	1.36±0.10
32	26.63±0.01	35.00±0.08	1.32±4.98	92.92±8.67	0.56±0.04
33	26.62±0.01	35.08±0.01	1.10±7.35	95.37±11.89	0.86±0.13
34	26.50±0.03	35.06±0.01	0.53±0.03	94.59±6.32	0.65±0.04

Table 13: **Water-column profiler statistics for the 10 March 2011 survey.**

Station ID	Mean temperature ± 1 std deviation [^{o}C]	Mean salinity ± 1 std. deviation [PSU]	Mean turbidity ± 1 std. deviation [NTU]	Mean light transmission ± 1 std. deviation [percent]	Mean fluorescence ± 1 std deviation [mg/m^3]
1	25.12±0.006	34.55±0.01	1.12±5.92	94.35±11.68	0.48±0.07
2	25.13±0.069	34.37±0.06	0.48±0.59	92.74±12.84	0.28±0.04
3	25.20±0.028	34.42±0.06	1.60±4.03	93.49±8.29	0.30±0.03
4	25.24±0.023	34.59±0.01	2.41±5.57	95.64±8.53	0.27±0.05
5	25.16±0.011	34.48±0.05	0.59±0.71	93.69±11.72	0.33±0.05
6	25.22±0.005	34.47±0.02	4.24±17.64	94.56±6.68	0.29±0.03
7	25.25±0.006	34.59±0.01	1.00±6.89	93.96±9.83	0.26±0.05
8	25.29±0.034	34.57±0.01	0.41±1.84	94.94±5.92	0.20±0.04
9	25.26±0.033	34.49±0.06	3.71±12.26	92.03±14.22	0.33±0.03
10	25.32±0.043	34.53±0.05	3.20±12.54	93.52±10.30	0.31±0.02
11	25.29±0.031	34.58±0.00	0.66±1.24	95.32±8.51	0.28±0.03
12	25.28±0.023	34.60±0.01	0.32±0.13	96.13±7.00	0.31±0.05
13	25.53±0.121	34.32±0.23	4.58±14.26	90.62±14.81	0.43±0.10
14	25.32±0.003	34.60±0.00	0.38±0.44	93.33±11.30	0.30±0.04
15	25.29±0.014	34.58±0.01	1.19±7.06	94.49±7.09	0.29±0.06
16	25.39±0.035	34.54±0.03	6.65±24.52	91.35±11.07	0.27±0.02
17	25.48±0.008	34.38±0.08	6.95±14.50	79.79±15.88	0.34±0.06
18	25.62±0.070	34.35±0.08	3.18±0.95	76.15±3.31	0.63±0.09
19	25.40±0.008	34.55±0.02	7.52±20.38	91.24±13.64	0.35±0.02
20	25.31±0.012	34.59±0.02	0.42±0.24	94.50±0.17	0.34±0.06
21	25.33±0.034	34.59±0.01	1.22±7.60	94.16±1.96	0.32±0.08
23	26.13±0.070	34.05±0.15	3.80±2.77	70.47±11.92	0.83±0.13
24	26.49±0.012	33.73±0.12	20.24±20.24	44.79±8.22	1.77±0.10
25	25.53±0.012	34.49±0.01	6.17±15.33	95.09±1.54	0.25±0.02
26	25.35±0.057	34.58±0.01	0.33±0.05	94.95±11.84	0.23±0.03
27	25.29±0.033	34.59±0.02	1.07±6.94	93.45±3.39	0.28±0.08
28	25.32±0.018	34.58±0.00	0.38±0.76	96.09±6.24	0.29±0.04
29	25.43±0.117	34.60±0.03	1.57±7.94	93.15±8.52	0.41±0.12
30	25.30±0.005	34.57±0.01	0.99±3.83	95.48±8.29	0.20±0.02
31	25.28±0.022	34.58±0.01	0.67±3.71	92.91±5.61	0.28±0.04
32	25.27±0.025	34.58±0.02	1.36±3.41	95.39±6.80	0.19±0.02
33	25.25±0.007	34.58±0.01	1.73±12.62	96.08±8.67	0.23±0.04
34	25.05±0.057	34.32±0.27	0.70±1.99	93.79±11.89	0.25±0.07

Table 14. Sediment trap location and depth information.

[Note: simple tube traps (STT) were deployed with their openings 0.4 m above the seabed; the rotary sediment trap (RST) was deployed with its opening 1.4 m above the seabed, hence the different orders of magnitude in the collection rates between trap types]

USGS Sample Identifier	Site name	Sample type	Average trap collection rate [mg/cm^2/day]	Latitude [decimal degrees]	Longitude [decimal degrees]	Depth [m]
BI-0311-13	Central 2 m	STT	156.70	20.02709	-155.82425	2
BI-0311-14	South 15 m	STT	531.91	19.98671	-155.83380	15
BI-0311-15	North 15 m	STT	501.55	20.02923	-155.83551	15
BI-0311-16	Central 5 m	STT	306.34	20.02330	-155.82774	5
BI-0311-17	South 5 m	STT	537.24	20.01173	-155.82702	5
BI-0311-18	Central 15 m	STT	359.10	20.01947	-155.83154	15
BI-0311-19	Central 5 m	RST	0.01	20.02330	-155.82774	5
BI-0311-20	Central 5 m	RST	0.02	20.02330	-155.82774	5
BI-0311-21	Central 5 m	RST	1.23	20.02330	-155.82774	5
BI-0311-22	Central 5 m	RST	0.27	20.02330	-155.82774	5
BI-0311-23	Central 5 m	RST	0.19	20.02330	-155.82774	5
BI-0311-24	Central 5 m	RST	0.20	20.02330	-155.82774	5
BI-0311-25	Central 5 m	RST	0.30	20.02330	-155.82774	5
BI-0311-26	Central 5 m	RST	0.11	20.02330	-155.82774	5
BI-0311-27	Central 5 m	RST	0.49	20.02330	-155.82774	5
BI-0311-28	Central 5 m	RST	0.14	20.02330	-155.82774	5
BI-0311-29	Central 5 m	RST	1.05	20.02330	-155.82774	5
BI-0311-30	Central 5 m	RST	7.92	20.02330	-155.82774	5
BI-0311-31	Central 5 m	RST	3.20	20.02330	-155.82774	5
BI-0311-32	Central 5 m	RST	12.91	20.02330	-155.82774	5

Table 15. Sediment trap grain size and composition information.

USGS Sample Identifier	Sand [percent]	Silt [percent]	Clay [percent]	Mean size [mm]	Carbonate [percent]	Terrigenous [percent]
BI-0311-13	6.61	71.50	21.79	0.011	6.72	93.28
BI-0311-14	88.64	7.47	3.36	0.137	83.74	16.26
BI-0311-15	95.59	1.87	1.60	0.188	94.31	5.69
BI-0311-16	83.74	10.45	5.53	0.194	90.38	9.62
BI-0311-17	93.01	3.87	1.96	0.179	76.01	23.99
BI-0311-18	80.74	10.60	5.17	0.135	89.82	10.18
BI-0311-19	3.53	66.04	30.42	0.008	34.85	65.15
BI-0311-20	3.11	63.53	33.36	0.008	45.92	54.08
BI-0311-21	9.16	70.26	20.59	0.011	43.25	56.75
BI-0311-22	8.77	66.28	24.95	0.010	37.73	62.27
BI-0311-23	7.53	74.80	17.67	0.012	31.46	68.54
BI-0311-24	9.99	72.84	17.17	0.013	35.41	64.59
BI-0311-25	10.03	69.06	20.92	0.012	57.85	42.15
BI-0311-26	8.19	64.23	27.57	0.010	60.13	39.87
BI-0311-27	8.78	62.90	28.32	0.010	61.55	38.45
BI-0311-28	6.84	61.67	31.49	0.009	62.42	37.58
BI-0311-29	9.40	68.12	22.48	0.011	63.93	36.07
BI-0311-30	37.90	42.70	19.33	0.022	80.68	19.32
BI-0311-31	18.09	59.86	22.05	0.013	75.61	24.39
BI-0311-32	80.21	13.09	5.80	0.150	92.33	7.67

Table 16. Seabed sample location and depth information.

USGS Sample Identifier	Site Name	Sample Type	Latitude [decimal degrees]	Longitude [decimal degrees]	Depth [m]
BI-0311-1 – S15	South 15 m	Grab	19.98671	-155.83380	15
BI-0311-2 – C5	Central 5 m	Grab	20.02330	-155.82774	5
BI-0311-3 – N15	North 15 m	Grab	20.02923	-155.83551	15
BI-0311-4 – C15	Central 15 m	Grab	20.01947	-155.83154	15
BI-0311-5 – S5	South 5 m	Grab	20.01173	-155.82702	5
BI-0311-6 – C2	Central 2 m	Grab	20.02709	-155.82425	2

Table 17. Seabed grain size and composition.

USGS Sample Identifier	Sand [percent]	Silt [percent]	Clay [percent]	Mean Size [mm]	Carbonate [percent]	Terrigenous [percent]
BI-0311-1 – S15	98.72	0.77	0.16	0.225	89.65	10.35
BI-0311-2 – C5	99.21	0.22	0.15	0.477	96.15	3.85
BI-0311-3 – N15	98.17	0.47	0.27	0.254	96.83	3.17
BI-0311-4 – C15	90.16	0.19	0.18	0.682	94.99	5.01
BI-0311-5 – S5	98.67	0.27	0.16	0.450	47.54	52.46
BI-0311-6 – C2	84.30	7.58	6.94	0.105	49.08	50.92

Table 18: Geochronologic results for core PC3.

Mid depth [cm]	Mass depth [g/cm^2]	Cum. mass [g/cm^2]	Total ^{210}Pb ± 1 std. deviation [dpm/g]	Total ^{226}Ra ± 1 std. deviation [dpm/g]	Excess ^{210}Pb [dpm/g]	Total ^{137}Cs [dpm/g]	Linear sed. rate [cm/yr]	Mass accumulation rate [mg/cm^2/yr]	Avg. year interval ± 1 std. deviation [A.D.]
0.5	1.26	1.26	3.53±0.33	0.32±0.07	3.22	0.16	-	-	-
2.5	1.24	2.50	3.46±0.40	0.49±0.05	2.97	0.19	-	-	-
4.5	1.25	3.74	3.90±0.51	0.24±0.08	3.65	0.16	-	-	-
6.5	1.18	4.93	3.89±0.42	0.53±0.07	3.36	0.18	-	-	-
8.5	1.30	6.23	3.27±0.47	0.42±0.07	2.85	0.18	-	-	-
11	1.33	7.56	3.80±0.25	0.52±0.06	3.27	0.18	2.48	550.28	2008.8±1.1
13	1.29	8.85	3.80±0.50	0.57±0.07	3.23	0.21	1.36	475.74	2003.6±0.9
15	1.29	10.14	3.79±0.56	0.58±0.09	3.21	0.18	0.95	397.58	1997.7±0.9
17	1.22	11.35	3.34±0.51	0.48±0.07	2.86	0.17	0.77	364.39	1991.1±1.1
19	1.25	12.60	3.37±0.48	0.49±0.09	2.88	0.17	0.62	284.68	1983.3±1.5
21	1.19	14.99	2.78±0.63	0.42±0.08	2.36	0.20	0.53	263.01	1974.3±2.3
23	1.25	17.48	2.75±0.61	0.52±0.07	2.23	0.21	0.44	200.42	1963.5±4.0
25	1.32	20.12	2.23±0.36	0.54±0.07	1.70	0.26	0.37	170.88	1949.3±7.1
28	1.15	22.41	1.80±0.35	0.26±0.06	1.54	0.17	-	-	-

Table 19: **Wave-current critical shear stress statistics.**

Site name	Condition [time period, in 2010 Year Days]	Depth [m]	Mean shear stress ± 1 std. deviation [N/m^2]	Time shear stress exceeded threshold for suspension of silt-sized particles [percent]	Time shear stress exceeded threshold for suspension of clay-sized particles [percent]
North 15-m	Experiment [310–390]	15	0.22±0.34	19.68	44.82
	Trade winds [317–320]	15	0.09±0.05	0.62	22.45
	Wave resuspension [380–383]	15	0.79±0.63	80.08	99.17
Central 15-m	Experiment [310–390]	15	0.34±0.50	31.65	58.40
	Trade winds [317–320]	15	0.12±0.46	1.60	41.60
	Wave resuspension [380–383]	15	1.19±0.91	95.40	99.59
Central 5-m	Experiment [310–390]	5	0.26±0.38	20.15	62.05
	Trade Winds [317–320]	5	0.15±0.06	3.12	59.67
	Wave resuspension [380–383]	5	0.65±0.57	75.52	99.17
Central 2-m*	Experiment [310–390]	1	0.08±0.08	4.74	20.09
	Trade winds [317–320]	1	0.09±0.06	1.37	26.03
	Wave resuspension [380–383]	1	0.29±0.13	52.05	89.04
South 15-m	Experiment [310–390]	15	0.24±0.36	22.44	46.75
	Trade winds [317–320]	15	0.09±0.05	0.83	18.50
	Wave resuspension [380–383]	15	0.85±0.67	83.40	99.59
South 5-m	Experiment [310–390]	5	0.80±1.25	61.17	85.27
	Trade winds [317–320]	5	0.30±0.13	57.59	84.8
	Wave resuspension [380–383]	5	2.88±2.15	100.00	100.00

*Statistics were calculated using a proxy current velocity of 0.025 m/s and average wave periods

Table 20: Suspended-sediment flux statistics.

Site Name	Condition [time period, in 2010 Year Days]	Depth [m]	Average daily suspended-sediment flux [metric tons/m²]	Direction of transport [°True]
North 15-m MiniProbe	Experiment [310–390]	15	3.67	87.36
	Trade winds [317–320]	15	0.07	145.27
	Flood [322–325]	15	0.07	9.04
	Wave resuspension [380–383]	15	2.48	94.19
Central 15-m MiniProbe	Experiment [310–390]	15	20.64	147.95
	Trade winds [317–320]	15	0.10	119.65
	Flood [322–325]	15	0.24	156.40
	Wave resuspension [380–383]	15	4.05	161.68
Central 15-m Mooring	Experiment [310–390]	2	8.63	128.39
	Trade winds [317–320]	2	0.14	148.72
	Flood [322–325]	2	0.07	247.64
	Wave resuspension [380–383]	2	5.52	112.93
Central 5-m MiniProbe	Experiment [310–390]	5	58.04	248.16
	Trade winds [317–320]	5	0.21	95.96
	Flood [322–325]	5	1.08	120.53
	Wave resuspension [380–383]	5	49.38	259.24
Central 5-m mooring	Experiment [310–390]	2	133.93	266.37
	Trade winds [317–320]	2	0.03	64.67
	Flood [322–325]	2	0.07	130.13
	Wave resuspension [380–383]	2	95.97	277.51
Central 2-m MiniProbe	Experiment [310–390]	1	N.D.*	N.D.*
	Trade winds [317–320]	1	N.D.*	N.D.*
	Flood [322–325]	1	N.D.*	N.D.*
	Wave resuspension [380–383]	15	N.D.*	N.D.*
South 15-m MiniProbe	Experiment [310–390]	15	5.41	147.65
	Trade winds [317–320]	15	0.03	21.49
	Flood [322–325]	15	0.03	128.51
	Wave resuspension [380–383]	15	4.51	218.80
South 5-m MiniProbe	Experiment [310–390]	5	37.33	358.20
	Trade winds [317–320]	5	0.24	333.50
	Flood [322–325]	5	0.94	332.26
	Wave resuspension [380–383]	5	18.26	5.05

*N.D. = No data.

Appendix 1. Acoustic Doppler Current Profiler (ADCP) Information

RD Instruments 600 kHz Workhorse Monitor upward-looking acoustic Doppler current profiler
s/n: 2074

Transmitting Frequency:	614 kHz
Depth of Transducer:	12.8 m
Blanking Distance:	0.25 m
Height of First Bin above Transducer:	1.45 m
Bin Size:	1.0 m
Number of Bins:	18
Operating Mode:	High-resolution, broad bandwidth
Sampling Frequency:	2 Hz
Time per Ping:	00:04.00
Pings per Ensemble:	50
Profile Ensemble Interval:	0:15:00.00
Wave Ensemble Interval:	1:00:00.00
Sound Speed Calculation:	Set salinity, updating temperature via sensor

RD Instruments 600 kHz Workhorse Monitor upward-looking acoustic Doppler current profiler
s/n: 2432

Transmitting Frequency:	614 kHz
Depth of Transducer:	13.6 m
Blanking Distance:	0.25 m
Height of First Bin above Transducer:	1.45 m
Bin Size:	1.0 m
Number of Bins:	18
Operating Mode:	High-resolution, broad bandwidth
Sampling Frequency:	2 Hz
Time per Ping:	00:04.00
Pings per Ensemble:	50
Profile Ensemble Interval:	0:15:00.00
Wave Ensemble Interval:	1:00:00.00
Sound Speed Calculation:	Set salinity, updating temperature via sensor

Nortek Instruments 2 MHz Aquadopp upward-looking acoustic Doppler current profiler
s/n: 1861

Transmitting Frequency:	2 MHz
Depth of Transducer:	5 m
Blanking Distance:	0.20 m
Height of First Bin above Bed:	1.00 m
Bin Size:	0.5 m

Number of Bins:	12
Average interval:	0:08:00.00
Profile interval:	0:15:00.00
Wave interval:	1:00:00.00
Wave cell size:	0.5 m
Operating Mode:	High-resolution
Sound Speed Calculation:	Set salinity, updating temperature via sensor

Nortek Instruments 2 MHz Aquadopp upward-looking acoustic Doppler current profiler
s/n: 1852

Transmitting Frequency:	2 MHz
Depth of Transducer:	5 m
Blanking Distance:	0.20 m
Height of First Bin above Bed:	1.00 m
Bin Size:	0.5 m
Number of Bins:	12
Average interval:	0:08:00.00
Profile interval:	0:15:00.00
Wave interval:	1:00:00.00
Wave cell size:	0.5 m
Operating Mode:	High-resolution
Sound Speed Calculation:	Set salinity, updating temperature via sensor

Nortek Instruments 2 MHz Aquadopp upward-looking acoustic Doppler current profiler
s/n: 1757

Transmitting Frequency:	2 MHz
Depth of Transducer:	3 m
Blanking Distance:	0.20 m
Height of First Bin above Bed:	1.00 m
Bin Size:	0.5 m
Number of Bins:	10
Average interval:	0:08:00.00
Profile interval:	0:15:00.00
Wave interval:	1:00:00.00
Wave cell size:	0.5 m
Operating Mode:	High-resolution
Sound Speed Calculation:	Set salinity, updating temperature via sensor

Nortek Instruments 1 MHz AWAC upward-looking acoustic Doppler current profiler
s/n: 5156

Transmitting Frequency:	1 MHz
Depth of Transducer:	15 m
Blanking Distance:	0.40 m

Height of First Bin above Bed: 1.50 m
Bin Size: 1.00 m
Number of Bins: 18
Average interval: 0:06:00.00
Profile interval: 0:15:00.00
Wave interval: 1:00:00.00
Wave cell size: 1.8 m
Operating Mode: High-resolution
Sound Speed Calculation: Set salinity, updating temperature via sensor

Data Processing:

The RDI current data were processed using the WinADCP program and the wave data using the WavesMon program. The Nortek current data were processed using the Prof2NDP program and the wave data using the QuickWave program.

The data were averaged over 1 hour ensembles, all of the spurious data above the water surface were removed, and all of the data in bins where the beam correlation dropped below 80% were removed for visualization and analysis.

Appendix 2. Conductivity and Temperature (CT) Information

Seabird Microcat SBE-37SM temperature-conductivity (CT) sensors
s/n: 3800, 3801, 7046, and 7047
Sampling Frequency: 2 Hz
Measurements per Burst: 8
Time Between Bursts: 00:05:00.00

Data Processing:

The CT data were post-processed for visualization and analysis by removing all instantaneous (only one data point in time) data spikes that exceeded the deployment mean ± 3 standard deviations.

Appendix 3. Turbidity Sensor (SLOBS) Information

Aquatec/Seapoint 200-TY self-logging optical backscatter sensors (SLOBS)
s/n: 371-026
Aquatec/Seapoint 210-TYT self-logging optical backscatter sensors (SLOBS)
s/n: 024-002, 024-005, 024-006, 024-013, 024-018 ,024-052
Sampling Frequency: 2 Hz
Measurements per Burst: 8
Time Between Bursts: 00:05:00.00

Data Processing:

      The SLOBS data were post-processed for visualization and analysis by removing all instantaneous (only one data point in time) data spikes that exceeded the deployment mean ± 3 standard deviations.

Appendix 4. Weather Station (WS), Terrestrial Imaging System (TIS), and Coral Imaging System (CIS) Information

NovaLynx WS-16N-A Marine-grade Weather Station:

Anemometer:	200-05106-MA (marine model)
Temperature & Relative Humidity:	110-WS-16TH-A w/radiation shield
Barometric Pressure Sensor:	110-WS-16BP
Rain Gage:	110-WS-16RC
Sampling Frequency:	1 Hz
Measurements per Burst:	1800
Time Between Bursts:	00:30:00.00

USGS Terrestrial Imaging System

Camera:	Canon EOS Digital Rebel Xti 10.1 megapixel
Programmable Automated Controller:	Campbell Scientific Scientific CR200
Sampling Times:	07:00, 08:00, 09:00, 10:00, 11:00, 13:00, 15:00, and 17:00 HST

USGS Coral Imaging System

Camera:	Nikon CoolPix 8700 8-megapixel digital camera
Programmable Automated Controller:	Campbell Scientific Scientific CR200
Sampling Times:	00:00, 04:00, 08:00, 12:00, 16:00, and 20:00 HST

Appendix 5. Water-Column Profiler (WCP) Information

Conductivity/Temperature/Depth (CTD) Profiler with Optical Backscatter (OBS), Photosynthetically-Available Radiation (PAR), Dissolved Oxygen (DO), and Chlorophyll (chl) Sensors

Instruments:

Seabird 19plus CTD sensor; s/n:	5250
D&A Instruments OBS-3 sensor; s/n:	1134
Seabird pressure sensor; s/n:	2632709
Wet Labs CStar; s/n:	712
Sampling Frequency:	4 Hz

    Position Information:

        Garmin GPS-76 GPS; s/n: 80207465; USGS/CRP unit#1

Data Processing:
        The profiler data were processed using the SBEDataProcessing program.

        The data were averaged into 0.5 m vertical bins and all of the spurious data
        marked by a flag in the raw data were removed for visualization and analysis.
        Stratification were measured as the difference between the mean of the top
        three bins (0.5–1.5 m below the surface) and the bottom three bins (0.5–1.5 m
        above the bed).

Appendix 6. Water-Column Profiler (WCP) log: 6 November 2010

| Cast Number/Site	Date [MM/DD/YYY]	Time [HST]	Latitude [decimal degrees]	Longitude [decimal degrees]	Depth [m]
1	11/06/2010	09:57:46	20.0269961	-155.8242271	2
2	11/06/2010	10:03:30	20.0258809	-155.8241391	<1
3	11/06/2010	10:07:13	20.0248816	-155.8240163	<1
4	11/06/2010	10:11:02	20.0235571	-155.8238250	<1
5	11/06/2010	10:21:30	20.0117810	-155.8273887	16
6	11/06/2010	11:13:40	19.9443847	-155.8727774	28
7	11/06/2010	11:29:00	19.9785747	-155.8412896	70
8	11/06/2010	11:35:41	19.9758262	-155.8340876	12
9	11/06/2010	11:40:45	19.9815847	-155.8318523	14
10	11/06/2010	11:44:23	19.9844308	-155.8403968	60
11	11/06/2010	11:48:20	19.9869389	-155.8337882	38
12	11/06/2010	11:53:06	19.9922507	-155.8284970	16
13	11/06/2010	11:56:06	19.9931553	-155.8373494	62
14	11/06/2010	12:01:42	20.0052388	-155.8359194	63
15	11/06/2010	12:06:52	20.0043909	-155.8269207	15
16	11/06/2010	12:23:32	20.0122077	-155.8364979	68
17	11/06/2010	12:27:13	20.0177151	-155.8357232	93
18	11/06/2010	12:34:42	20.0170263	-155.8251168	10
19	11/06/2010	12:39:24	20.0194201	-155.8318590	35
20	11/06/2010	12:43:39	20.0231293	-155.8363725	103
21	11/06/2010	12:47:32	20.0249106	-155.8332369	68
22	11/06/2010	12:51:56	20.0232811	-155.8279341	15
23	11/06/2010	12:56:44	20.0260841	-155.8287010	15
24	11/06/2010	13:00:30	20.0264197	-155.8339061	50
25	11/06/2010	13:05:50	20.0289800	-155.8320484	12
26	11/06/2010	13:09:55	20.0290288	-155.8376493	91
27	11/06/2010	13:13:55	20.0293112	-155.8357052	43
28	11/06/2010	13:17:35	20.0353828	-155.8381160	111
29	11/06/2010	13:22:48	20.0380800	-155.8347245	20
30	11/06/2010	13:40:03	20.0494285	-155.8402751	30
31	11/06/2010	13:43:12	20.0479930	-155.8431138	70
32	11/06/2010	13:52:33	20.0655462	-155.8545657	20
33	11/06/2010	13:55:20	20.0644229	-155.8558560	86

Appendix 7. Water-column profiler (WCP) log: 10 March 2011

Cast Number/Site	Date [MM/DD/YYY]	Time [HST]	Latitude [decimal degrees]	Longitude [decimal degrees]	Depth [m]
1	03/10/2011	09:53:17	20.0654793	-155.8545055	22
2	03/10/2011	09:55:25	20.0643726	-155.8559496	85
3	03/10/2011	10:01:58	20.0479995	-155.8430153	67
4	03/10/2011	10:05:43	20.0495011	-155.8402219	28
5	03/10/2011	10:12:32	20.0381756	-155.8348914	28
6	03/10/2011	10:17:24	20.0353047	-155.8380641	110
7	03/10/2011	10:22:32	20.0288226	-155.8378312	126
8	03/10/2011	10:27:07	20.0293713	-155.8356479	42
9	03/10/2011	10:30:27	20.0290158	-155.8319154	9
10	03/10/2011	10:33:45	20.0263292	-155.8340037	50
11	03/10/2011	10:36:52	20.0248069	-155.8332565	67
12	03/10/2011	10:40:40	20.0231114	-155.8364469	110
13	03/10/2011	10:45:45	20.0175509	-155.8357611	108
14	03/10/2011	10:50:54	20.0194043	-155.8317982	35
15	03/10/2011	10:56:29	20.0233086	-155.8280029	13
16	03/10/2011	10:59:54	20.0261581	-155.8285829	13
17	03/10/2011	11:07:47	20.0237224	-155.8236656	7
18	03/10/2011	11:12:53	20.0248951	-155.8239361	6
19	03/10/2011	11:21:11	20.0269211	-155.8242938	3
20	03/10/2011	11:27:02	20.0256073	-155.8241111	5
21	03/10/2011	12:00:25	20.0170518	-155.8252093	11
22	03/10/2011	12:12:42	20.0121125	-155.8366229	67
23	03/10/2011	12:18:00	20.0116591	-155.8274271	19
24	03/10/2011	12:23:42	20.0045298	-155.8269249	14
25	03/10/2011	12:28:58	20.0052225	-155.8360652	68
26	03/10/2011	12:38:41	19.9929535	-155.8374674	63
27	03/10/2011	12:46:05	19.9920303	-155.8283855	16
28	03/10/2011	12:50:48	19.9869106	-155.8339371	27
29	03/10/2011	12:55:10	19.9844524	-155.8405241	70
30	03/10/2011	13:02:33	19.9814444	-155.8318827	16
31	03/10/2011	13:08:02	19.9759981	-155.8340725	18
32	03/10/2011	13:14:26	19.9785870	-155.8415335	71
33	03/10/2011	13:27:55	19.9443606	-155.8729729	28

Appendix 8. Topographic and bathymetric plots of Pelekane Bay
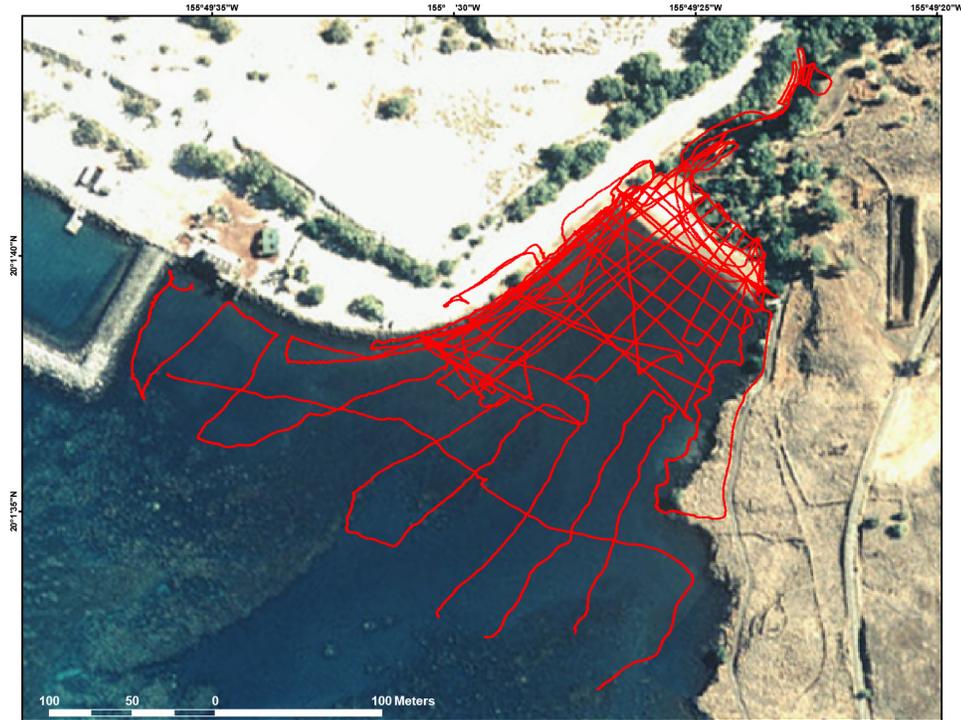
Appendix 8.1. Track lines from the topographic survey of the beach and nearshore portions of Pelekane Bay, Hawaii, conducted on March 11–12, 2011.
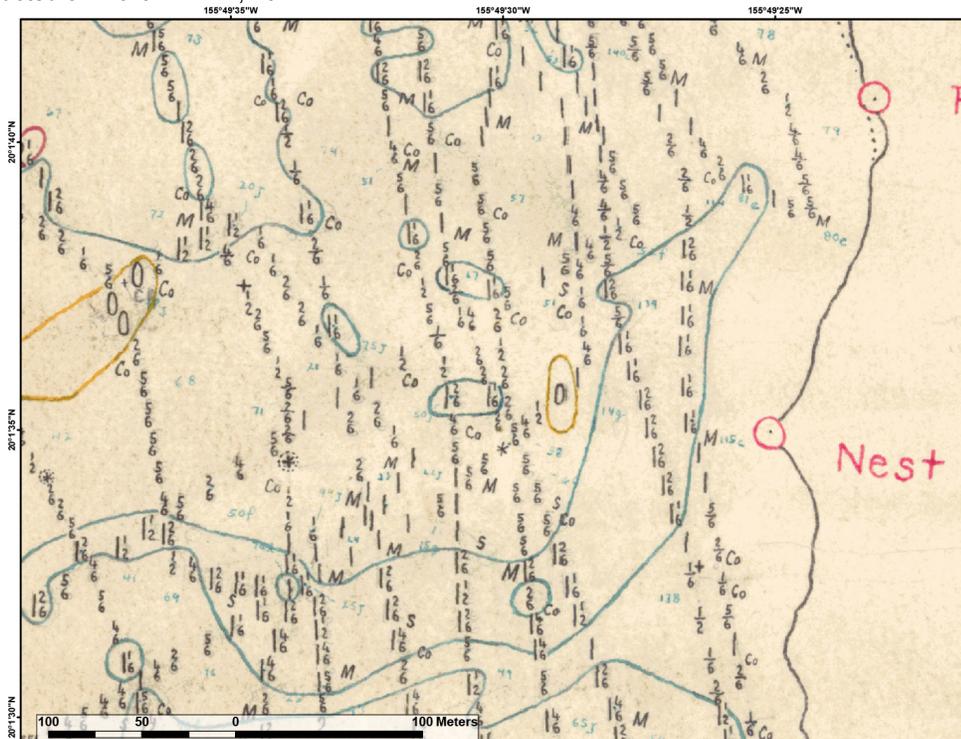
Appendix 8.2. Map showing the historical bathymetric data from the 1928 U.S. Coast and Geodetic Hydrographic Survey #5007. Sounding depths given in fathoms.

Appendix 9. Time-series plots of variations in water level, wave heights, wave periods, and wave directions from the acoustic Doppler current profilers (ADCPs)
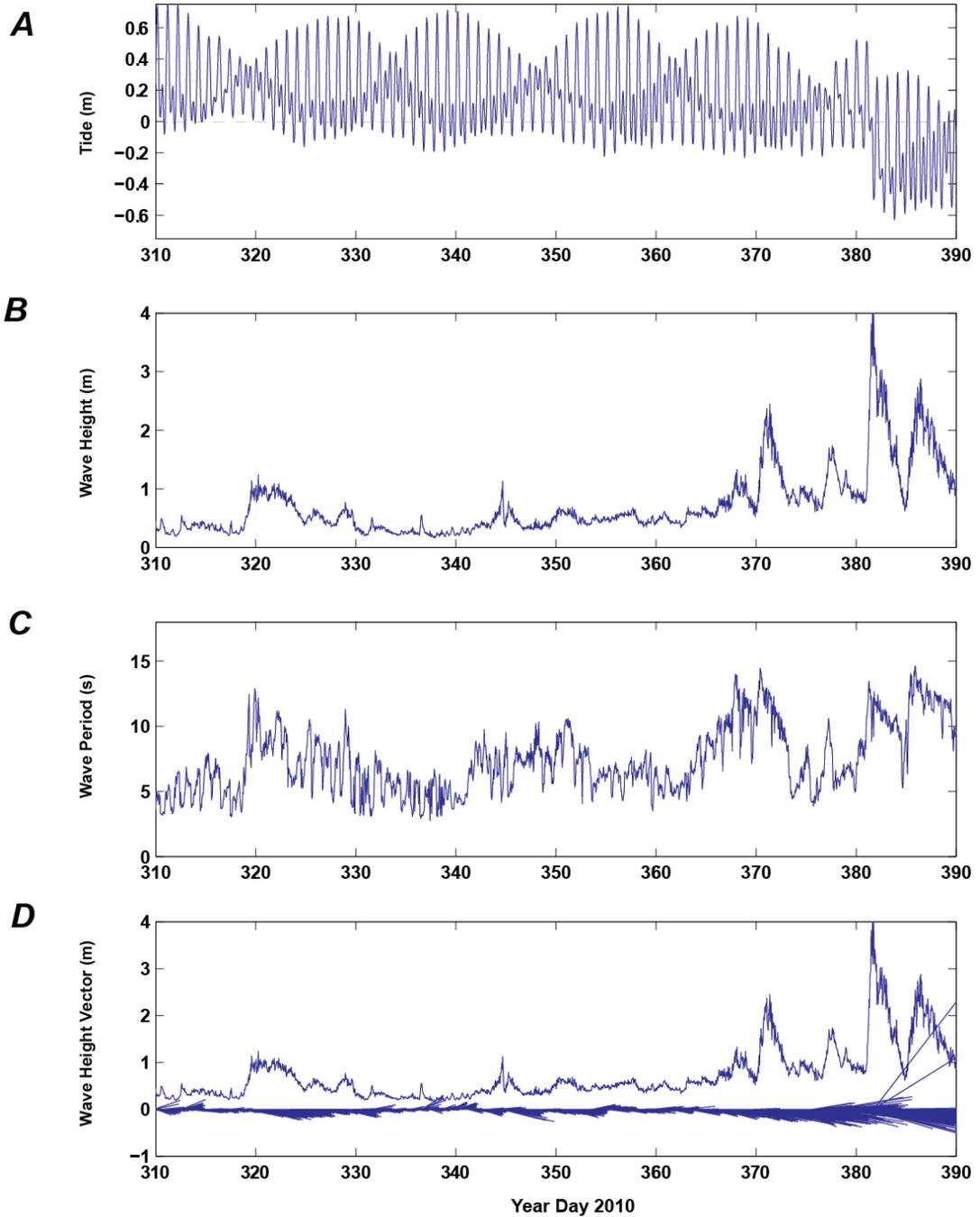
Appendix 9.1. Tide and wave data from the ADCP at Central 15-m site. *A*. Tidal height, in meters. *B*. Wave height, in meters. *C*. Wave period, in seconds. *D*. Wave height (red), in meters, and wave vectors (blue), with directions given as "going to," measured in degrees clockwise from true north.
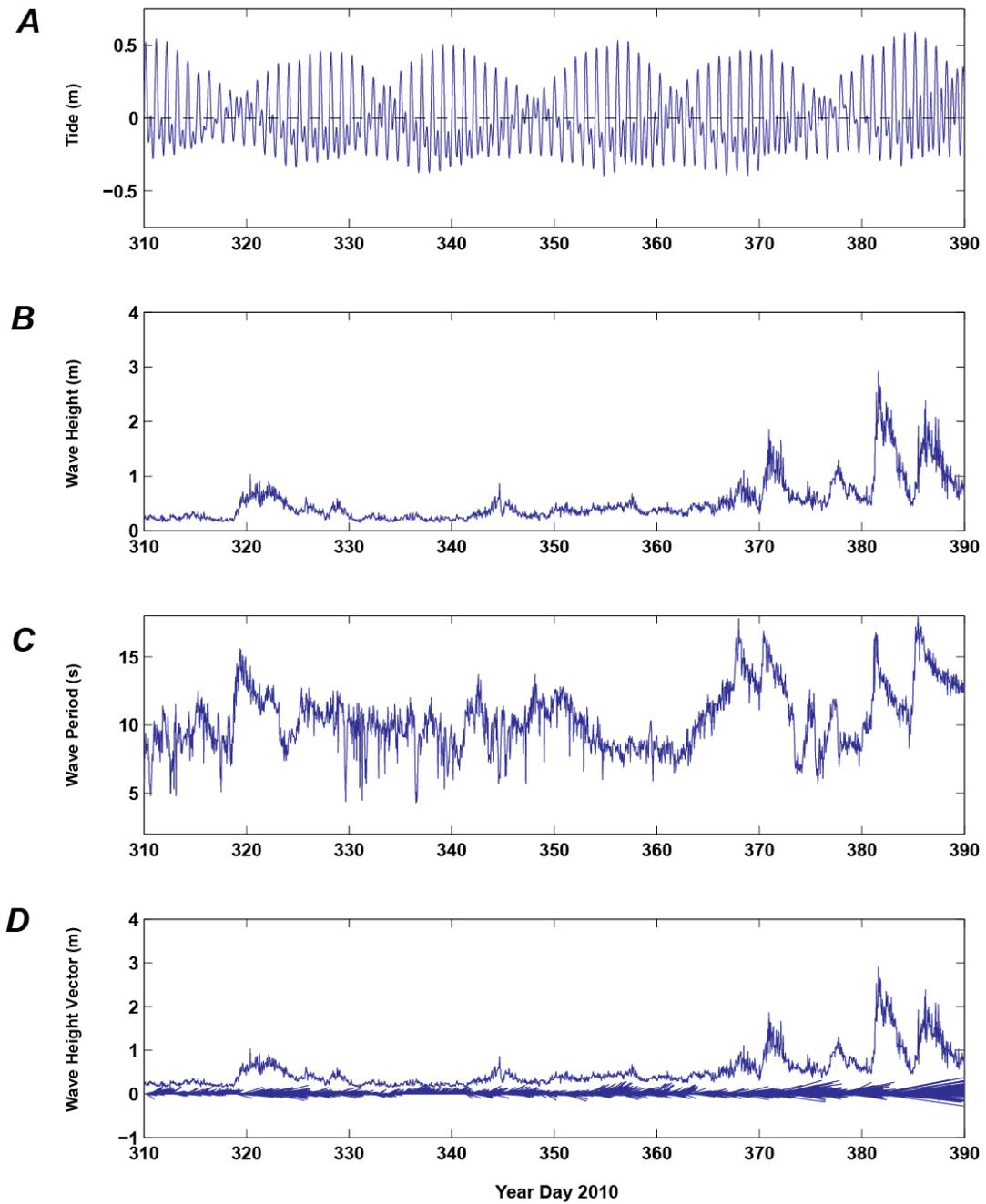
Appendix 9.2. Tide and wave data from the ADCP at the North 15-m site. *A*, Tidal height, in meters. *B*, Wave height, in meters. *C*, Wave period, in seconds. *D*, Wave height (red), in meters, and wave vectors (blue), with directions given as "going to," measured in degrees clockwise from true north.
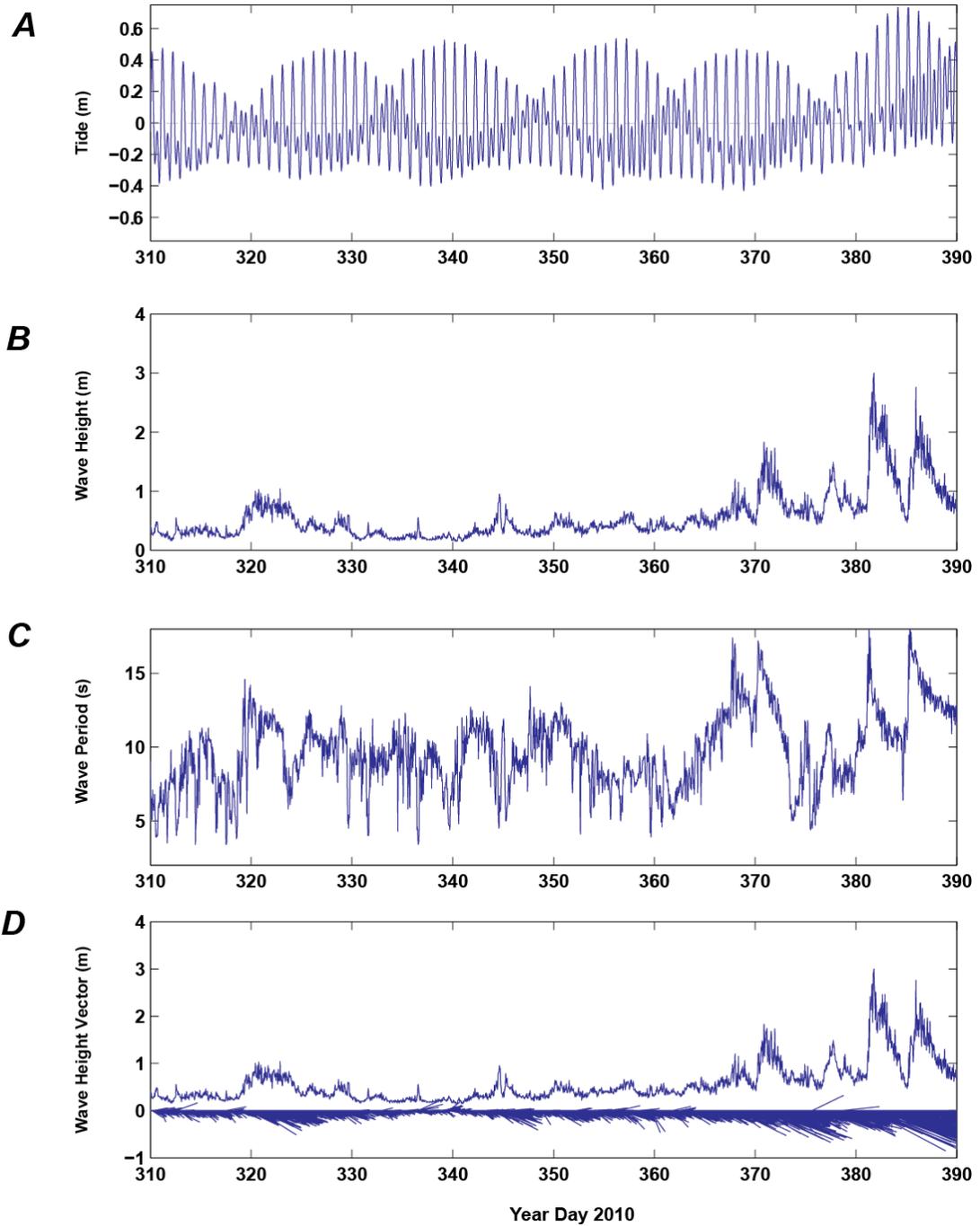
Appendix 9.3. Tide and wave data from the ADCP at the South 15-m site. *A*, Tidal height, in meters. *B*, Wave height, in meters. *C*, Wave period, in seconds. *D*, Wave height (red), in meters, and wave vectors (blue), with directions given as "going to," measured in degrees clockwise from true north.
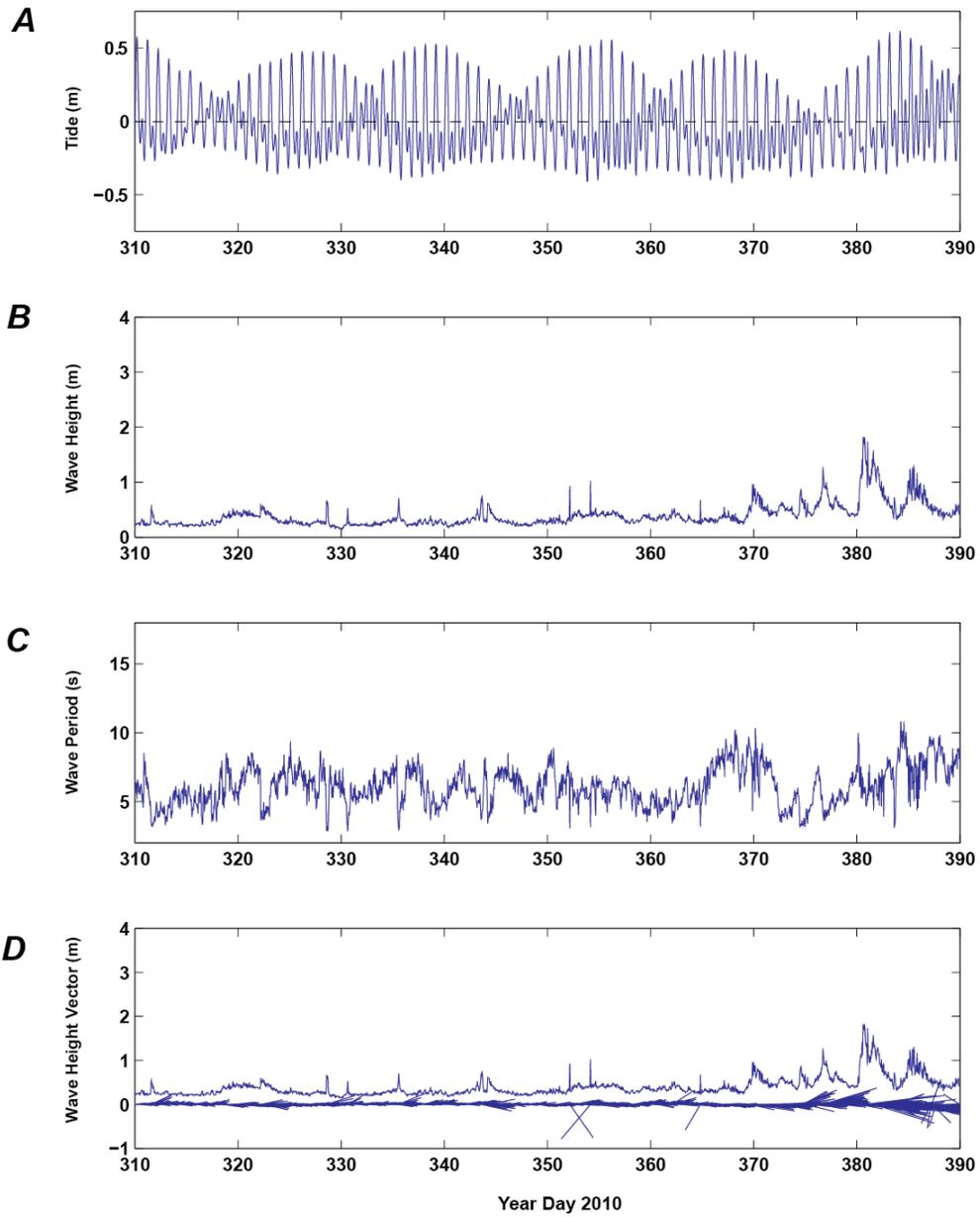
Appendix 9.4. Tide and wave data from the ADCP at the Central 5-m site. *A*, Tidal height, in meters. *B*, Wave height, in meters. *C*, Wave period, in seconds. *D*, Wave height (red), in meters, and wave vectors (blue), with direction given as "going to," measured in degrees clockwise from true north.
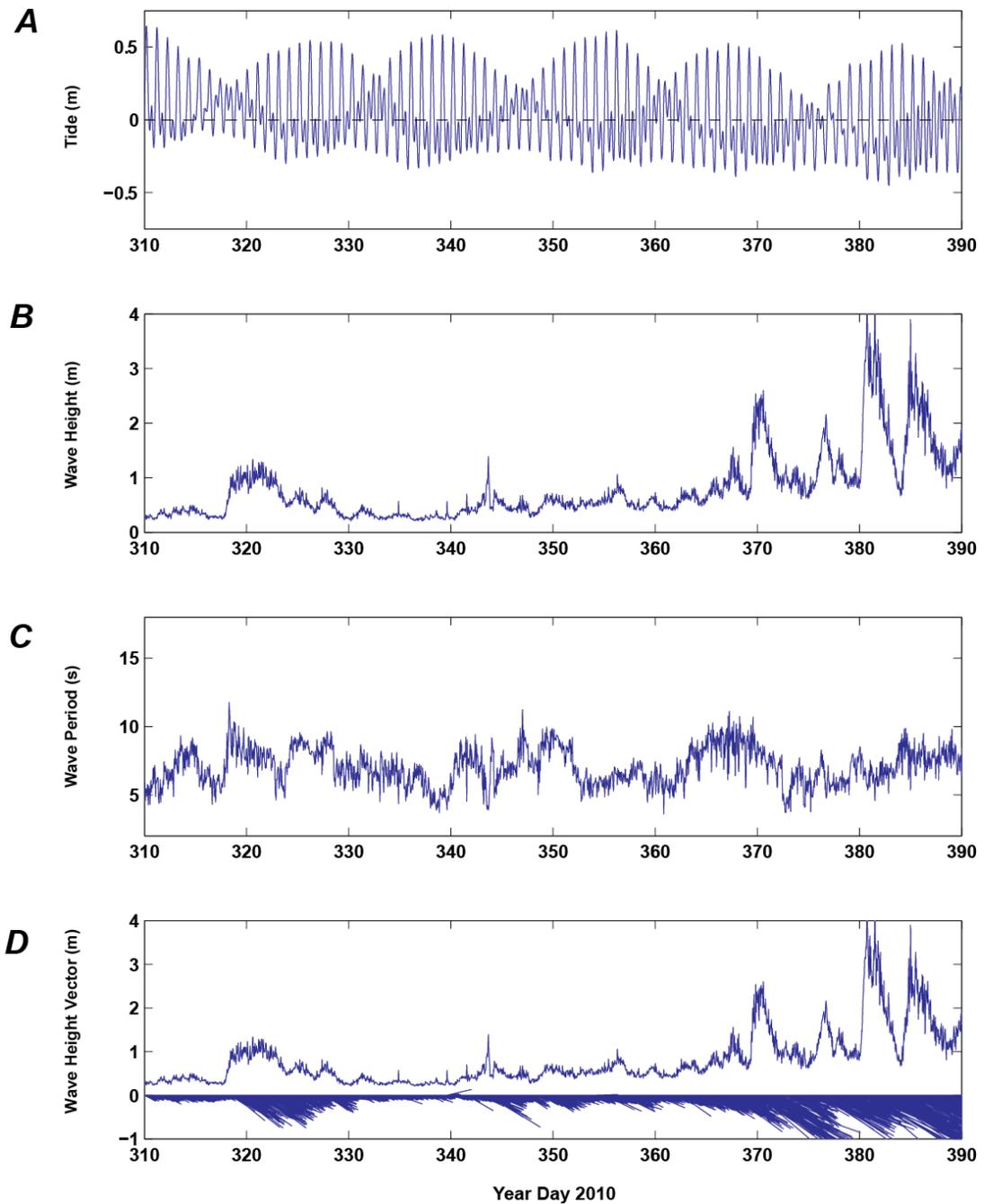
Appendix 9.5. Tide and wave data from the ADCP at the South 5-m site. *A*, Tidal height, in meters. *B*, Wave height, in meters. *C*, Wave period, in seconds. *D*, Wave height (red), in meters, and wave vectors (blue), with direction given as "going to," measured in degrees clockwise from true north.
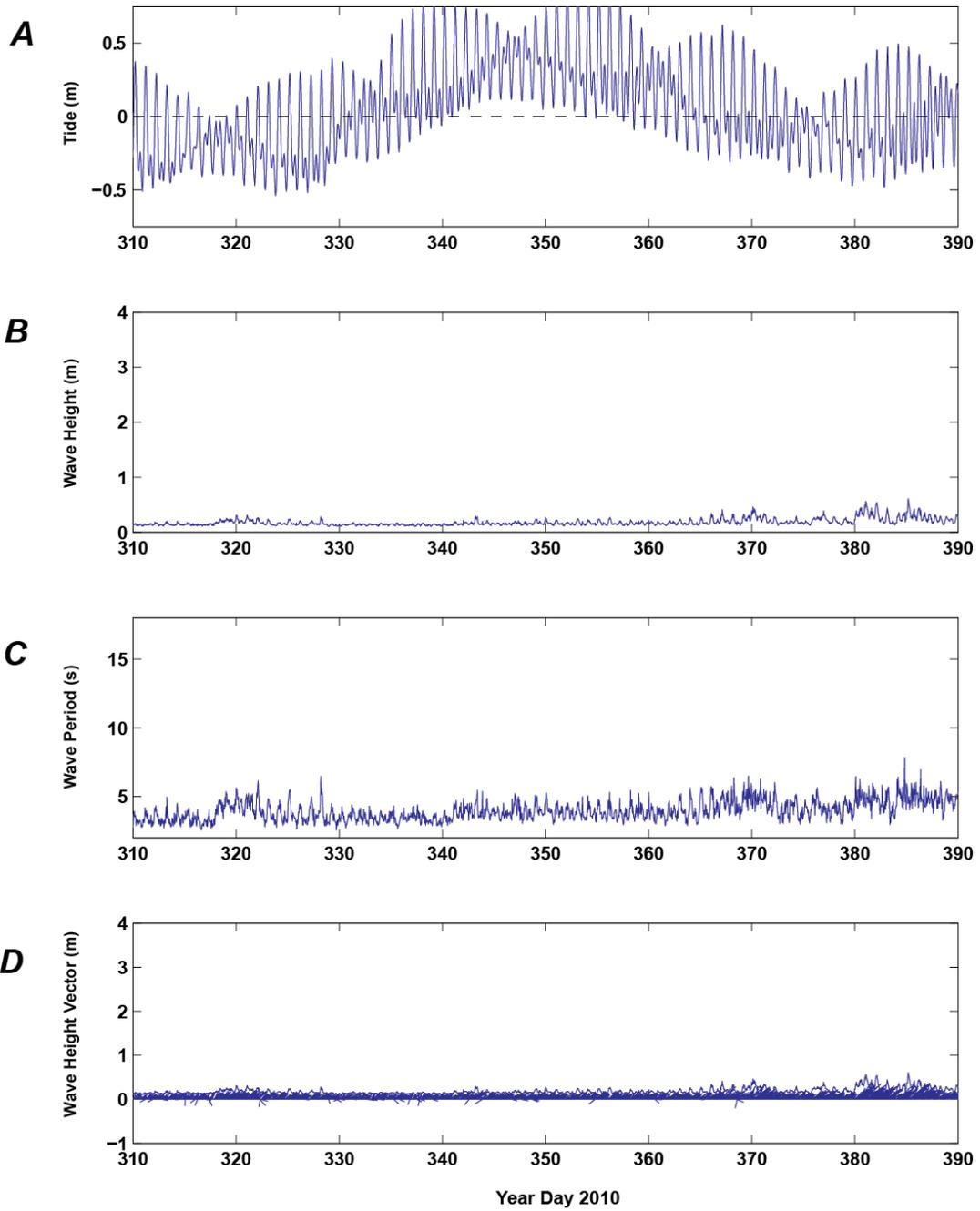
Appendix 9.6. Tide and wave data from the ADCP at the Central 2-m site. *A*, Tidal height, in meters. *B*, Wave height, in meters. *C*, Wave period, in seconds. *D*, Wave height (red), in meters, and wave vectors (blue), with direction given as "going to," measured in degrees clockwise from true north.

Appendix 10. Time-series plots of variations in water level, currents, and temperature from the acoustic Doppler current profilers (ADCPs).
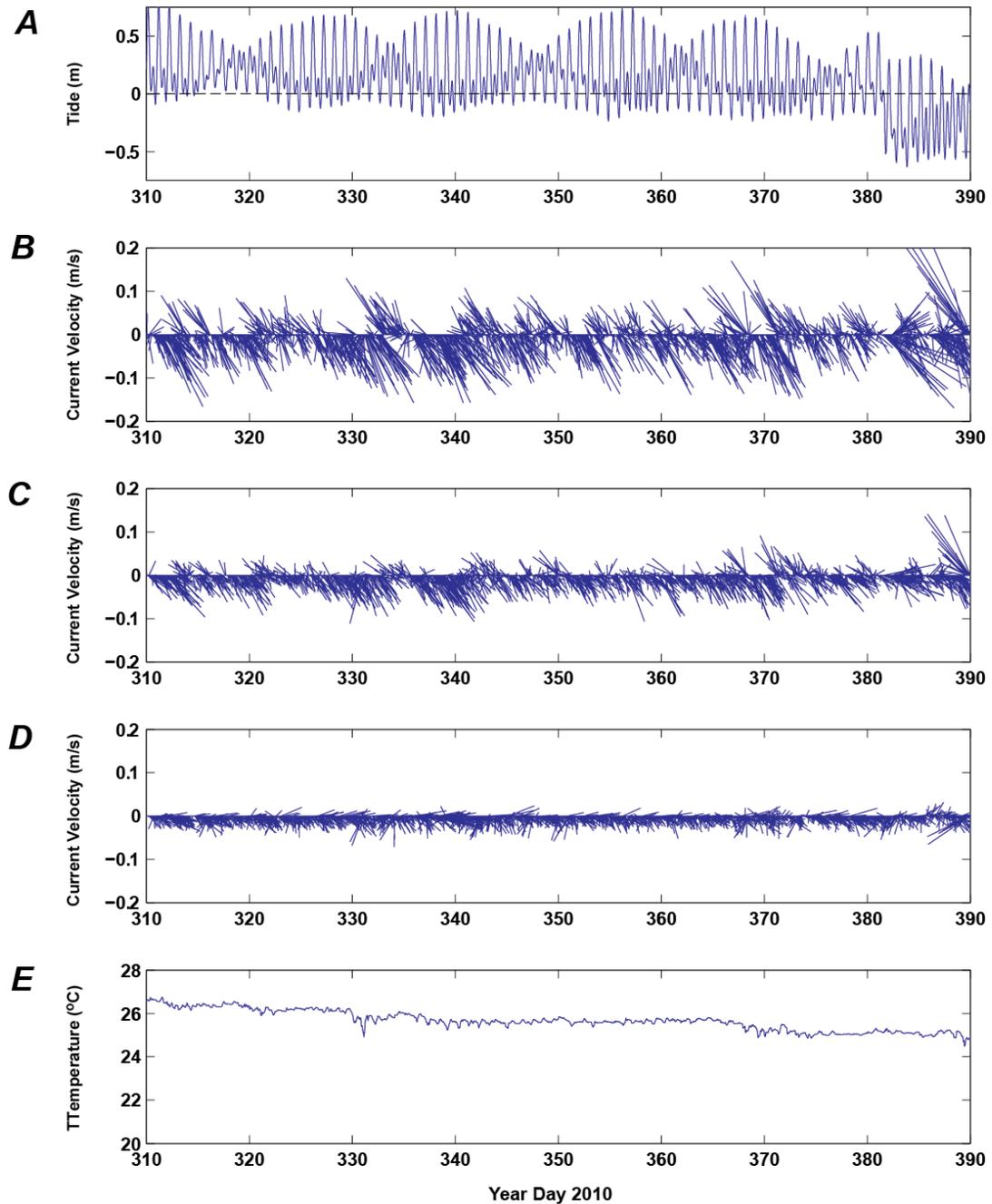

Appendix 10.1. Tide, current, and water temperature data from the ADCP at the Central 15-m site. *A*, Tidal height, in meters. *B*, Near-surface current velocity, with direction given in degrees clockwise from true north and speed given in meters per second. *C*, Mid-depth current velocity, with direction given in degrees clockwise from true north and speed given in meters per second. *D*, Near-bed current velocity, with direction given in degrees clockwise from true north and speed in meters per second. *E*, Water temperature, in degrees Celsius.
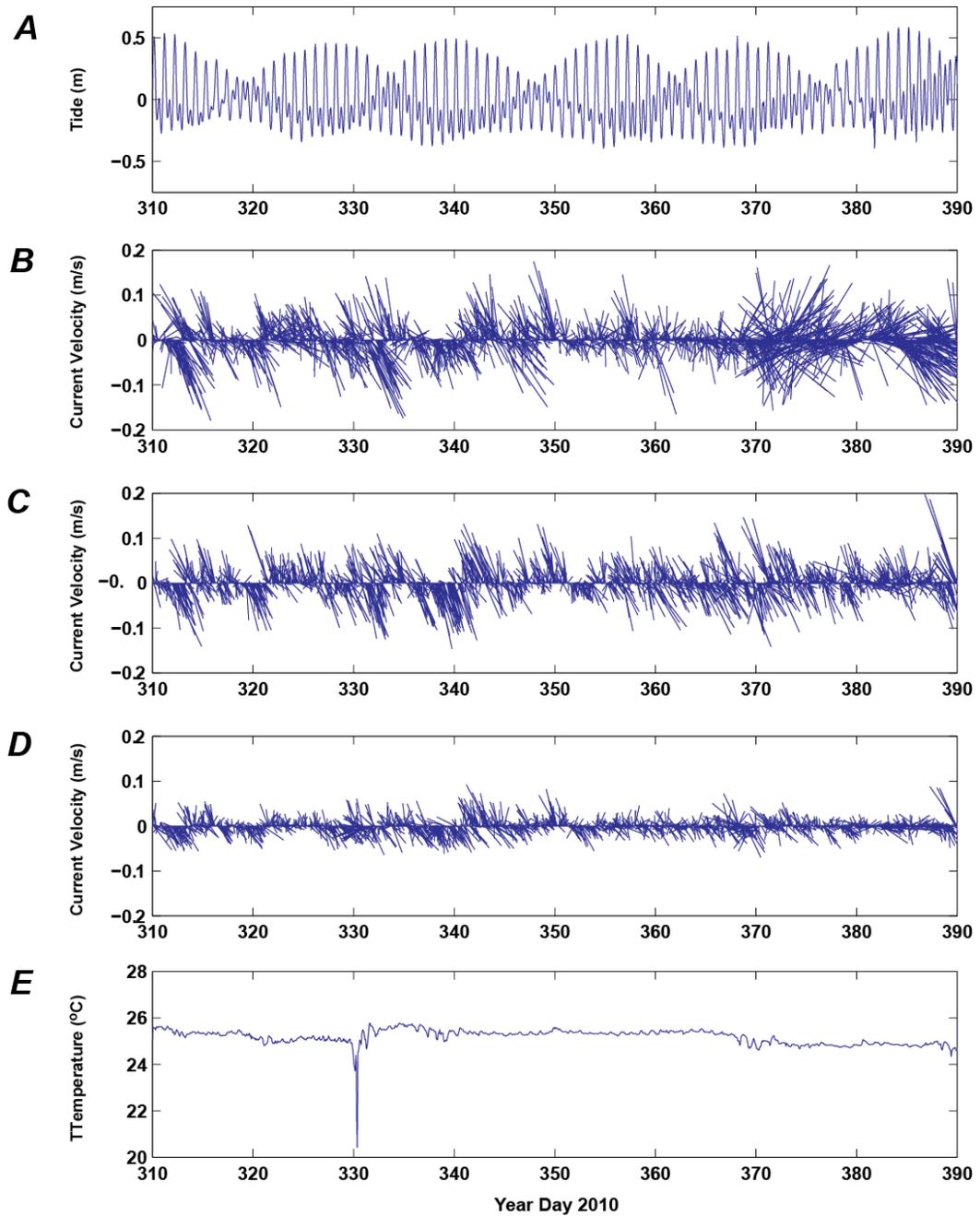
Appendix 10.2. Tide, current, and water temperature data from the ADCP at the North 15-m site. *A*, Tidal height, in meters. *B*, Near-surface current velocity, with direction in degrees from true north and speed in meters per second. *C*, Mid-depth current velocity, with direction in degrees from true north and speed in meters per second. *D*, Near-bed current velocity, with direction in degrees from true north and speed in meters per second. *E*, Water temperature, in degrees Celsius.
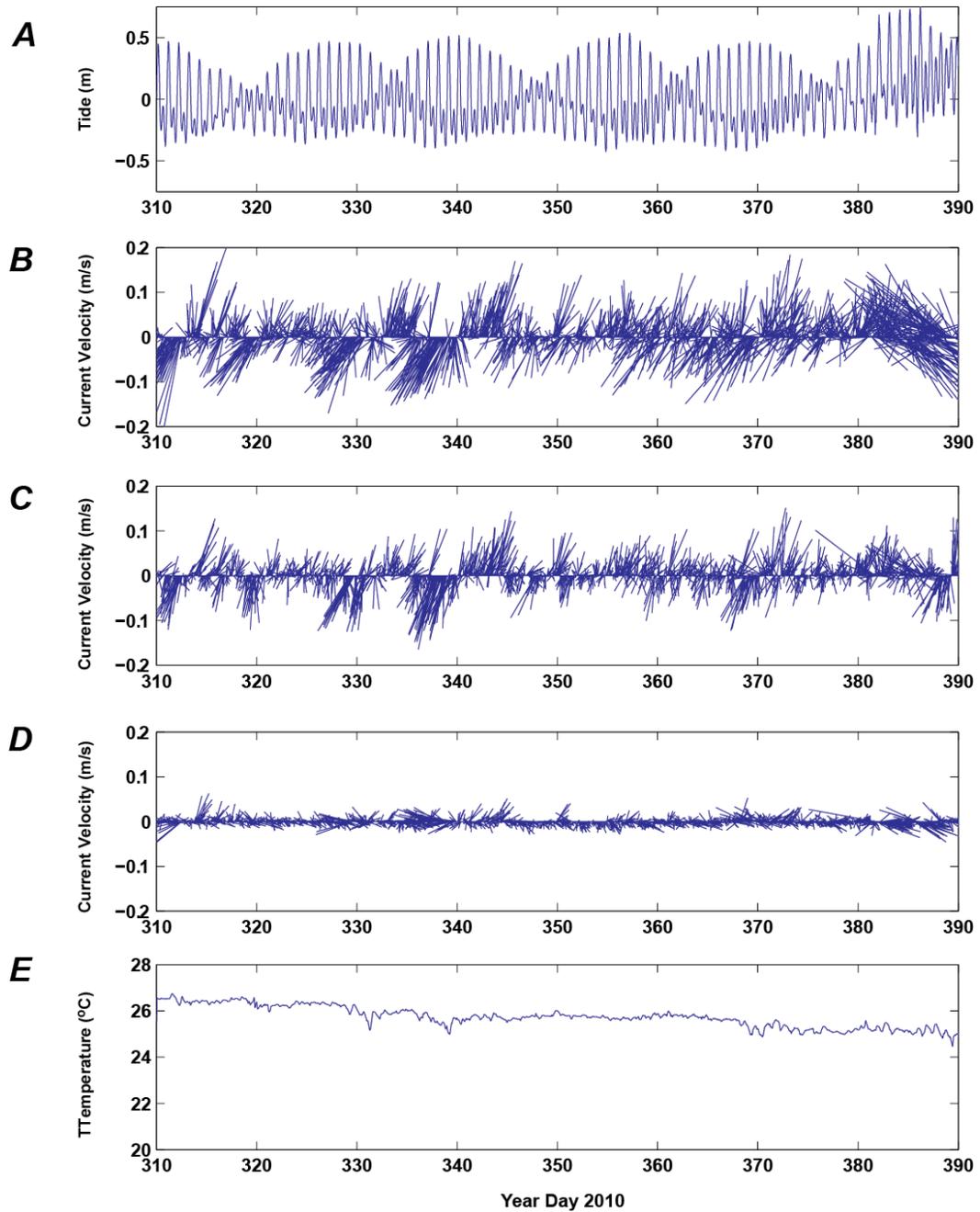
Appendix 10.3. Tide, current, and water temperature data from the ADCP at the South 15-m site. *A*,Tidal height, in meters. *B*, Near-surface current velocity, with direction in degrees from true north and speed in meters per second. *C*, Mid-depth current velocity, with direction in degrees from true north and speed in meters per second. *D*, Near-bed current velocity, with direction in degrees from true north and speed in meters per second. *E*, Water temperature, in degrees Celsius.
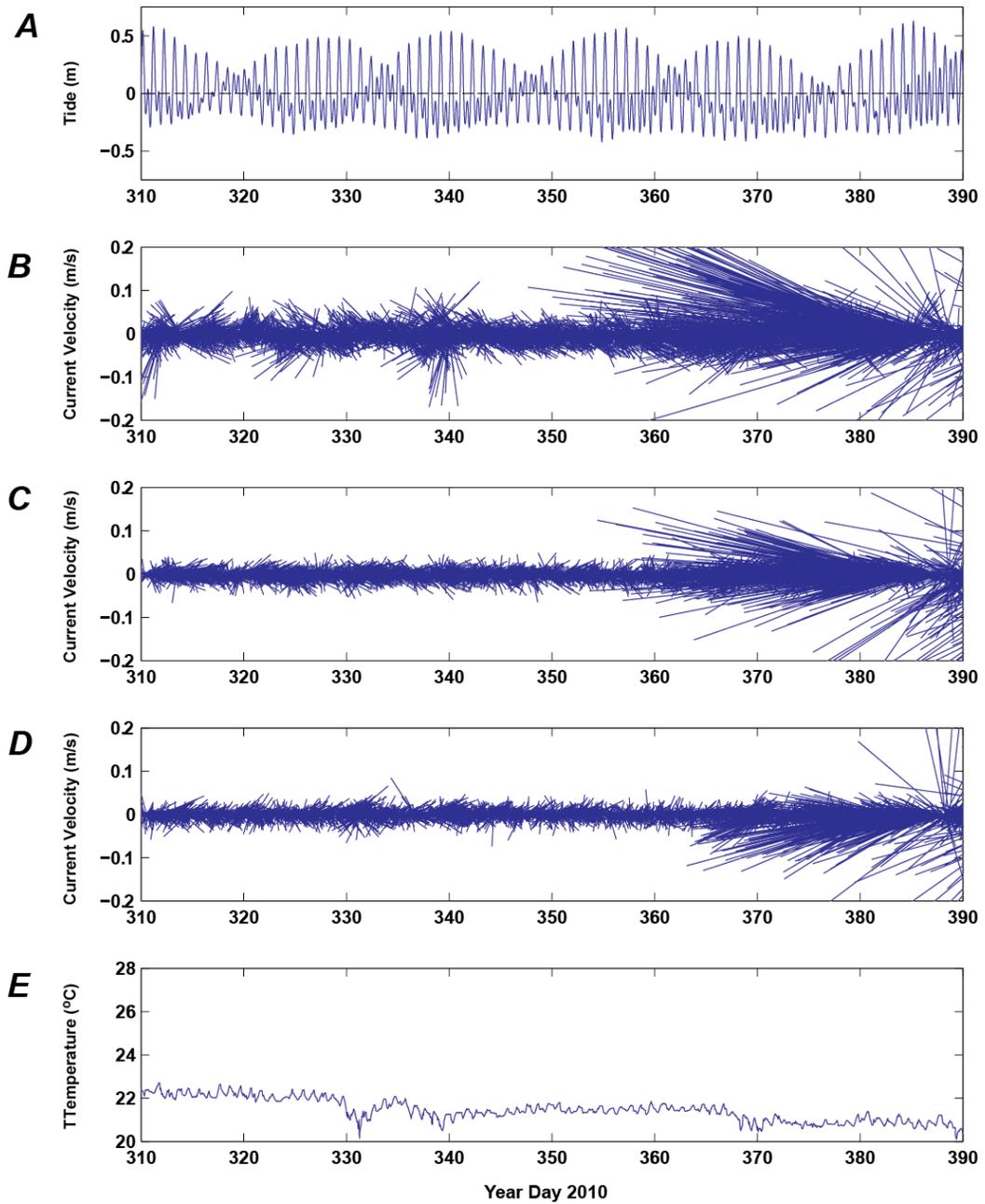
Appendix 10.4. Tide, current, and water temperature data from the ADCP at the Central 5-m site. *A*, Tidal height, in meters. *B*, Near-surface current velocity, with direction in degrees from true north and speed in meters per second. *C*, Mid-depth current velocity, with direction in degrees from true north and speed in meters per second. *D*, Near-bed current velocity, with direction in degrees from true north and speed in meters per second. *E*, Water temperature, in degrees Celsius.
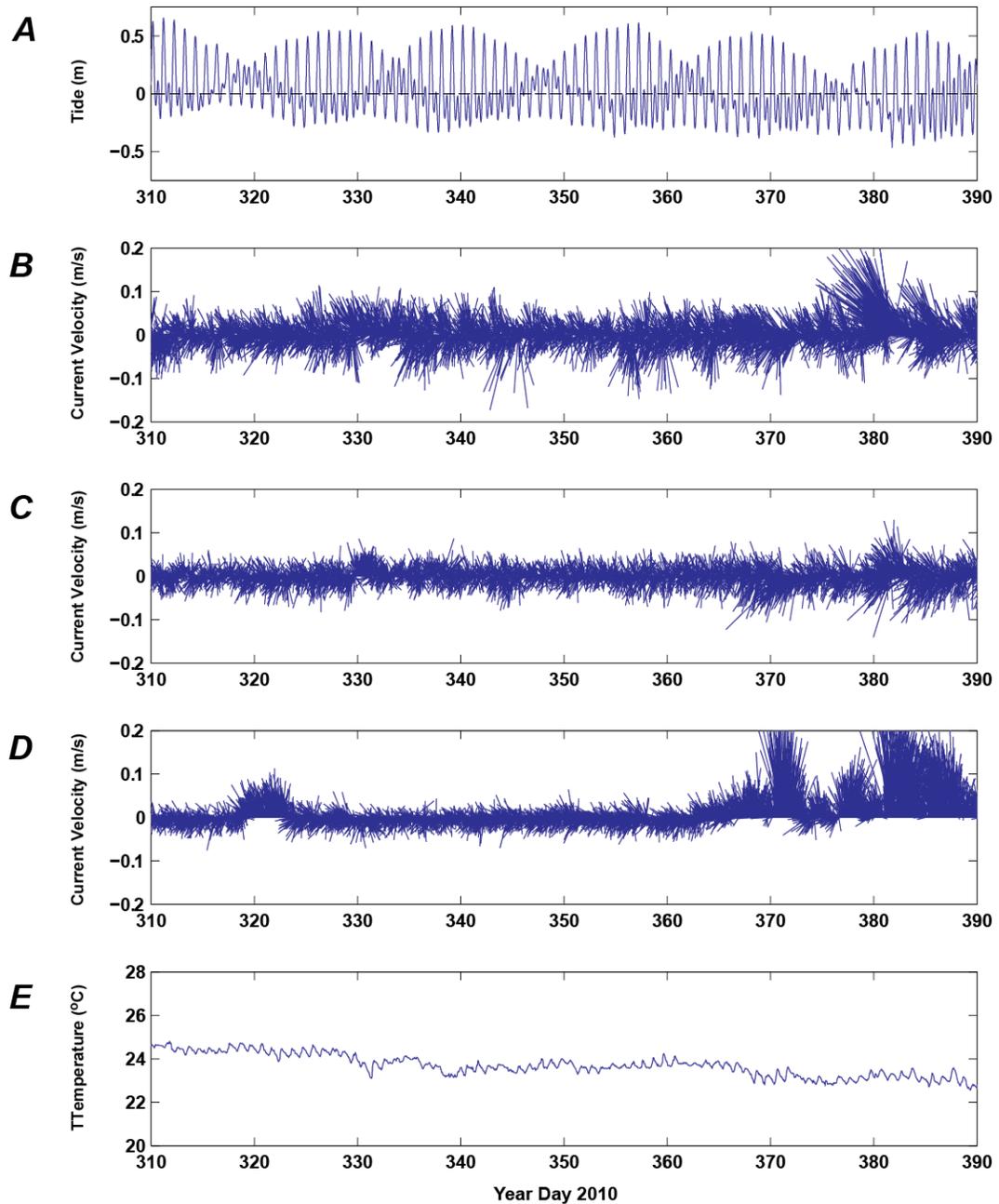
Appendix 10.5. Tide, current, and water temperature data from the ADCP at the South 5-m site. *A*, Tidal height, in meters. *B*, Near-surface current velocity, with direction in degrees from true north and speed in meters per second. *C*, Mid-depth current velocity, with direction in degrees from true north and speed in meters per second. *D*, Near-bed current velocity, with direction in degrees from true north and speed in meters per second. *E*, Water temperature, in degrees Celsius.

Appendix 11. Time-series plots of data from the conductivity and temperature (CT) sensors
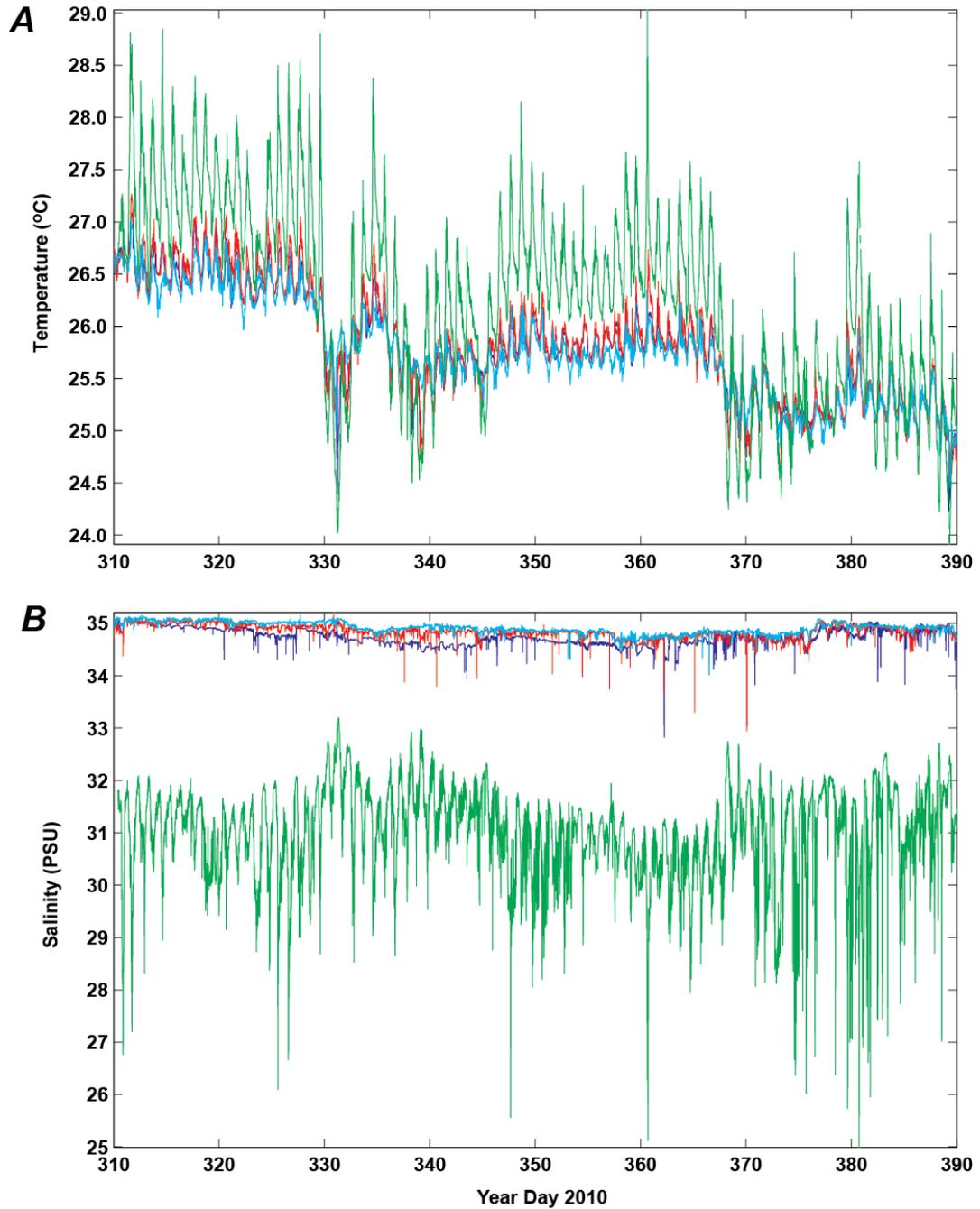
Appendix 11.1. Temperature and salinity data from the CT sensors at the instrument sites. *A*, Water temperature, in degrees Celsius. Green, Central 2-m MiniProbe; blue, Central 5-m MiniProbe; red, Central 5-m ,mooring; cyan, Central 15-m mooring. *B*, Salinity, in Practical Salinity Units (PSU). Green, Central 2-m MiniProbe; blue, Central 5-m MiniProbe; red, Central 5-m mooring; cyan, Central 15-m mooring.

Appendix 12. Time series plots of variations in turbidity from the self-logging optical backscatter sensors (SLOBS)
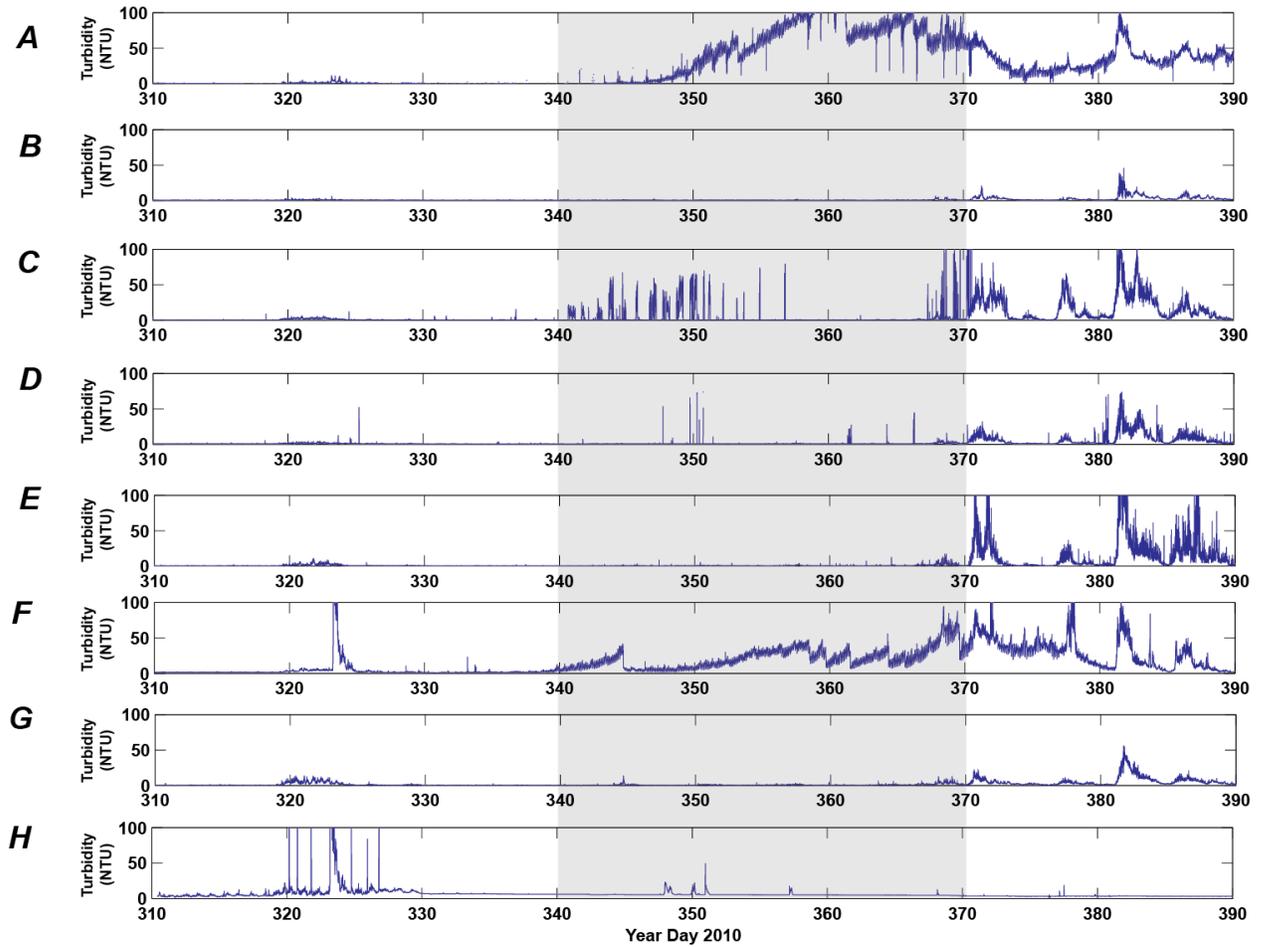
Appendix 12.1. Turbidity data for the 2010–2011 winter from the SLOBSs, in Nephelometric Turbidity Units (NTU); data from the shaded areas were not used for statistics or analysis. *A*, Turbidity at the Central 5-m mooring. *B*, Turbidity at the Central 15-m mooring. *C*, Turbidity at the Central 15-m MiniProbe. *D*, Turbidity at the North 15-m MiniProbe. *E*, Turbidity at the South 15-m MiniProbe. *F*, Turbidity at the Central 5-m MiniProbe. *G*, Turbidity at the South 5-m MiniProbe. *H*, Turbidity at the Central 2-m MiniProbe.

Appendix 13. Maps showing the spatial variability in water parameters from the water-column profiler (WCP) casts in November 2010 and March 2011
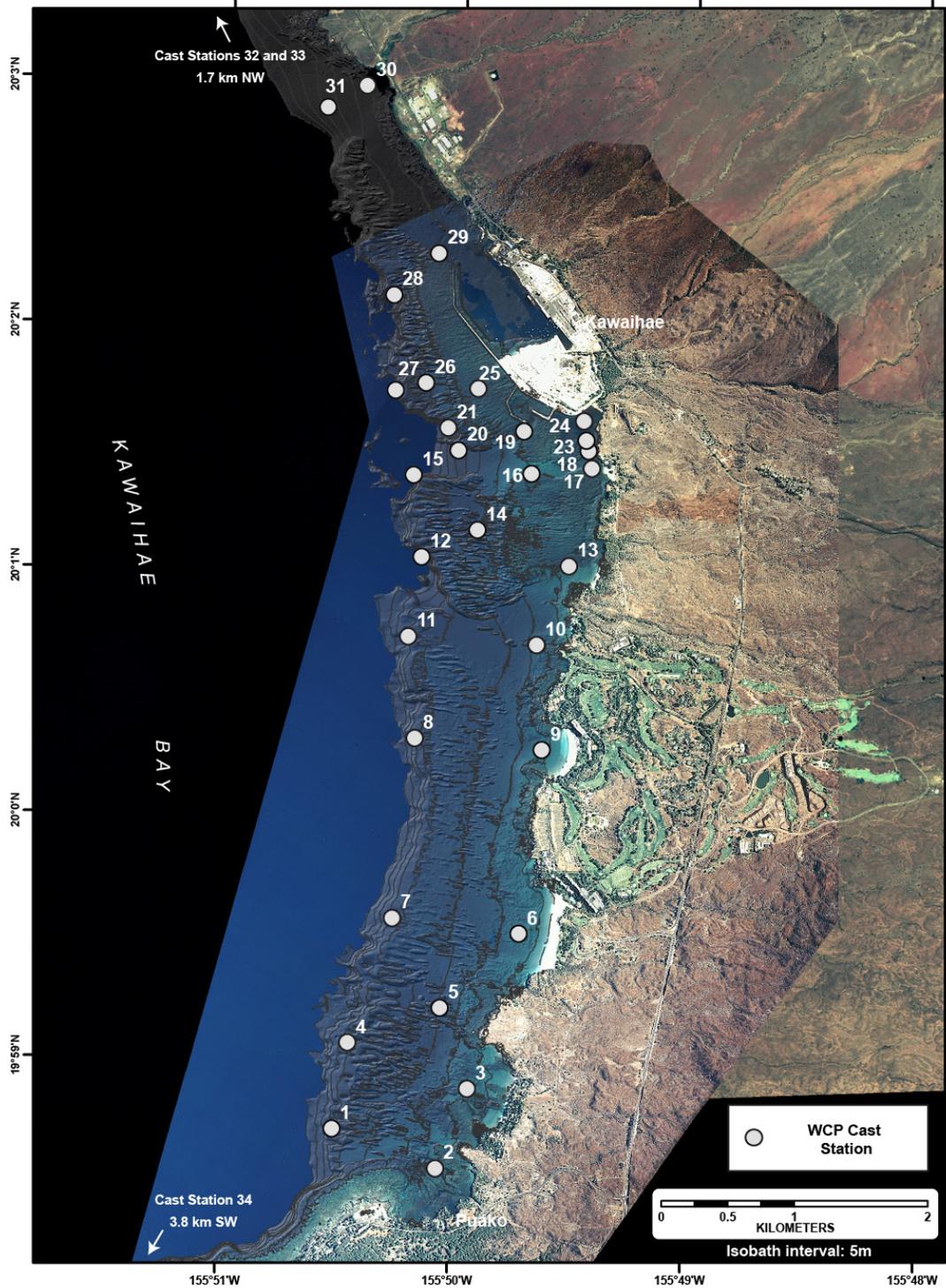
**Appendix 13.1.** Map showing the locations for the WCP casts in November 2010 and March 2011.
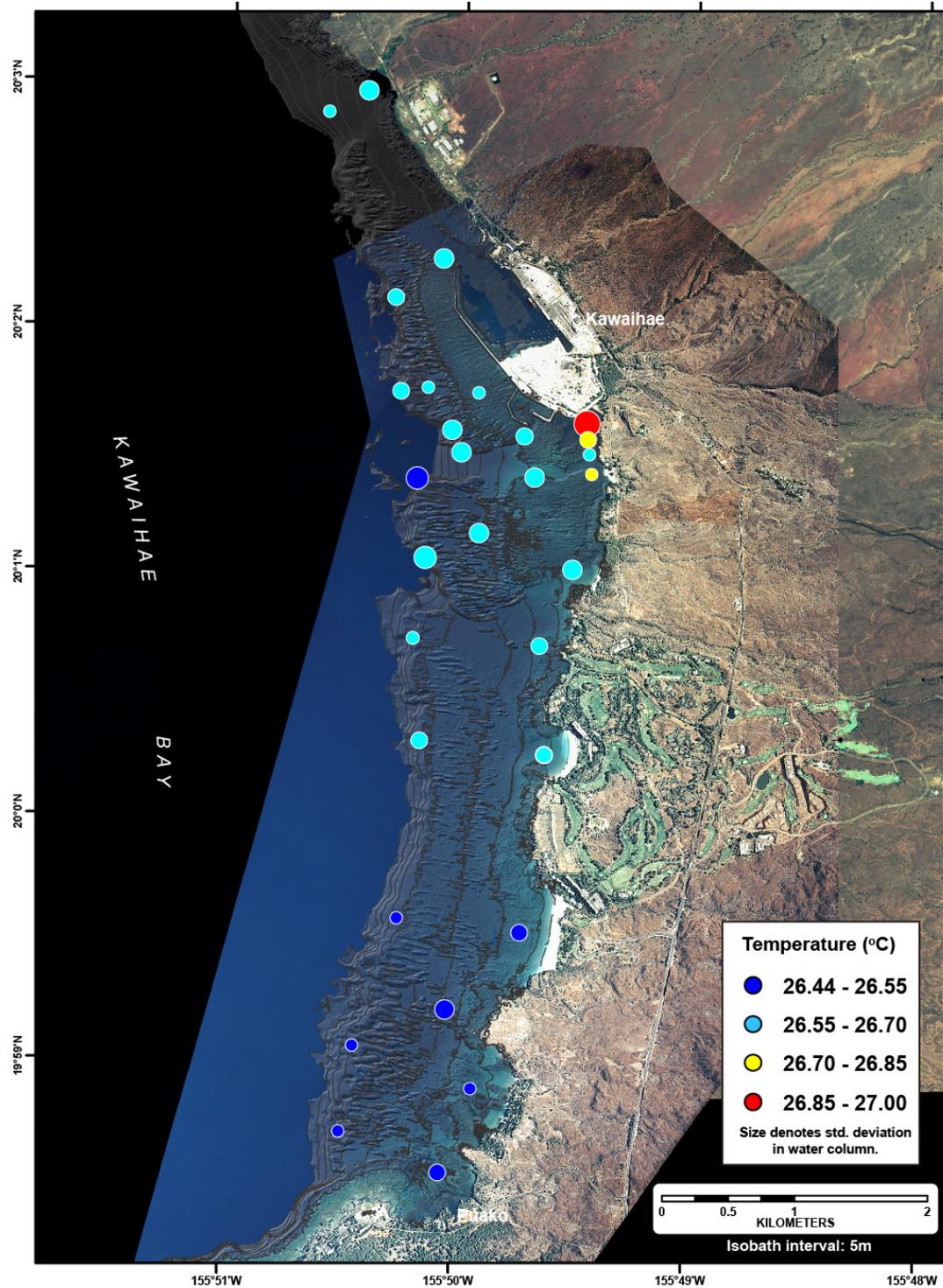
Appendix 13.2. Map showing the spatial variability of water temperature, in degrees Celsius, during the survey on 6 November 2010. The warmest area measured was in Pelekane Bay, possibly due to the shallow depths. The coldest area of the survey was located to the south, near Puako.

93
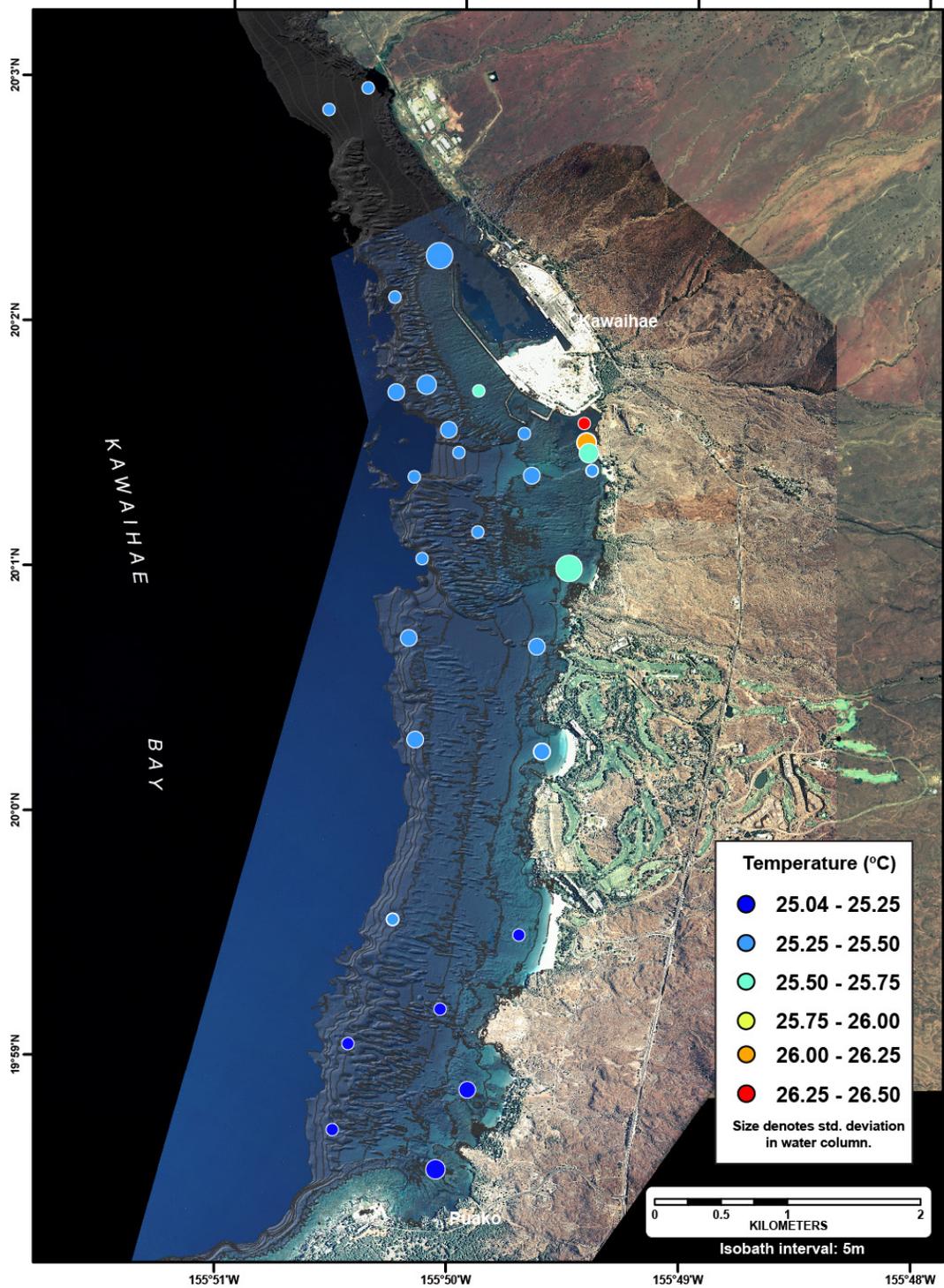
Appendix 13.3. Map showing the spatial variability of temperature, in degrees Celsius, during the survey on 10 March 2011. The warmest area of the survey was located near shore in Pelekane Bay. The coldest temperatures were measured to the south, near Puako. Overall, the temperatures during the March 2011 survey were colder than the November 2010 survey, due to seasonal cooling.
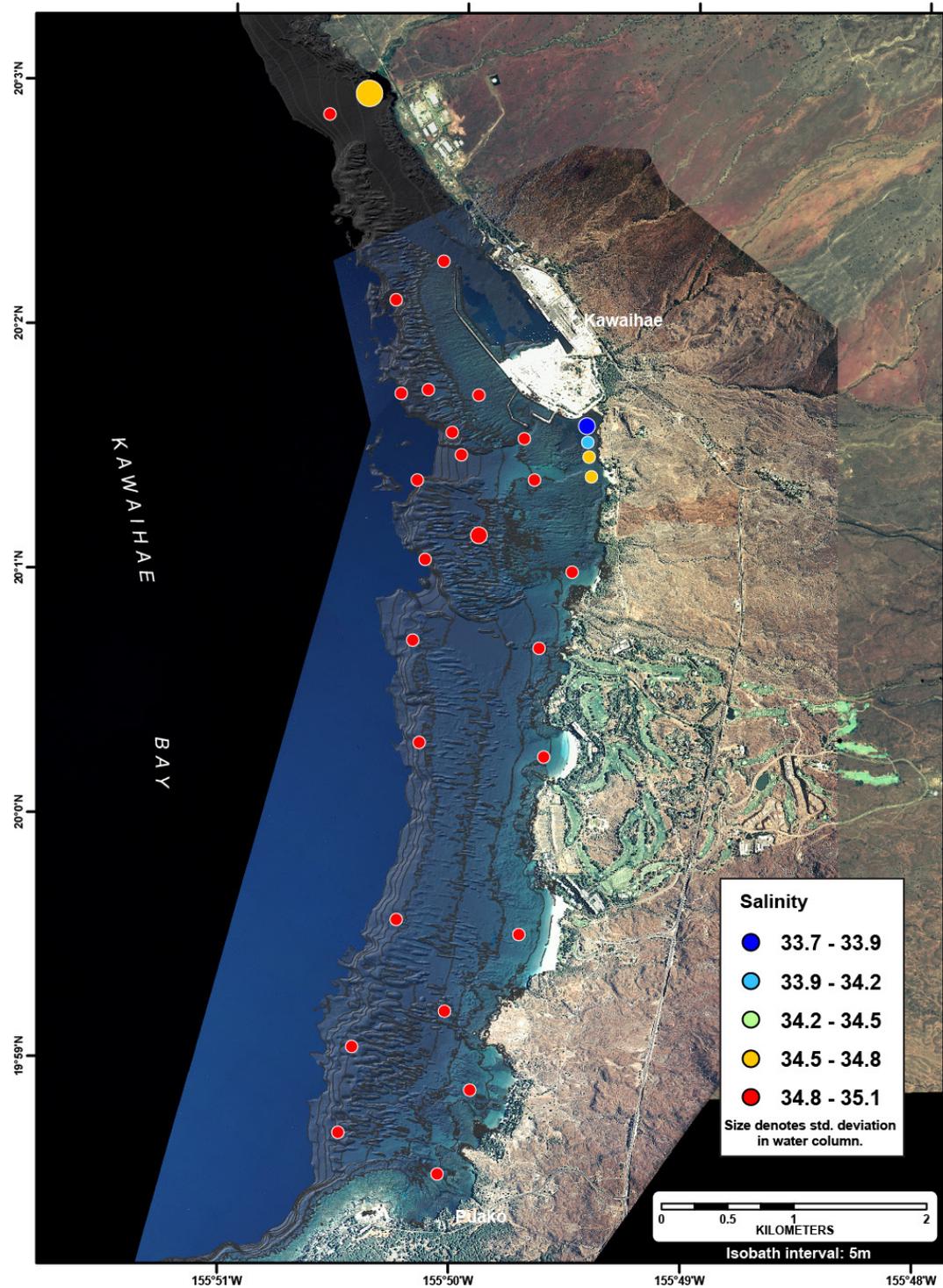
Appendix 13.4. Map showing the spatial variability of salinity, in Practical Salinity Units (PSU), during the survey on 6 November 2010. Salinity values were lower offshore of streams in the northern part of the survey and near Pohokohaule stream in Pelekane Bay.
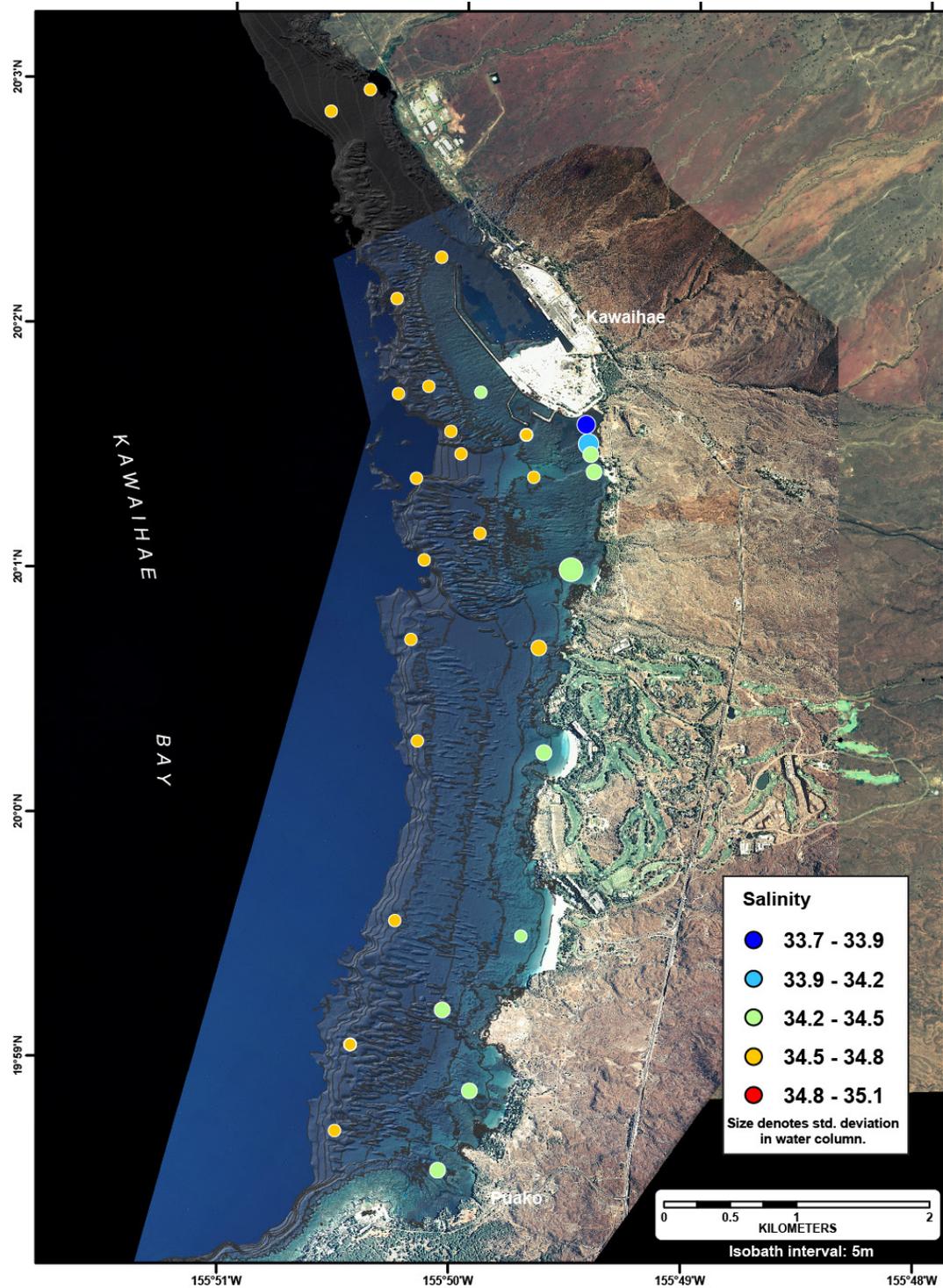
Appendix 13.5. Map showing the spatial variability of salinity, in Practical Salinity Units (PSU), during the survey on 10 March 2011. Salinity values during this survey were lower overall than during the November survey, possibly due to an increase in surface runoff and submarine groundwater discharge following rainfall during the winter months.
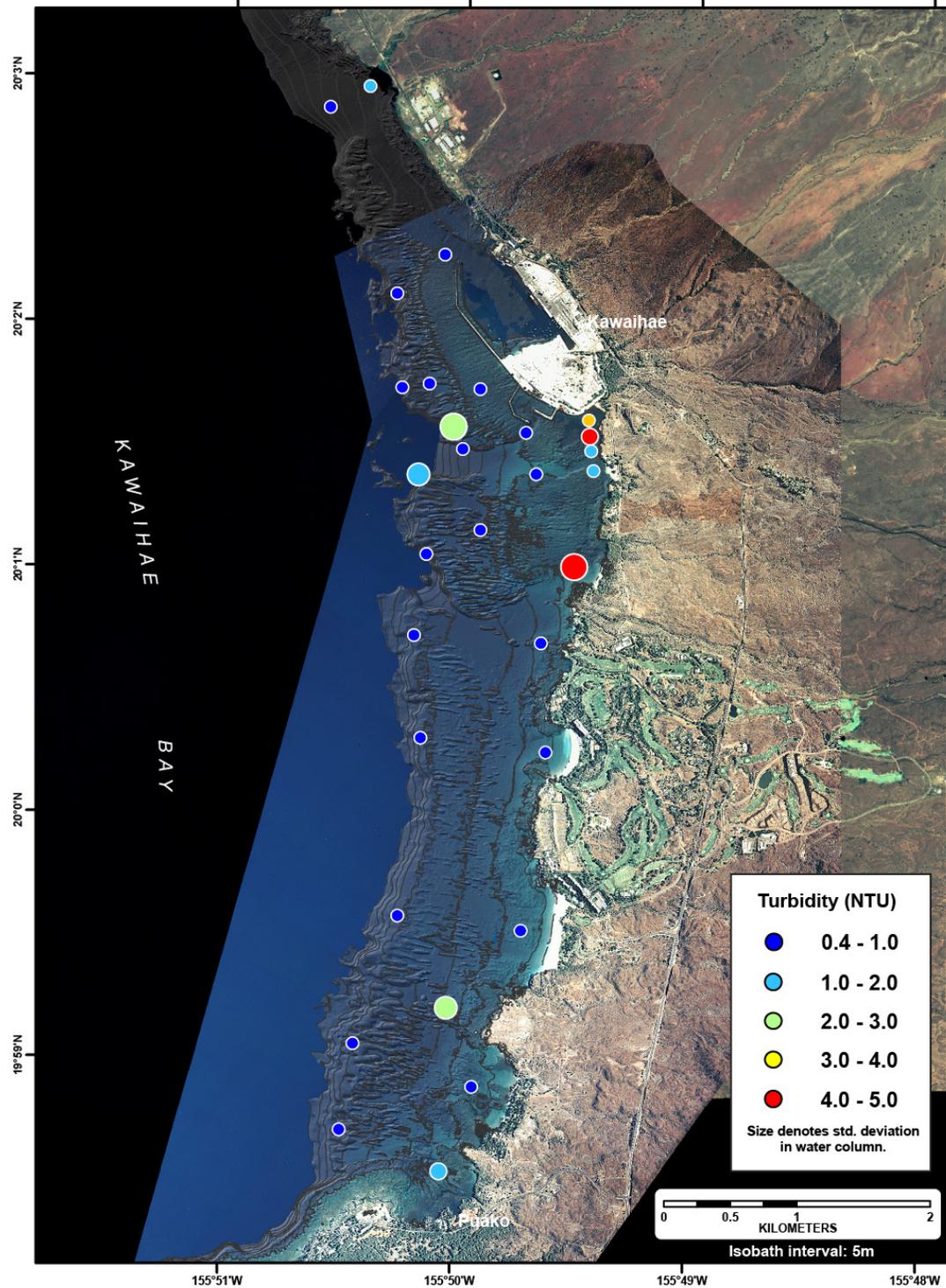
Appendix 13.6. Map showing the spatial variability of turbidity, measured by optical backscatter, in Nephelometric Turbidity Units (NTU), during the survey on 6 November 2010. There was relatively clear water overall, with the highest turbidity in Pelekane Bay.
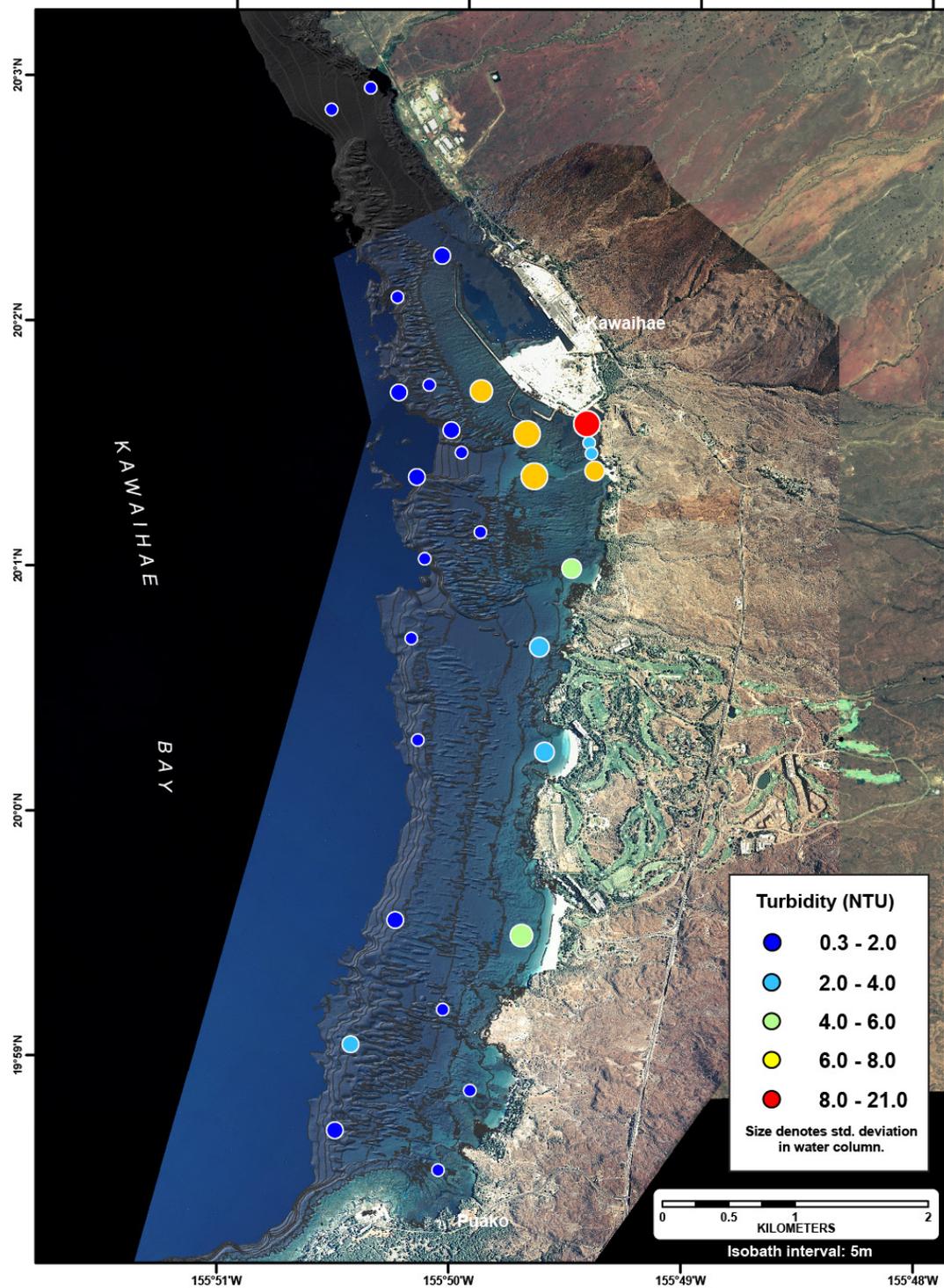
Appendix 13.7. Map showing the spatial variability of turbidity, measured by optical backscatter, in Nephelometric Turbidity Units (NTU), during the survey on 10 March 2011. The water was relatively clear overall, with the highest turbidity in Pelekane Bay and just south of the bay. The turbidity was higher than the early-November 2010 survey, possibly due to the input of sediment from the late November 2010 flood.
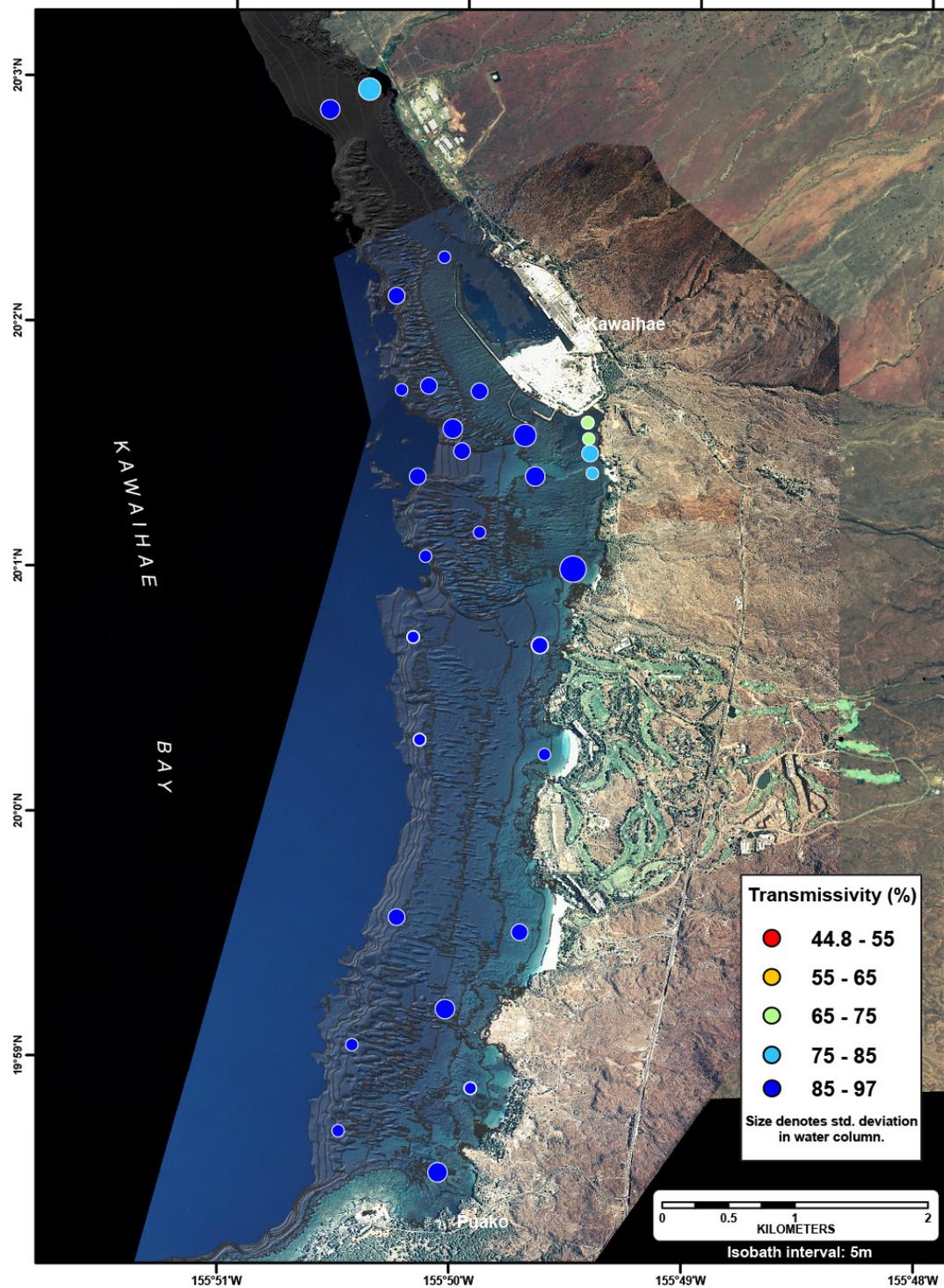
Appendix 13.8. Map showing the spatial variability of light transmission, in percent, during the survey on 6 November 2010. There was relatively clear water overall with lower light transmission (higher turbidity) in Pelekane Bay.
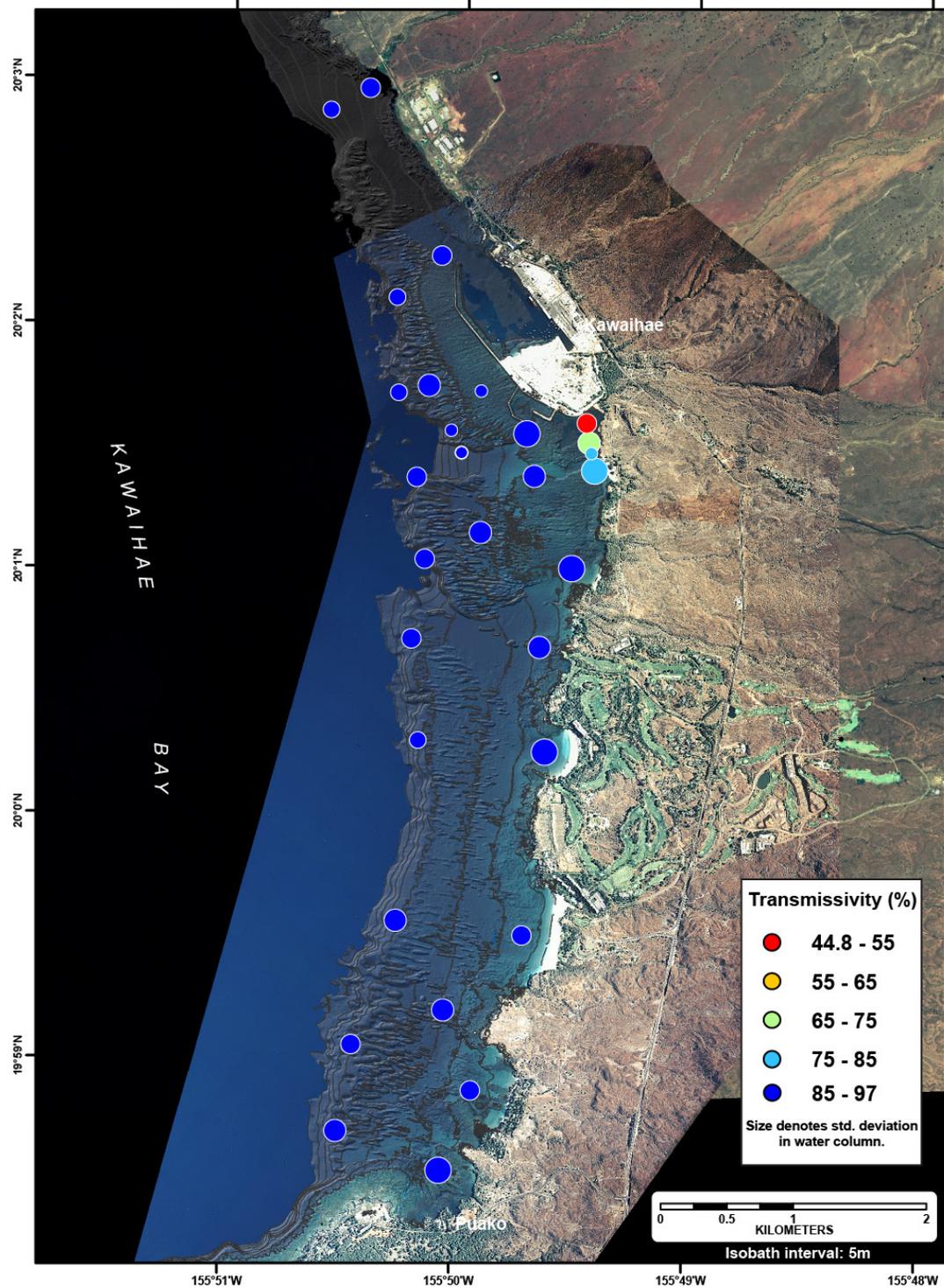
Appendix 13.9. Map figure showing the spatial variability of light transmission, in percent, during the survey on 10 March 2011 survey. There survey showed relatively clear water overall with lower light transmission (higher turbidity) in Pelekane Bay. The light transmission was lower in Pelekane Bay at this time than during the early November 2010 survey, possibly due to the input of sediment from the late November 2010 flood.
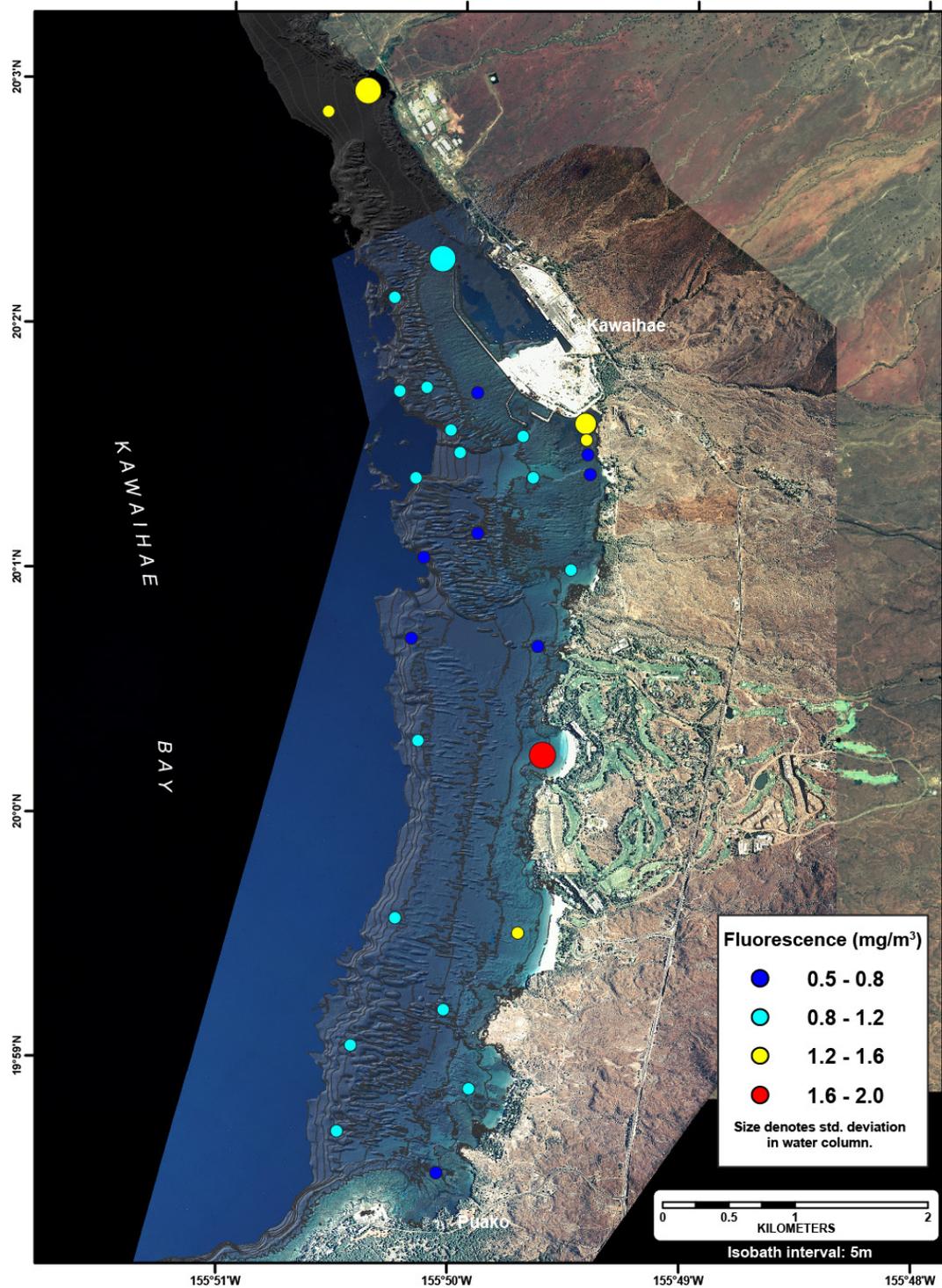
Appendix 13.10. Map showing the spatial variability of fluorescence, in milligrams per cubic meter, during the survey on 6 November 2010. The areas with greatest fluorescence were located near shore in the vicinity of streams and human development. The offshore casts show low fluorescence and little variability.

101
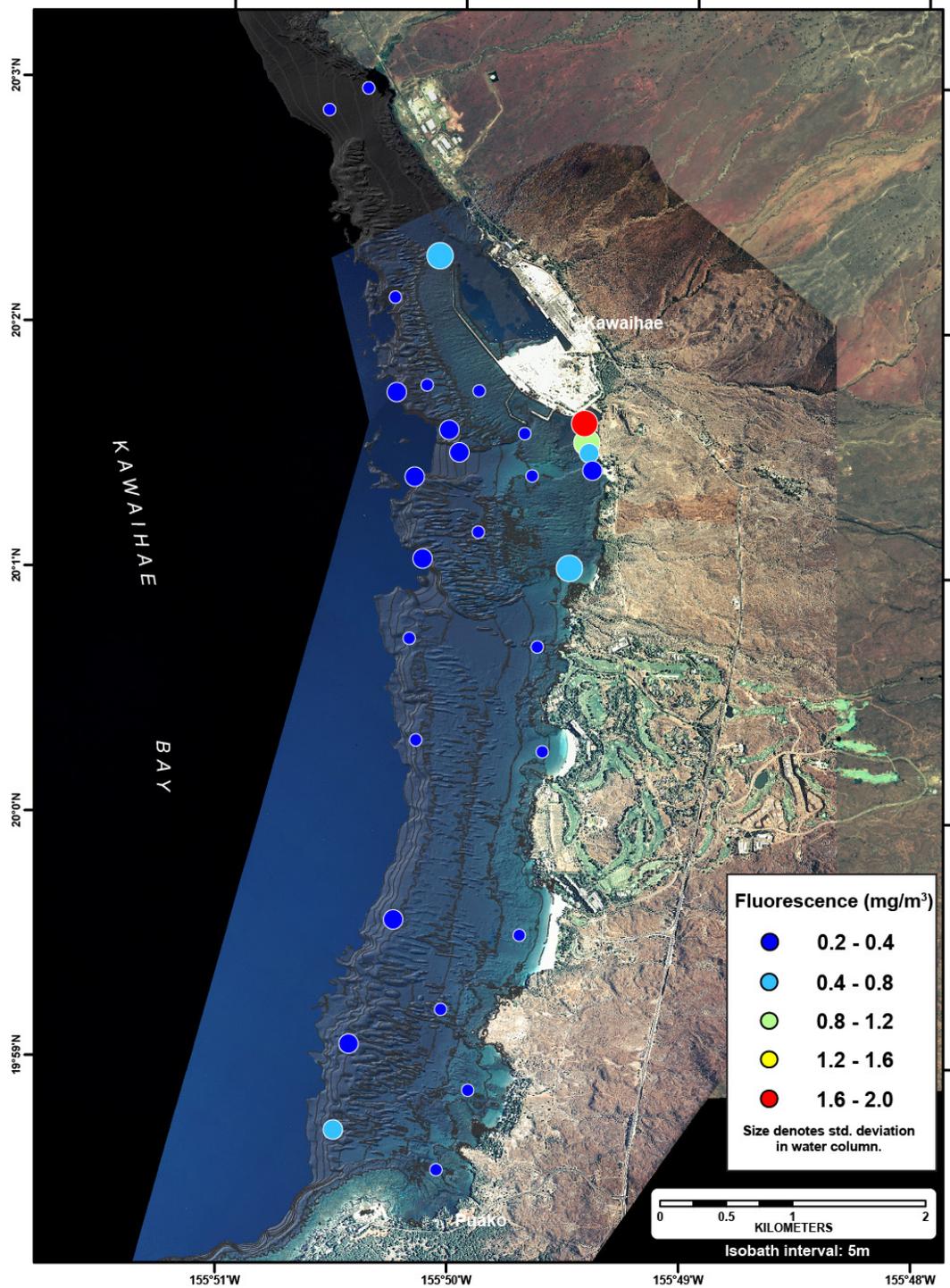
Appendix 13.11. Map showing the spatial variability of fluorescence, in milligrams per cubic meter, during the survey on 10 March 2011. The area with greatest fluorescence was located nearshore in Pelekane Bay. The fluorescence was lower in the rest of the areas of the survey.

Appendix 14. Time-series plots of variations in current, wave, and combined wave-current critical shear stresses for silt- and clay-sized particles
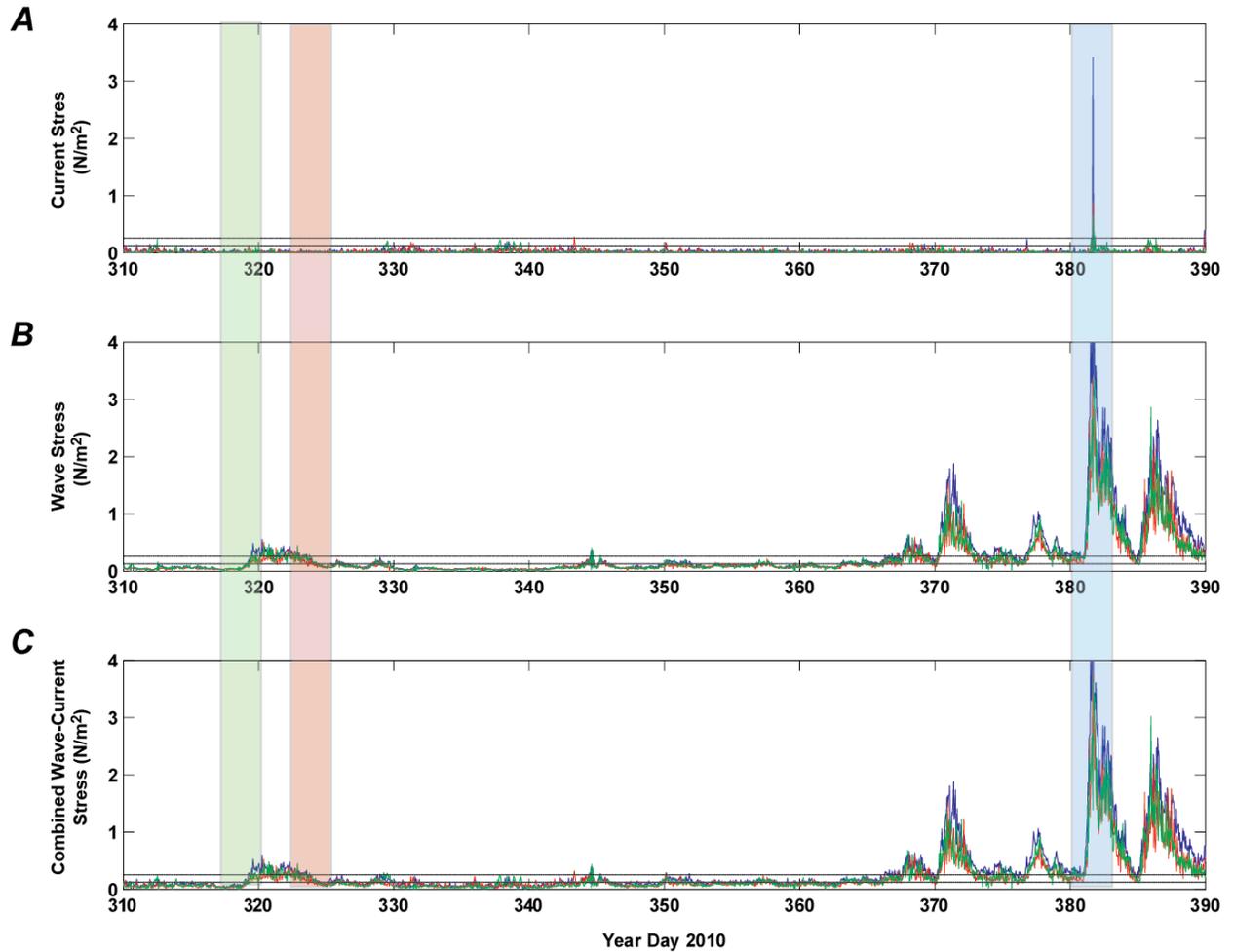
Appendix 14.1. Calculated critical shear stress values from the acoustic Doppler current profiler (ADCP) sensors at the deep (>15 m) instrument sites. *A*, Current shear stress, in Newtons per square meter (N/m^2). *B*, Wave shear stress, in Newtons per square meter. *C*, Combined wave-current shear stress, in Newtons per square meter. Blue lines, Central 15-m site; red lines, North 15-m site; green lines, South 15-m site. Green shading, trade-wind conditions; orange shading, flood event; blue shading, large-wave event. The black lines at 0.10 Newtons per square meter is the critical shear stress for carbonate sand and terrigenous mud. If the shear stress exceeds this value, the material will be resuspended from the seabed; if not, the material will remain stable on the seabed.
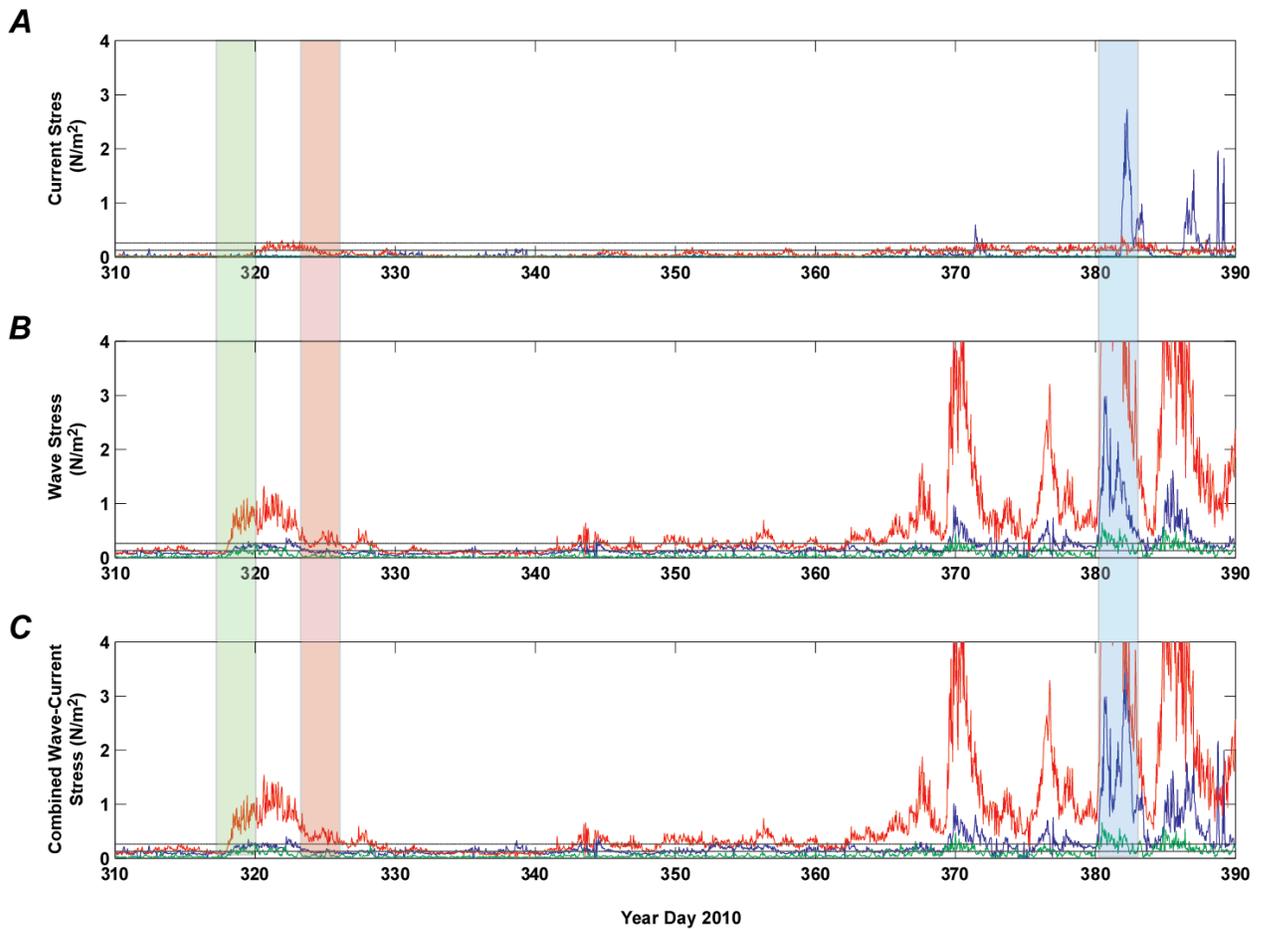
Appendix 14.2 Calculated critical shear stress values from the acoustic Doppler current profiler (ADCP) sensors at the shallow (<5 m) instrument sites. *A*, Current shear stress, in Newtons per square meter (N/m^2). *B*, Wave shear stress, in Newtons per square meter. *C*, Combined wave-current shear stress, in Newtons per square meter. Blue lines, Central 5-m site; red lines, South 5-m site; green lines, Central 2-m site. Green shading, trade-wind conditions; orange shading, flood event; blue shading, large-wave event. The black lines at 0.10 Newtons per square meter is the critical shear stress for carbonate sand and terrigenous mud. If the shear stress exceeds this value, the material will be resuspended from the seabed; if not, the material will remain stable on the seabed.